

**The Pennsylvania State University**

**The Graduate School**

**Department of Agricultural and Biological Engineering**

**REMOTE SENSING OF NUTRIENT DEFICIENCY IN *LACTUCA SATIVA*  
USING NEURAL NETWORKS FOR TERRESTRIAL AND ADVANCED LIFE  
SUPPORT APPLICATIONS**

**A Thesis in**

**Agricultural and Biological Engineering**

**by**

**Eddie Seldon Sears**

**Submitted in Partial Fulfillment  
of the Requirements  
for the Degree of**

**Doctor of Philosophy**

**May 2001**

UMI Number: 3014695

**UMI<sup>®</sup>**

---

UMI Microform 3014695

Copyright 2001 by Bell & Howell Information and Learning Company.

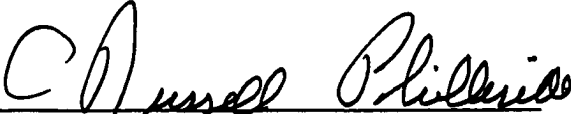
All rights reserved. This microform edition is protected against  
unauthorized copying under Title 17, United States Code.

---

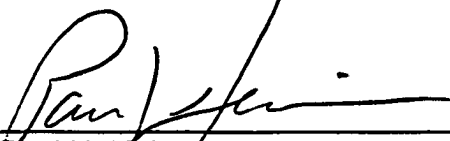
Bell & Howell Information and Learning Company  
300 North Zeeb Road  
P.O. Box 1346  
Ann Arbor, MI 48106-1346

We approve the thesis of Edie S. Sears.

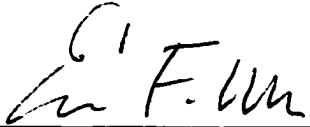
Date of Signature

  
C. Russell Philbrick  
Professor of Electrical Engineering  
Thesis Co-Advisor  
Co-Chair of Committee

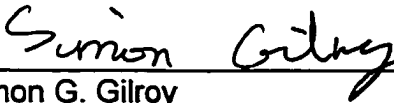
11 April 2001

  
Paul H. Heinemann  
Professor of Agricultural Engineering  
Thesis Co-Advisor  
Co-Chair of Committee

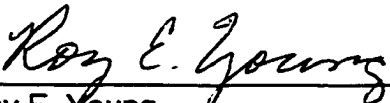
4/9/01

  
Eileen F. Wheeler  
Assistant Professor of Agricultural Engineering

March 27, 2001

  
Simon G. Gilroy  
Associate Professor of Biology

April 2, 2001

  
Roy E. Young  
Professor of Agricultural Engineering  
Head of the Department of Agricultural and Biological Engineering

April 9, 2001

## ABSTRACT

A remote sensing study using reflectance and fluorescence spectra of hydroponically grown *Lactuca sativa*, 'Ostinata' (lettuce) canopies was conducted. An optical receiver was designed and constructed to interface with a commercial fiber optic spectrometer for data acquisition. Optical parameters were varied to determine the effects of field of view and distance to target on vegetation stress assessment over the complete growth cycle of the test plants. Feedforward backpropagation neural networks (NN) were implemented to predict the presence of canopy stress and vegetation nutrient status based on spectral inputs of canopy reflectance and fluorescence. Effects of spatial and spectral resolutions on stress predictions of the neural network were also examined.

Visual inspection and fresh mass values failed to differentiate between controls and plants cultivated with 25% of the recommended concentration of phosphorous (P) in solution. There was also difficulty discerning 25% nitrogen (N) from 5%P based on fresh mass and visual inspection. The NN's were trained on input vectors created using reflectance and test day, fluorescence and test day, and reflectance, fluorescence, and test day. Four networks were created representing four levels of spectral resolution: the COLORBLOCK NN with wavelength resolution of  $\Delta\lambda\approx 100\text{-nm}$ , 10-nm NN ( $\Delta\lambda\approx 10\text{-nm}$ ), 1-nm NN ( $\Delta\lambda\approx 1\text{-nm}$ ), and 0.1-nm NN ( $\Delta\lambda\approx 0.1\text{-nm}$ ).

Results from the NN validation classification demonstrated that all four types of network could be used as a remote sensing method for detecting extreme nitrogen deficiency early in the growth cycle. For the lower resolution models, COLORBLOCK and 10-nm NN, the best classification results of 5%N occurred using both reflectance and fluorescence spectra and a field of view (FOV) encompassing a 7.5-cm diameter spot size or 0.8 of a

plant. For the higher resolution models, 1-nm NN and 0.1-nm NN, 5%N specimens were classified the best using reflectance spectra without fluorescence. For the highest resolution model, 0.1-nm NN, the best classification results coincided with the largest FOV, a 15-cm spot size or area encompassing 3 plants.

The 10-nm resolution was found to be sufficient for classifying extreme nitrogen deficiency in freestanding hydroponic lettuce. As a result of leaf angle and canopy structure broadband scattering intensity in the 700-nm to 1000-nm range was found to be the most useful portion of the spectrum in this study. More subtle effects of “greenness” and fluorescence emission were obscured by canopy structure and leaf orientation.

Scans having higher than acceptable variation should then be deleted from the neural network training and testing. This would enhance the robustness of the system. As field of view was not as found to be as significant as originally believed, systems implementing higher repetitions over more uniformly oriented, i.e. smaller, flatter, target areas would provide for more discernible neural network input vectors.

It is believed that this technique holds considerable promise for the early detection of extreme nitrogen deficiency in *Lactuca Sativa* cultivated in NASA Advanced Life Support well as in terrestrial hydroponic systems. Further research is recommended using stereoscopic digital cameras to quantify leaf area index, leaf shape, and leaf orientation as well as reflectance. Given the additional information provided by stereoscopic vision systems, fluorescence emission may also prove to be a useful biological assay of freestanding vegetation.

## Table of Contents

<b>LIST OF TABLES .....</b>	<b>VII</b>
<b>LIST OF FIGURES .....</b>	<b>VIII</b>
<b>LIST OF ABBREVIATIONS AND SYMBOLS .....</b>	<b>XI</b>
<b>ACKNOWLEDGEMENTS.....</b>	<b>XIII</b>
<b>1. INTRODUCTION.....</b>	<b>1</b>
1.1 PROJECT JUSTIFICATION .....	1
1.2 SYSTEM SUMMARY .....	2
<b>2. LIGHT INTERACTION WITH LEAVES .....</b>	<b>4</b>
2.1 REFLECTANCE.....	4
2.2 FLUORESCENCE .....	10
<b>3. REMOTE SENSING REVIEW.....</b>	<b>13</b>
3.1 HISTORY OF REMOTE SENSING.....	14
3.2 PASSIVE REMOTE SENSING.....	19
3.3 ACTIVE REMOTE SENSING.....	21
<b>4. HARDWARE FOR DATA COLLECTION.....</b>	<b>27</b>
4.1 EXCITATION LIGHT SOURCE.....	27
4.2 INSTRUMENTATION FOR OPTICAL SPECTROSCOPY .....	31
4.3 OPTICAL RECEIVER .....	35
4.4 RESULTS OF PLANT STRESS MEASUREMENTS .....	38
<b>5. ARTIFICIAL NEURAL NETWORKS (ANN's).....</b>	<b>41</b>
5.1 HISTORY OF ARTIFICIAL NEURAL NETWORKS .....	43
5.1.1 <i>Bain's Concept of Memory</i> .....	43
5.1.2 <i>The First Logic Circuits</i> .....	45
5.1.3 <i>Perceptron and ADELIN</i> .....	47
5.1.4 <i>Multilayered Backpropagation Association Networks</i> .....	51
5.2 NEURAL NETWORK OPERATION .....	53
5.3 NEURAL NETWORK TERMINOLOGY .....	57
5.4 PREDICTION OF SPECIFIC NUTRIENT LEVELS IN VEGETATION .....	59
<b>6. HYPOTHESIS AND OBJECTIVES.....</b>	<b>60</b>
6.1 HYPOTHESIS .....	60
6.2 OBJECTIVES.....	61
<b>7. METHODOLOGY.....</b>	<b>62</b>
7.1 LETTUCE CULTIVATION.....	62

<b>7.2</b>	<b>ELECTROMAGNETIC RADIATION AND OPTICS.....</b>	<b>67</b>
7.2.1	<i>Electromagnetic Radiation Units.....</i>	67
7.2.2	<i>Reflectance Light Source.....</i>	70
7.2.3	<i>Fluorescence Excitation Source.....</i>	72
7.2.4	<i>Plant Angle.....</i>	73
7.2.5	<i>Optical Receiver.....</i>	73
<b>7.3</b>	<b>DATA ANALYSIS.....</b>	<b>80</b>
7.3.1	<i>Test Bias.....</i>	82
7.3.2	<i>Reflectance Spectra.....</i>	83
7.3.3	<i>Fluorescence Spectra.....</i>	95
7.3.4	<i>Combination of Reflectance and Fluorescence Spectra.....</i>	102
7.3.5	<i>Spatial Resolution.....</i>	103
7.3.6	<i>Spectral Resolution.....</i>	103
<b>8.</b>	<b>RESULTS AND CONCLUSIONS.....</b>	<b>106</b>
8.1	<b>PLANT CULTIVATION.....</b>	<b>106</b>
8.2	<b>TEST BIAS.....</b>	<b>110</b>
8.3	<b>NEURAL NET OUTPUT.....</b>	<b>110</b>
8.3.1	<i>COLORBLOCK.....</i>	120
8.3.2	<i>The 10-nm NN.....</i>	122
8.3.3	<i>The 1-nm NN.....</i>	123
8.3.4	<i>The 0.1-nm NN.....</i>	125
8.4	<b>CANOPY STRUCTURE AND PLANT ANGLE.....</b>	<b>126</b>
8.5	<b>CONCLUSIONS.....</b>	<b>135</b>
	<b>REFERENCES.....</b>	<b>140</b>
	<b>APPENDIX A.) CULTIVATION INFORMATION.....</b>	<b>151</b>
	<b>APPENDIX B.) RESULTS FOR COLORBLOCK NEURAL NET.....</b>	<b>173</b>
	<b>APPENDIX C.) RESULTS FOR 10-NM NEURAL NET.....</b>	<b>183</b>
	<b>APPENDIX D.) RESULTS FOR 1-NM NEURAL NET.....</b>	<b>193</b>
	<b>APPENDIX E.) RESULTS FOR 0.1-NM NEURAL NET.....</b>	<b>203</b>

**LIST OF TABLES**

<b>TABLE 3.1.) MILESTONES IN THE HISTORY OF REMOTE SENSING .....</b>	<b>.18</b>
<b>TABLE 7.1.) EXPERIMENTAL DESIGN FOR HYDROPONIC LETTUCE CULTIVATION ...</b>	<b>63</b>
<b>TABLE 7.2.) CONTROL NUTRIENT SOLUTION (WELLS, 1995) AND TAP WATER CONCENTRATIONS .....</b>	<b>65</b>
<b>TABLE 7.3) EXPERIMENTAL LAYOUT USING RANDOMIZED BLOCK DESIGN .....</b>	<b>.67</b>
<b>TABLE 8.1.) PAIRED TWO SAMPLE T-TEST FOR MEANS, 2-TAILED P-VALUES .....</b>	<b>109</b>
<b>TABLE 8.2.) BEST NEURAL NETWORK (NN) VALIDATION OUTPUT FOR EACH LEVEL OF SPECTRAL RESOLUTION AS A FUNCTION OF TEST DAY .....</b>	<b>138</b>



## LIST OF FIGURES

<b>FIGURE 1.1.) GRID SCANNING BY SPECTROMETER WITHIN A SELF-MONITORING PLANT GROWTH CHAMBER .....</b>	<b>3</b>
<b>FIGURE 2.1. A.) LEAF ANATOMY, IDEALIZED LEAF CROSS (CAMPBELL 1996) AND B.) GENERALIZED CHLOROPLAST IN CROSS SECTION (NOBEL, 1991).....</b>	<b>6</b>
<b>FIGURE 2.2.) BLUE, GREEN, RED, AND INFRARED LIGHT INTERACTING WITH A GENERALIZED LEAF CROSS SECTION (CAMPBELL, 1996).....</b>	<b>7</b>
<b>FIGURE 2.3.) IDEALIZED SPECTRAL REFLECTANCE CURVE FOR VEGETATION (HTTP://PIRLWWW.LPL.ARIZONA.EDU/BIOSPHERE/ ECO/PLANTSPEX2.GIF .....</b>	<b>9</b>
<b>FIGURE 3.1.) THE FLUORESCENCE INDUCTION OR KAUTSKY CURVE (ROSEMA, ET AL., 1992).....</b>	<b>22</b>
<b>FIGURE 3.2. A.) LIF SPECTRA OF PURIFIED PLANT PIGMENTS. B.) LIF SPECTRA OF PLANT TYPES (CHAPPELLE AND WILLIAMS, 1987) .....</b>	<b>26</b>
<b>FIGURE 4.1) LABORATORY CONFIGURATION OF CHAPPELLE AND WILLIAMS 1987 LIF EXPERIMENTS .....</b>	<b>28</b>
<b>FIGURE 4.2) LABORATORY CONFIGURATION FOR SAITO ET AL. 1998 LIF EXPERIMENTS. A) EXPERIMENTAL SETUP AND B) CONFIGURATION OF LEAF, LASER BEAM, AND FIBER .....</b>	<b>31</b>
<b>FIGURE 4.3) BLOCK DIAGRAM OF EXPERIMENTAL HARDWARE CONFIGURATION ...</b>	<b>32</b>
<b>FIGURE 4.4) EFFECT OF NUTRIENT DEFICIENCIES ON 8-WEEK OLD CORN PLANTS A) LIF INTENSITY AT 440-NM AND B) LIF INTENSITY AT 685-NM (CHAPPELLE AND WILLIAMS, 1987) .....</b>	<b>39</b>
<b>FIGURE 5.1.) RASHEVSKY'S BINARY LOGIC OPERATION, EXCLUSIVE OR .....</b>	<b>45</b>
<b>FIGURE 5.2.) McCULLOCH AND PITTS'S THRESHOLD LOGIC CIRCUIT FOR AN AND OPERATION .....</b>	<b>46</b>
<b>FIGURE 5.3.) ROSENBLATT'S ORIGINAL PERCEPTRON CIRCUIT .....</b>	<b>48</b>
<b>FIGURE 5.4.) THE BASIC BACKPROPAGATION NODE (OLMSTED, 1998).....</b>	<b>52</b>

<b>FIGURE 7.1.) EXPERIMENTAL SETUP FOR HYDROPONIC CULTIVATION OF TEST PLANT .....</b>	<b>63</b>
<b>FIGURE 7.2.) INTENSITY OF A BLACKBODY EMITTER AT 3200K USING PLANCK'S LAW.....</b>	<b>71</b>
<b>FIGURE 7.3.) RAY DIAGRAM OF OPTICAL RECEIVER FOCUSING LENS ONTO 1-MM DIAMETER FIBER OPTIC .....</b>	<b>77</b>
<b>FIGURE 7.4.) ENCLOSED ENERGY DIAGRAM FOR OPTICAL RECEIVER .....</b>	<b>78</b>
<b>FIGURE 7.5.) SPOT DIAGRAM FOR OPTICAL RECEIVER.....</b>	<b>79</b>
<b>FIGURE 7.6. REFLECTANCE SPECTRA OF MEDIUM SPOT SIZE ON TEST DAY 28 OF TEST 1. A.) SPECTROMETER CHANNEL 1, 800 TO 1000-NM. B.) SPECTROMETER CHANNEL 2, 625 TO 865-NM. C.) SPECTROMETER CHANNEL 3, 400 TO 690-NM</b>	<b>86</b>
<b>FIGURE 7.7.) SPECTRAL QUALITY FOR MEDIUM SPOT SIZE FOV ON DAY 28 OF TEST 1 .....</b>	<b>89</b>
<b>FIGURE 7.8.) REFLECTANCE SPECTRA OF MEDIUM SPOT SIZE ON TEST DAY 32 OF TEST 1. A.) SPECTROMETER CHANNEL 1, 800 TO 1000-NM. B.) SPECTROMETER CHANNEL 2, 625 TO 865-NM. C.) SPECTROMETER CHANNEL 3, 400 TO 690-NM</b>	<b>90</b>
<b>FIGURE 7.9.) SPECTRAL QUALITY FOR MEDIUM SPOT SIZE FOV ON DAY 32 OF TEST 1 .....</b>	<b>93</b>
<b>FIGURE 7.10.) RAW DATA OF SPECTROMETER CHANNEL 1 FOR REFLECTANCE OF MEDIUM FOV ON DAY 32 OF TEST 1.....</b>	<b>94</b>
<b>FIGURE 7.11.) FLUORESCENCE SPECTRA OF MEDIUM SPOT SIZE ON TEST DAY 28 OF TEST 1. A.) SPECTROMETER CHANNEL 1, 800 TO 1000-NM. B.) SPECTROMETER CHANNEL 2, 625 TO 865-NM. C.) SPECTROMETER CHANNEL 3, 400 TO 690-NM.....</b>	<b>96</b>
<b>FIGURE 7.12.) FLUORESCENCE SPECTRA OF MEDIUM SPOT SIZE ON TEST DAY 32 OF TEST 1. A.) SPECTROMETER CHANNEL 1, 800 TO 1000-NM. B.) SPECTROMETER CHANNEL 2, 625 TO 865-NM. C.) SPECTROMETER CHANNEL 3, 400 TO 690-NM.....</b>	<b>99</b>
<b>FIGURE 8.1.) EFFECT OF NUTRIENT DEFICIENCY ON LETTUCE FRESH MASS .....</b>	<b>106</b>
<b>FIGURE 8.2.) NEURAL NETWORK RESULTS FOR A.) LARGE FIELD OF VIEW (FOV), B.) MEDIUM FIELD OF VIEW, AND C.) SMALL FIELD OF VIEW.....</b>	<b>111</b>

<b>FIGURE 8.3.) RESULTS OF NEURAL NETWORKS USING FLUORESCENCE SPECTRA AS INPUT VECTOR FOR A.) LARGE FIELD OF VIEW (FOV), B.) MEDIUM FIELD OF VIEW, AND C.) SMALL FIELD OF VIEW .....</b>	<b>114</b>
<b>FIGURE 8.4.) RESULTS OF NEURAL NETWORKS USING BOTH REFLECTANCE AND FLUORESCENCE SPECTRA AS INPUT VECTOR FOR A.) LARGE FIELD OF VIEW (FOV), B.) MEDIUM FIELD OF VIEW, AND C.) SMALL FIELD OF VIEW.....</b>	<b>117</b>
<b>FIGURE 8.5.) DIRECTION OF ROTATION FOR PLANT ANGLE EXPERIMENTS WITH RESPECT TO OPTICAL RECEIVER ZENITH AND LAMP ANGLED AT 45°. .....</b>	<b>127</b>
<b>FIGURE 8.6.) EFFECT OF LEAF ANGLE ON REFLECTANCE SPECTRA. A.) SPECTROMETER CHANNEL 1. B.) SPECTROMETER CHANNEL 2. C.) SPECTROMETER CHANNEL 3.....</b>	<b>128</b>
<b>FIGURE 8.7.) EFFECT OF LEAF ANGLE ON FLUORESCENCE SPECTRA. A.) SPECTROMETER CHANNEL 1. B.) SPECTROMETER CHANNEL 2. C.) SPECTROMETER CHANNEL 3.....</b>	<b>131</b>
<b>FIGURE 8.8.) SUMMARY OF NN VALIDATION RESULTS FOR CLASSIFICATION OF 5%N SPECIMENS AS A FUNCTION OF TEST DAY .....</b>	<b>139</b>

## LIST OF ABBREVIATIONS AND SYMBOLS

Quantity	Description
A:	Amps
A/D:	Analogue to Digital
ADALINE:	ADaptive LInear Element
ALS:	Advanced Life Support
ALSS:	Advanced Life Support System
ANN:	Artificial Neural Network
ATP:	Adenosine TriPhosphate
c:	centi (as a prefix $10^{-2}$ )
CCD:	Charged Couple Device
CI:	Certainty Index
COLORBLOCK	Low spectral resolution neural network, spectral input vectors consist of temporal parameter and five spectral bands: UV (370-399nm), blue (400-499nm), green (500-599nm), red (600-699nm), and NIR (700-1030nm)
CWF:	Cool White Fluorescent
DCMU:	3-(3-4-DiChlorophenyl)-1-1-Dimethyl Urea
ERTS	Earth Resources Technology Satellite
EOS:	Earth Observation System (Satellite)
Fe:	Illuminated chlorophyll fluorescence steady state intensity
Fo:	Dark level chlorophyll fluorescence intensity
Fp:	Illuminated chlorophyll fluorescence peak intensity
f/D ratio:	lens focal length to lens diameter ratio
FWHM:	Full Width Half Maximum
g:	gram
GOES:	Geostationary Operational Environmental Satellite
Hz:	Hertz
J:	Joule
K:	Kelvin
LANDSAT:	LAND SATellite
LIDAR:	Llght Detection And Ranging
LIF:	Laser Induced Fluorescence
m:	milli (as a prefix $10^{-3}$ )
m:	meter
n:	nano (as a prefix $10^{-9}$ )
NA:	Numerical Aperature
NADP <sup>+</sup> :	Nicotinamide Adenine Dinucleotide Phosphate (oxidized form)

<b>NADPH:</b>	<b>Nicotinamide Adenine Dinucleotide Phosphate (reduced form)</b>
<b>NASA:</b>	<b>National Aeronautics and Space Administration</b>
<b>NDVI:</b>	<b>Normalized Difference Vegetation Index</b>
<b>Nd-YAG:</b>	<b>Neodymium Yttrium Argon Garnet</b>
<b>NIR:</b>	<b>Near InfraRed</b>
<b>NN:</b>	<b>Neural Network</b>
<b>NOAA AVHRR:</b>	<b>National Oceanic and Atmospheric Administration's Advanced Very High Resolution Radiometer</b>
<b>p:</b>	<b>pico (as a prefix <math>10^{-12}</math>)</b>
<b>PAR:</b>	<b>Photosynthetically Active Radiation</b>
<b>PC:</b>	<b>Personal Computer</b>
<b>PSI:</b>	<b>PhotoSystem One</b>
<b>PSII:</b>	<b>PhotoSystem Two</b>
<b>pH:</b>	<b><math>-\log(a_{H^+})</math></b>
<b>PPFD</b>	<b>Photosynthetic Photon Flux Density</b>
<b><math>r^2</math>:</b>	<b>coefficient of determination (or) proportion of explained variation</b>
<b>s:</b>	<b>second</b>
<b>SPOT:</b>	<b>Système Pour l' Observation de la Terre (Satellite)</b>
<b>sr:</b>	<b>steradian</b>
<b>UV:</b>	<b>UltraViolet</b>
<b>W:</b>	<b>Watt</b>
<b>0.1-nm NN</b>	<b>Ultra high spectral resolution neural net trained using a temporal parameter and detailed spectrum (<math>\Delta\lambda\approx 0.1</math>-nm) from 370-nm to 1030-nm.</b>
<b>1-nm NN</b>	<b>High spectral resolution neural net trained using a temporal parameter and detailed spectrum (<math>\Delta\lambda\approx 1</math>-nm) from 370-nm to 1030-nm.</b>
<b>10-nm NN</b>	<b>Medium spectral resolution neural net trained using a temporal parameter and detailed spectrum (<math>\Delta\lambda\approx 10</math>-nm) from 370-nm to 1030-nm.</b>
<b><math>\mu</math>:</b>	<b>micro (as a prefix <math>10^{-6}</math>)</b>

## ACKNOWLEDGEMENTS

This research was made possible by a GSRP grant from NASA Office of Life and Microgravity Science. Additional funding and assistance was provided by The Pennsylvania State University Graduate College, the Department of Agricultural and Biological Engineering, and the Department of Electrical Engineering.

The author wishes to extend sincerest thanks to those who contributed to her doctoral program. Deepest appreciation to Professor C. R. Philbrick for his exceptional support during the course of this dissertation. Special thanks to Dr.'s Paul Heinemann, Simon Gilroy, and Eileen Wheeler for their much valued time and input. The author also wishes to acknowledge the assistance of: Alex Achey, Linda Becker, Ginnipal Chadha, Michael Connelly, Randall Bock, Steven Esposito, Guangkun (Homer) Li, Gioia Massa, Karoline Mulik, Ed Novitsky, Wanda Nyman, Gregory Omarr, Natalie Sharbaugh, Walter Gottlieb Mathias Schneider III, Paul Walker, and Roy Young. Finally, heart-felt thanks goes to my family and to those who lent their kindness and unwavering support during the more arduous phases of this endeavor.

# **Remote Sensing of Nutrient Deficiency in *Lactuca Sativa* Using Neural Networks for Terrestrial and Advanced Life Support Applications**

## **1. Introduction**

### **1.1 Project Justification**

The primary goal of this research was to develop a robust and automated technique for monitoring crop nutrient stress in controlled environments. Remote sensing of plant canopies with multiple leaves and random orientation was investigated using both reflectance and fluorescence spectra to detect nitrogen or phosphorous deficiencies in hydroponic *Lactuca sativa*, lettuce. Extended duration space travel or extraterrestrial colonization requires bioregeneration of all resources in order to minimize resupply from Earth and reduce system mass. The goal of NASA's Advanced Life Support (ALS) program is to provide life-support, self-sufficiency for human beings to carry out research and exploration productively in space for benefits on Earth and to open the door for planetary explorations (Rummel, et al. 1998). ALS utilizes higher plants to convert CO<sub>2</sub> to O<sub>2</sub>, recycle nutrients, filter water, and provide a vegetarian diet for the crew. Thus, plant condition with respect to growth, vigor, and stress levels must be monitored continuously to ensure stability of the regenerative biological system. Physiological plant stresses

resulting in degraded system performance or failure include: nutrient imbalances, drought, anaerobic root zone, phytotoxin accumulation, pathogen attack, extreme temperatures, and otherwise inadequate environmental conditions. Since astronauts have only limited time for monitoring vegetative canopy health, this task must be partially to fully automated. Computer-driven remote sensing is a logical and potentially effective solution.

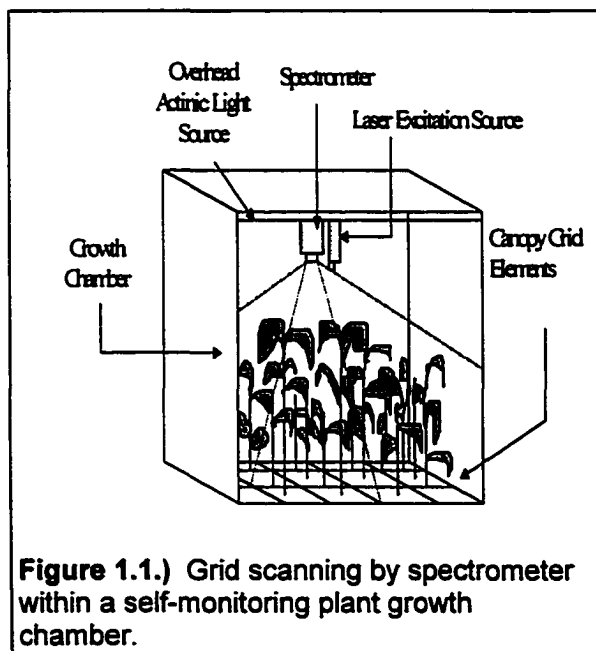
In addition to ALSS applications, remote detection of plant status has significant terrestrial application as well. Satellite observations of bulk canopy cover on Earth provides valuable information on vegetative health, abundance, and dynamics on a global scale. Aerial remote sensing from planes and other airborne platforms provide local environmental data on field and forest conditions. Remote sensing techniques are also of considerable economic and academic value when incorporated into biological monitoring systems for greenhouses, growth chambers, and other research facilities.

## **1.2 System Summary**

The traditional laboratory technique for active remote sensing as a vegetational assay is to mechanically secure a single excised leaf in the horizontal plane coinciding with a non-fluorescent sample plate and to monitor resultant fluorescent emission from a very small,  $<1\text{-cm}^2$ , segment of the adaxial target. This technique is not only labor intensive but also may not sufficiently represent the entire *in situ* plant canopy status as seemingly



random and localized variations are common attributes of biological materials. In order to negate complications from this inherent variability it was desirable to monitor vegetative status on a canopy level rather than point source. Target spot size at canopy level is a necessary design specification for the fabrication of a self-monitoring growth chamber as conceptualized in *Figure 1.1*. The research described herein monitored reflectance and fluorescence from 177-cm<sup>2</sup>, 44-cm<sup>2</sup>, and 11-cm<sup>2</sup> canopy spot sizes to assess effects of sampling area on the accuracy of nutrient stress predictions.



## **2. Light Interaction with Leaves**

### **2.1 Reflectance**

When an electromagnetic wave is incident on an interface between two materials, some of the energy is reflected in the specular direction, some is scattered in all directions of the incident medium (diffuse scattering), and some of it is transmitted through the interface (Elachi, 1987). In recent years, many theoretical and experimental investigations of vegetation, environment variables, and the resulting spectral reflectance have been undertaken. On the theoretical side, one type of study has been the modeling of crop canopy reflectance (Jacquemoud et al., 1995; Kuusk, 1994; Sellers et al., 1992; Goel and Strebel, 1983; Goel, 1982; Kimes and Kirchner, 1982; Smith, 1982; Suits, 1972). In this case one defines, or derives, an algorithm to predict reflectance given specific variables describing the canopy. These variables generally include: optical properties of the vegetation components, e.g., wavelength dependent reflectance and transmittance of leaves, stalks, heads, etc.; physical parameters defining the canopy geometry, e.g., density, angular inclination, and distribution of vegetation components; variables defining the soil, e. g., wavelength dependent reflectance; variables defining source of radiation and the properties of the detector, e.g., sun zenith angle, detector zenith and azimuth angles (Goel and Strebel, 1983). On the experimental side, an extensive amount of data has been collected on the reflectance as a

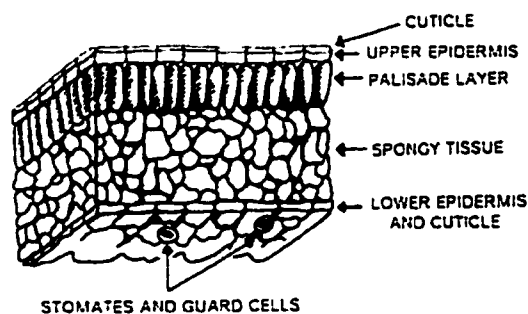
function of the canopy variables for crops like corn, soybeans, and wheat, for different growth stages and cultural practices (Wiegand et al., 1992; Neu et al., 1990; Biehl et al., 1982).

Vegetation reflects light quasi-spectrally, where scattered radiation is enhanced at angles near the angle of incidence, as well as diffuse scattering of light in all directions. The contribution of the specular component of leaf reflectance can be described using the Fresnel law and results primarily from the presence of the waxy leaf cuticle (Ross and Marshak, 1988). Light scattering by the leaf surface can best be described as a pseudo-Lambertian distribution.

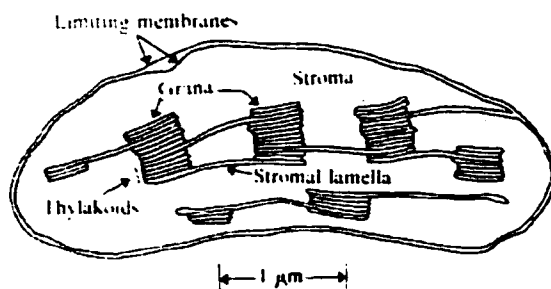
The mechanism of pseudo-Lambertian reflectance is the interaction of electromagnetic radiation with the chemical constituents along the leaf surface and within the leaf cells. Visible light interacts primarily with the chlorophyll in cells along the leaf surface while infrared interacts with air pockets inside cells. Chlorophyll absorbs with visible light and is the primary plant photopigment housed in granum (stacks of thylakoids), within the chloroplasts of palisade and spongy mesophyll cells (*Figure 2.1*). There are about half a million chloroplasts per  $\text{mm}^2$  in the palisade mesophyll layer of a leaf surface (Campbell, 1990) which is the layer of primary interaction for visible wavelengths, (*Figure 2.2*). The architecture and composition of a leaf determine how far light penetrates into the surface layer of a leaf.

Conversely, plant type and light environment are two of the factors that

determine leaf architecture and composition, for example an electron micrograph of leaves taken from the same tree show that the palisade cells of leaves grown in higher sunlight are 10 to 25- $\mu\text{m}$  longer (Taiz and Zeigler, 1991). The spongy parenchyma cells then absorb as much of the light energy as possible that goes through the first layer of palisade cells because of sieve and light guide effects.



a.)



b.)

**Figure 2.1. a.) Leaf anatomy, idealized leaf cross (Campbell 1996), and b.) generalized chloroplast in cross section; the chloroplasts make up the light absorbing material of the palisade and spongy leaf layers (Nobel, 1991).**

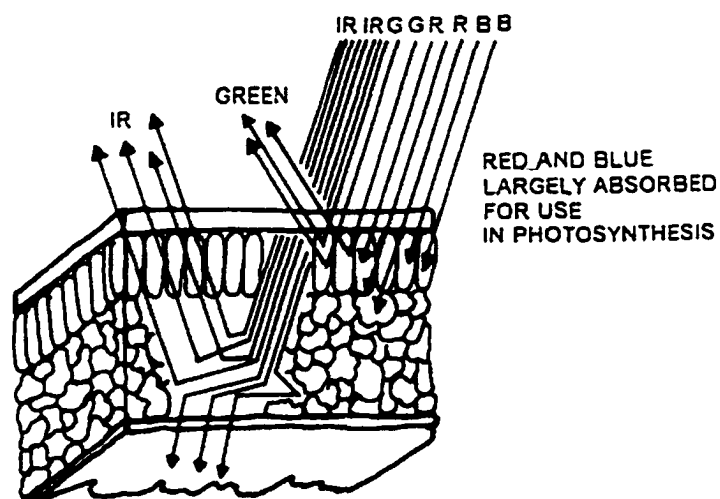


**Figure 2.2.)** Blue, green, red, and infrared light interacting with a generalized leaf cross section (Campbell, 1996).

---

Plant photopigments include chlorophyll-a, chlorophyll-b, and carotenoids. Chlorophyll-a molecules absorption maximum occurs near 670-nm and chlorophyll-b molecules absorb maximally at 650-nm (Taiz and Zeigler, 1991). Both chlorophyll molecules also have blue band absorption components near 440-nm, known as the Soret band (Nobel, 1991). The chlorophylls appear green to the human eye because green wavelengths are absorbed less readily than blue and red so more green wavelengths are scattered back to the eye. Chlorophyll-a is grass green in appearance while chlorophyll-b is yellow green as a wider range of wavelengths in the 500 to

600-nm region are scattered (*Figure 2.2*). Non-green photopigments include carotenes and xanthophylls which are carotenoids and anthocyanin, a plant pigment responsible for the wide assortment of flower coloration. The carotenoids act as both accessory pigments and photoprotective agents. As accessory pigments, carotenoids absorb in the 400 to 500-nm region giving them a characteristic orange coloration. Anthocyanin absorbs primarily in the 400-600 nm region and typically appears red. During the spring and summer seasons, the chlorophylls become the dominant photopigment in plants causing them to appear green to the human eye. In the Fall seasons, it is the carotenoids outliving the chlorophylls during organized leaf senescence that creates the glorious yellow-golden-red palette of autumn foliage.

Visible light is absorbed and scattered primarily by chlorophyll rich palisade mesophyll cells, while infrared rays interact mainly with air pockets among spongy mesophyll cells. When leaves are young or wilted from drought stress, there is less air between spongy mesophyll and less infrared scattered.

*Figure 2.3* shows the spectral reflectance characteristics of plants again illustrating the preferential red and blue absorption of chlorophyll. Reflectance, due to scattering, also notably increases at NIR wavelengths between 0.7- $\mu\text{m}$  and 1.3- $\mu\text{m}$  demonstrating the effect of air content in the biological cell structure. Absorption features in the scattered light spectrum in the 1.4- $\mu\text{m}$  to 2.6- $\mu\text{m}$  region is mainly attributed to water absorption. Spectral

reflectance varies between plant species, as a function of growth cycle, and in response to plant stresses.

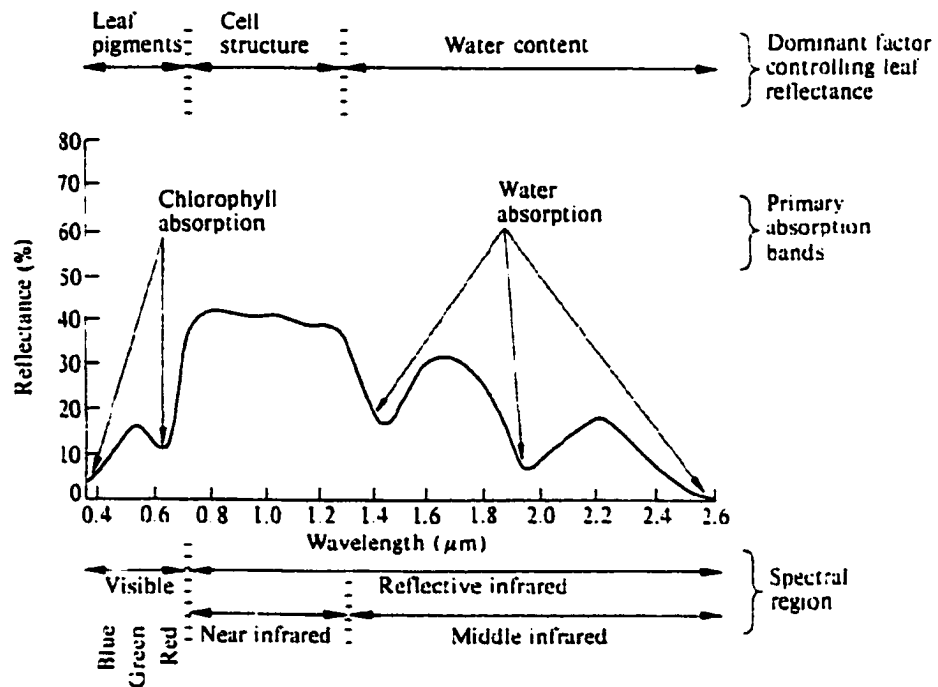


**Figure 2.3.)** Idealized spectral reflectance curve for vegetation (<http://pirlwww.lpl.arizona.edu/Biosphere/Eco/plantspex2.gif>).

## **2.2 Fluorescence**

Electrons of an atom or molecule can only occupy specific quantized orbits with specific energy levels or electronic states (Elachi, 1987). Fluorescence is the radiative decay of excited electronic states within molecules. Fluorescent emission is almost always at a lower frequency and longer wavelength than the exciting radiation. This is due to radiational loss as some of the energy is transmitted by vibrational modes and other processes to surrounding molecules. As energy is lost from a molecule, the excited molecule progresses downwards through a combination of radiating and radiationless transitions associated with each electronic state. At the lowest vibrational level of the particular electronic state, an excited molecule is often unable to impart to its neighbors the extra energy required to fully drop down to the next state. The excess energy may be given off by the excited molecule as a photon of light. The rare and frequently overlooked exception to this process is resonance fluorescence where emitted radiation has the same frequency as incident radiation. Resonant fluorescence is an uncommon mechanism for radiative decay however, because interactions between an excited molecule and surrounding molecules are usually quite prevalent.

Visible light photons absorbed by canopy leaves may be captured by plant photopigments, in the photosynthetic pathway, or re-emitted as fluorescence or heat. Plant fluorescence is very closely associated with the



photosynthetic pathway. Photosynthesis, the manner plants convert carbon dioxide and water into glucose and oxygen, takes place in the chloroplasts and is summarized by the following equation:



Chloroplasts house structures called thylakoids which have vital functions in initial photosynthetic processes. Chlorophyll-*a*, chlorophyll-*b*, and carotenoids reside within the thylakoid membranes. These photopigments function collectively as light gathering antennas absorbing photons and relaying them to the reaction center where chlorophyll-*a* reduces the primary electron acceptor. The primary electron acceptor is the first component in a complex series of redox reactions generating the necessary negative and positive charge gradients within the cell to convert light energy into chemical energy. The light energy absorbed by the reaction center drives photosynthetic electron transport through the two light harvesting units of the thylakoid membrane, PhotoSystem II (PSII) and PhotoSystem I (PSI), leading to the oxidation of water, oxygen evolution, the reduction of NADP<sup>+</sup> to NADPH, membrane proton transport and eventually to Adenosine TriPhosphate (ATP) synthesis. Steps using this chemical energy to convert carbon dioxide to sugar occur in the stroma, the dense fluid filling the chloroplasts (*Figure 2.1*). The interaction of electromagnetic radiation with chlorophyll, carotenoids,

other accessory pigments, stroma, and water determines the nature of fluorescence spectra emission.

N. J. C. Muller (1874) was the first to observe chlorophyll fluorescence by visually using colored glass filters. He also correctly observed that fluorescence changes occurring in green leaves are correlated with photosynthetic assimilation.

Absorbed photon energy is converted to the potential energy of electrons in photopigments raised from their ground states to excited states, and small percentage of absorbed photon energy is also lost in the form of heat and/or fluorescence. In an optimally functioning green leaf at relatively low light levels, the distribution of absorbed quanta can be observed as follows: 84% photosynthesis, 14% heat, 2% fluorescence; however, if the photosynthesis reaction is hampered due to adverse environmental conditions such as reduced light, drought stress, reduced CO<sub>2</sub>, nutrient stresses, etc. then more energy is lost to heat and fluorescence emission (Rosema, et al., 1992). These values for loss represent minimum fluorescent quantum efficiency that would be expected. Thus, fluorescent emission can be exploited as a pre-visual remote sensing method to detect photosynthetic activity in plants and also used to detect physiological stress.

### **3. Remote Sensing Review**

Optical remote sensing is a nondestructive analytic procedure where the interaction of a material with electromagnetic radiation is detected and processed in order to determine specific characteristics of a target. The term "remote sensing" in its broadest sense merely means "reconnaissance at a distance" (Colwell, 1966). Scientific objectives that may be obtained using remote sensing methods include: automated nondestructive *in situ* testing of materials on a micro or macro-scale; rapid surveying of large areas; and inspecting objects at a considerable distance. One class of remote sensing activity derives information about the Earth's land and water surfaces using images acquired from an overhead perspective in one or more regions of the electromagnetic spectrum, as the radiation is reflected or emitted from the Earth's surface (Campbell, 1996). Hence, remote sensing is a technique enabling detection and monitoring of plants on an individual or community basis.

Instruments used for remote sensing are classified as either passive or active systems. Passive systems rely on sunlight as the primary excitation source and gather reflectance spectra as the primary signal. Active systems use a laser or another type of light source to induce reflectance and/or fluorescence.

In both optical techniques, spatial and spectral resolutions play critical roles in determining quality and quantity of the resultant data. Conventional spectrometers collect a single spectral curve representing an extended surface area and present it as raw numbers or graph form. However, spectral imagers may incorporate focal plane arrays of photon or thermal detectors or individual quantum detectors (Hardin, 1997). The number of wavelength bands that are imaged can be as few as one (spectral), multiple (multispectral), or as many as several hundred (hyperspectral). Once key bands have been identified for a particular crop or plant community, it is then possible to use spectral, multispectral, or hyperspectral scanning to study only these key bands in order to reduce the total quantity of data generated and stored.

### ***3.1 History of Remote Sensing***

Galileo was perhaps the founding father of remote sensing with his invention of the telescope in 1609, and his subsequent controversial discoveries. Galileo made very careful observations and measurements using his telescopes. He recorded these findings in detailed descriptions and drawings in his journals. This was possibly the most advanced method of remote sensing and recording for the next 200 years.

The first attempts to form images by photography date from the early 1800's. The first photograph was taken by Joseph Nicephore Niepce of his

French estate courtyard in 1827 (Estes, 1999). The exposure lasted eight hours and used an emulsion of Bitumen of Judea (Estes, 1999). The use of photography to record an aerial view of the Earth's surface from a balloon dates from 1858 (Campbell, 1996). In 1859 Gaspard Felix Tournachon, also known as Nadar, was a famous French photographer and balloonist who carried his bulky cameras aloft to make land surveys from aerial photographs (NASA's Observatorium, 1998). In April 1861 Professor Thaddeus Lowe, went up in a balloon near Cincinnati, Ohio, to make a weather observation. Unfortunately, strong winds carried him all the way to South Carolina, where he was arrested as a Union spy. Eventually released, he believed that tethered balloons could be useful for reconnaissance. After viewing a demonstration, President Lincoln agreed and authorized the US Army Balloon Corps, with Lowe in charge. Despite its advantage to the North during the American Civil War, the unit was deactivated in 1863 as the balloons had a not-surprising tendency to draw enemy fire (NASA's Observatorium, 1998).

The illustrious Bavarian pigeon corps was established in 1903 in an innovative attempt to avoid the dangers associated with balloons. The concept was very straightforward in that a light camera was simply attached to a carrier pigeon. These cameras took a picture every thirty seconds as the pigeon winged its way along an often uncertain course to its home shelter (NASA's Observatorium, 1998).

On December 17, 1903, Wilbur Wright piloted the first motor driven, heavier than air aircraft flight at Kitty Hawk, NC. The machine took off under its own power on level terrain, sustained controlled flight for a short period, then landed at a point at the same height at which it had started (Spick, 1994). This event marked the beginning of "modern" aerial photography and photogrammetry. In 1909, Wilbur Wright piloted the plane that acquired motion pictures of the Italian landscape near Centocelli, said to be the first aerial photographs taken from an airplane (Campbell, 1996).

World War I (1914-1918) marked the beginning of the acquisition of aerial photography on a routine basis (Campbell, 1996). The 1920's marked the development of instruments specifically designed to capture and analyze aerial photographs. During World War II (1939-1945), the use of the electromagnetic spectrum was extended from the visible to also include the infrared and microwave regions (Campbell, 1996). One of the most significant developments in the civilian sphere during this time was the work of Robert Colwell (1956) who used color infrared film and aerial photography to identify small grain cereal crops and their diseases.

The first meteorological satellite, TIROS-1, was launched in 1960 (Campbell, 1996). Although Schawlow and Townes (1958) and Maiman (1960) deserve recognition for their roles in creating the first laser, it was the giant-pulse technique, invented by McClung and Hellwarth (1962) that made remote optical probing really attractive (Measures, 1992). The first studies of

the atmosphere were undertaken by Fiocco and Smullin (1963), who recorded laser echoes from the upper regions of the atmosphere, and by Ligda (1963) who probed the troposphere (Measures, 1992).

In 1968 Apollo 8 returned the first pictures of the Earth from deep space. Images from the Apollo 9 multispectral four-lens camera were digitized and used to develop techniques for processing Landsat data (NASA's Observatorium, 1998).

In late July 1972 NASA launched the first Earth Resources Technology Satellite (ERTS-1). The multispectral data provided by the on-board sensors led to an improved understanding of crops, minerals, soils, urban growth, and many other Earth features and processes. The name of the satellite, and those that followed, was soon changed to a more pleasant-sounding Landsat. Landsats 2 through 7 have provided more data about the Earth than can ever be analyzed (NASA's Observatorium, 1998).

In the 1980's, scientists at NASA's Jet Propulsion Laboratory began to develop instruments that could create images of the Earth at unprecedented levels of detail. These instruments created the field of hyperspectral remote sensing which in the 1990's continued rapid development. Hyperspectral remote sensing forms the basis for a more thorough understanding of how to best apply more conventional remote sensing capabilities (Campbell, 1996). Table 3.1 summarizes some of the important milestones in the history of remote sensing.

---

 Table 3.1.) Milestones in the history of remote sensing
 

---

<b>Date</b>	<b>Occurrence</b>
1609	Galileo invents the telescope
1827	Beginning of practice of photography
1850-1860	Photography from balloons
1862	US Army establishes a balloon corps for photographic reconnaissance
1873	Theory of electromagnetic energy developed by James C. Maxwell
1909	Photography from airplanes
1910-1920	World War I: aerial reconnaissance
1920-1930	Developmental and initial applications of aerial photography and photogrammetry
1930-1940	Development of radar in Germany, United States, and United Kingdom
1940-1950	World War II: applications of nonvisible portions of electromagnetic spectrum
1950-1960	Military research and development
1956	Colwell's research on cereal crop disease detection with infrared photography
1960-1970	First use of term "remote sensing" TIROS weather satellite Skylab remote sensing observations from space
1962	McClung and Hellwarth invent the giant-pulse technique for laser remote sensing
1963	First laser studies of the atmosphere
1968	Apollo 8 acquires first pictures of Earth from space
1972	Launch of Landsat I
1970-1980	Rapid advances in digital image processing
1986	(SPOT) French Earth Observation Satellite
1990's	Development of hyperspectral sensors

---



### **3.2 *Passive Remote Sensing***

Many of Earth's surface features can be identified, mapped, and studied on the basis of their spectral characteristics. The thickness and texture of the waxy cuticle leaf covering characterizes spectral reflectance of plants. The green color of vegetation arises from the rapid rise in the relative absorption of blue and red wavelengths that results in more scattering in the green portion of the spectrum. Absorption is also quite pronounced in the near infrared region. The presence of chlorophyll in vegetative material leads to strong absorption at wavelengths shorter than 700-nm (up to approximately 400-nm) (Stephens, 1994). Plant material can be easily distinguished from inert substances by comparing the magnitudes of their visible versus NIR reflection. Vegetation has relatively high NIR reflectance while clouds, water, snow and soil all have higher visible reflectance than NIR. This difference can be calculated to determine total vegetation per unit area for specific locations. Differences in NIR reflectance and green reflectance intensity are also useful for detecting generic vegetation stresses, e.g. high, medium, low levels of stress, and for categorizing plant type, e.g. distinguishing between broad leaf and needle bearing trees.

Reflectance data from satellites, e.g. EOS, LANDSAT, SPOT, NOAA AVHRR (NVHRR), and GOES, have been used to calculate normalized vegetation indices using the following equation:

$$NDVI = \frac{NIR - RED}{NIR + RED}$$

where:        NDVI = Normalized Difference Vegetation Index  
                  NIR = Near Infrared wave band, e.g. NVHRR Ch.2  
                  RED = Red visible wave band, e.g. NVHRR Ch.1

Vegetation generally yields high positive NDVI while inanimate objects have near zero or negative NDVI values. The National Oceanic and Atmospheric Administration's (NOAA's) Advanced Very High Resolution Radiometer (AVHRR) has been used extensively for this purpose (Hixon, et al., 1980; Lillesand and Kiefer, 1987). AVHRR vegetation indices are used operationally by NOAA to assess global climate effects on vegetation and crop. Typically, the spectral bands used for this purpose have been the channel 1 visible band, 580 to 680 nm, and the channel 2 near-infrared band, 730 to 1100 nm (Lillesand and Kiefer, 1987). Other key bands for discerning information about plants include: 550-nm (chlorophyll density), 690 to 740 nm with 5 to 10 nm spectral resolution (plant stress), and 800 to 1200 nm (water stress index) (Hardin, 1997). This stress correlation to specific wavelengths is similar to but not the same as that shown in Figure 2.3 demonstrating the novelty and spectral variability associated with this area of research.

### **3.3 Active Remote Sensing**

Chlorophyll fluorescence studies were initially conducted in plant physiology laboratories to estimate photosynthetic efficiency for near range, point measurements on individual leaves oriented normal to the incident light source *via* holding plate and clamps. Over the last 15 years, three different laboratory methods for evaluating fluorescence were developed: 1.) time resolved measurements of induction kinetics in the  $\mu\text{s}$  to s domain for predarkened plants, 2.) measurements of the lifetime of the fluorescence in the ps to ns domain, and 3.) spectral resolved measurements of the fluorescence emission bands (Gunther, 1990).

The first laboratory measurement involving chlorophyll fluorescence kinetics as an indicator of higher plant photosynthetic status was discovered in 1931 (Kautsky and Hirsch, 1931). The fluorescence curve they observed over a single wavelength ( $\approx 690\text{-nm}$ ), initial peak, and sequential dampening of fluorescence is generally referred to as the fluorescence induction curve, Kautsky curve, or Kautsky-effect (*Figure 3.1*).

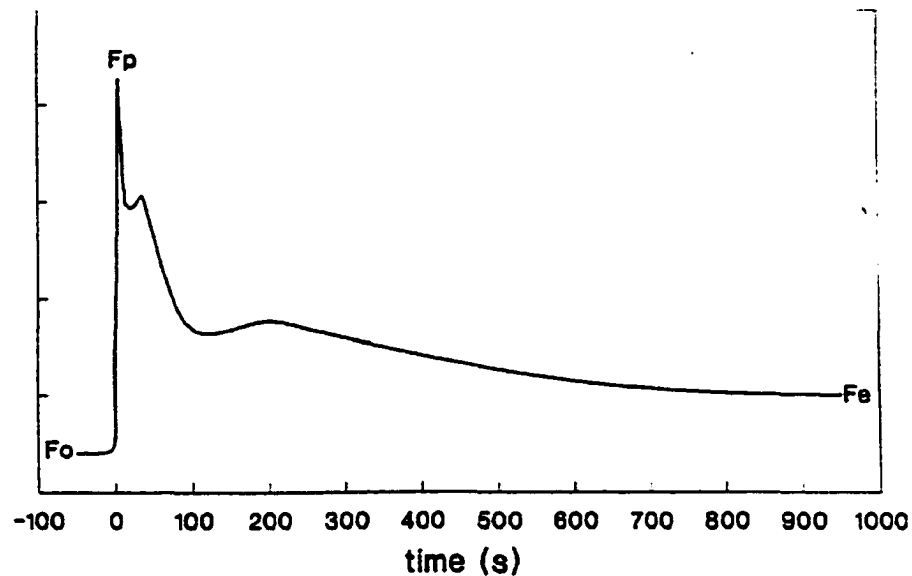


**Figure 3.1.)** The fluorescence induction or Kautsky curve where fluorescence is measured in relative intensity. (Rosema, et al., 1992).

---

$F_0$  represents the dark level of fluorescence relating to total chlorophyll content in the leaf. This is the fluorescence occurring when a dark-adapted leaf is suddenly illuminated by a high intensity light source. The light source is generally pulsed, e.g. 10 to 20-ns pulses, to enhance sensitivity of the receiver. After illumination, chlorophyll fluorescence rapidly increases to a maximum,  $F_p$ . This positive gradient is shaped by the primary electron acceptor changing from an oxidized to reduced state. The subsequent decrease from maximum to steady state indicates the ability of the regulatory

mechanism to adapt to a high light environment; in other words, it demonstrates how quickly photosystems come “online” and become fully functional. The steady-state emission,  $F_s$ , is representative of the actinic light intensity and the physiological status of the entire plant photosynthetic system. If the plant is subject to stress, or the photosynthetic process is in some way hindered, then the fluorescence peak,  $F_p$ , decreases and the steady-state emission,  $F_s$ , increases. The shape of the chlorophyll fluorescence induction curve is influenced by any factor that affects photosynthetic metabolism. Measures of chlorophyll fluorescence provide unique insights into the study of environmental effects on the thylakoid membrane system and can provide information on stress damage to the photosynthetic apparatus.

In general, fluorescence emission is not only characterized by the spectral shape but also by the decay time or lifetime of the excited state. The second laboratory technique is related to measurements of fluorescence lifetime in the ps to ns domain. It is similar to the Kautsky curve method, but makes use of lasers and is in a faster time domain. Using extremely short laser pulses as excitation light source (ps pulse width), it is possible to measure the fluorescence decay kinetics under laboratory conditions. Typical lifetimes are in the order of 50-2500 ps according to the state of the primary electron acceptor (Gunther, 1990). When the photosystem is dark-adapted, at least three exponential components are required to describe the

fluorescence decay. For chloroplasts and algae the lifetime of the very fast component is in the range of 80-130 ps, 300-600 ps for the middle component, and 1200-2500 ps for the long-lived component (Molzwarth, 1986). Thus, fluorescence lifetime is proportional to fluorescence quantum efficiency and describes quantum efficiency for photosynthesis which is useful for depicting plant type and vigor.

The third technique, fluorescence emission spectroscopy or laser induced fluorescence (LIF), detects the 1-3% of the absorbed energy that is emitted by the photopigments as characteristic fluorescence radiation. An active system for the excitation of chlorophyll fluorescence by LIF was first described by Hickman and Moore in 1970 for algae. In 1978 Brach *et al* were the first to use LIF on higher plants (Brach, et al., 1978a; Brach, et al., 1978b). Additional pioneering work improving this method and specific application was conducted by Emmett W. Chappelle; NASA Goddard and James E. McMurtrey III; USDA FCL (Chappelle, et al., 1984a; Chappelle, et al., 1984b; Chappelle, et al., 1985; Chappelle and Williams, 1987; Chappelle, et al., 1991; Chappelle, et al., 1992; McMurtrey, et al., 1994; Corp, et al., 1997).

Photosynthesis is dependent upon resonance fluorescence for the transfer of radiant energy absorbed by the accessory pigments to the primary photopigment, chlorophyll-a (Chappelle and Williams, 1987). The resonance fluorescence detected by LIF may be equated to the steady state

fluorescence,  $F_e$ , as described in the Kautsky curve. However, LIF, generally utilizes multiband spectra whereas Kautsky curves tend to be based on single waveband fluorescence (e.g. 690-nm). Multiband spectra would provide the additional information required for the development of algorithms needed for the correlation of fluorescence measurements with the physiological manifestations of specific environmental changes (Chappelle and Williams, 1987). *Figures 3.2a* and *3.2b* show multiband spectra data for various photopigments and for different plant types. The excitation source was a pulsed nitrogen laser, 337-nm, run at 30-Hz with average power output of 9-mJ. LIF spectra have been used to successfully differentiate among plant types, (*Figure 3.2b*) as well as to quantify specific environmental stresses exhibited in plant leaves. This will be demonstrated later in *Figure 4.4*.

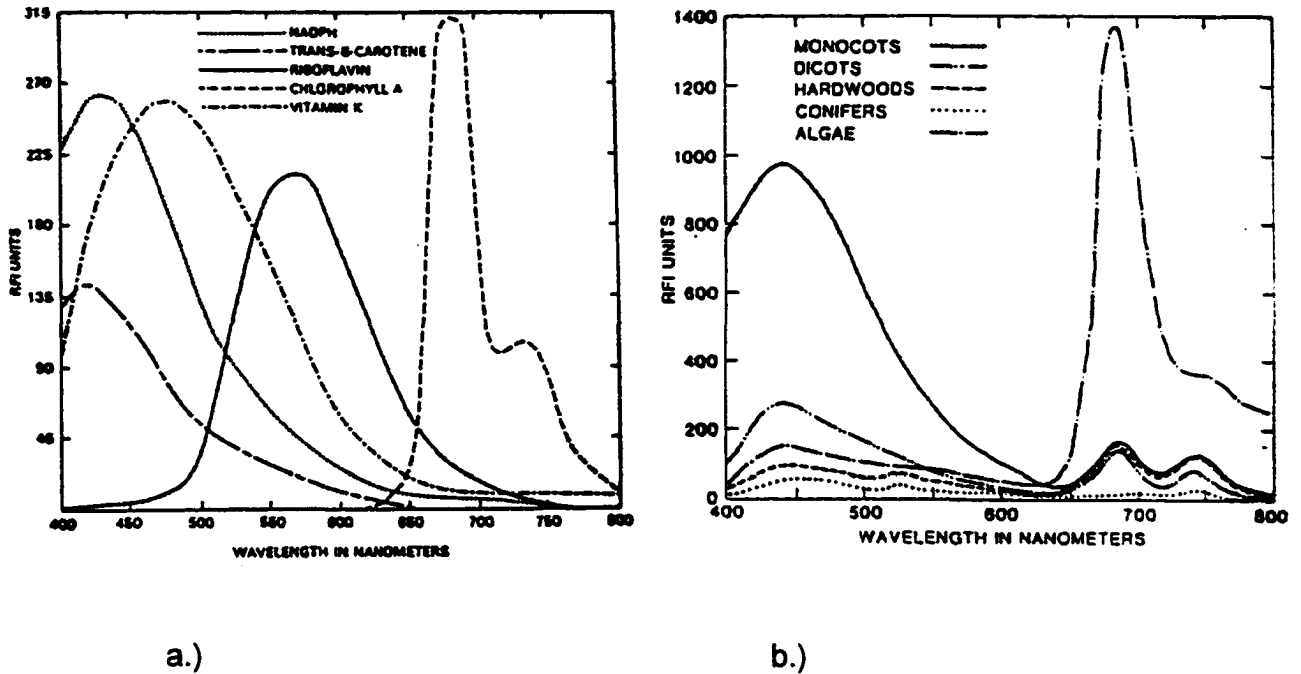


**Figure 3.2.** a.) LIF spectra of purified plant pigments. b.) LIF spectra of plant types (Chappelle and Williams, © 1987 IEEE).

Active field remote sensing of plants is defined here as using a laser as the emission source, a telescope to collect the fluorescent signal sent back from the target and a spectrometer for qualitative analysis or filter wheel and photon counter or diode for quantitative analysis. The hardware is mounted on mobile platforms such as planes or terrain vehicles to scan fields, trees, and forests. In this context, the method is most frequently referred to as Light Detection and Ranging (Lidar). Lidar systems used so far for biomass studies



are installed in aircraft where the nadir directed beam can be used to scan the plant matter at or near the surface. Hickman and Moore (1970) first suggested on the basis of laboratory studies that chlorophyll measurements with a sensitivity of better than  $10\text{-mg m}^{-3}$  were possible using an airborne pulsed neon laser from an altitude of 100-m. An improved system, incorporating a 250-mJ, 300-ns dye laser, was shown by Kim (1973) to be capable of detecting chlorophyll-a concentrations to a fraction of a  $\text{mg m}^{-3}$ .

Lidar systems are also often used on terrestrial platforms, usually a truck or van, to collect field measurements of plants. The variable leaf orientation and shadowing have been reported as the most common problems associated with using lidar for field measurements of plant life. Competitive absorption and fluorescence by other organic material has also been reported as problematic (Measures, 1992).

## **4. Hardware for Data Collection**

### ***4.1 Excitation Light Source***

Active remote sensing systems require light sources for excitation. Lasers and other high intensity UV light sources are used for active fluorescence studies. A 1987 laser excitation source optimization study by Chappelle and Williams supported the theory that UV wavelengths are the best, by enlisting a comprehensive comparison of excitation wavelengths. Chappelle and Williams (1987) evaluated the performance of excitation

source wavelengths ranging from 337 to 700-nm used to induce fluorescence from a soybean leaf. Fluorescent bands peaking at 440-nm, 685-nm, and 740-nm were deemed the to be the most useful in determining plant stress and were maximized in intensity with a nitrogen laser, 337-nm excitation source (at 30-Hz, 9-mJ, 10-ns pulses) compared to pumped tunable dye laser beams: BPBD, 357 to 395-nm; PBBO, 391 to 411-nm; coumarin 440, 417 to 473-nm; coumarin 540A, 515 to 583-nm, rhodamine B, 594 to 683-nm; Nile blue 690, 683 to 710nm. *Figure 4.1* depicts the 1987 Chappelle and Williams experimental set-up for LIF of a plant leaf.

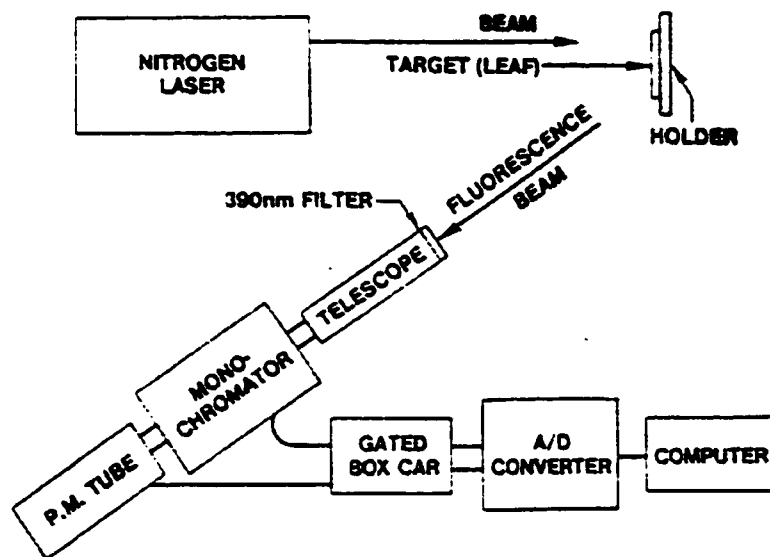


**Figure 4.1)** Laboratory configuration of Chappelle and Williams (© 1987 IEEE) LIF experiments.

In 1991, Schmuck, *et al.* used a Nd-YAG laser (355-nm with 35-ps pulses) to induce fluorescence from tobacco leaves at an optical path length of 26-m. The spot size diameter was 3-mm on a single leaf and the excitation energy was estimated at  $1 \times 10^{14}$  to  $5 \times 10^{14}$  photons per  $\text{cm}^2$ . In 1991, Chappelle *et al.* again made use of a nitrogen laser (337-nm at 30-Hz, 9-mJ, with 10-ns pulses) to induce fluorescence from plant extracts and intact clover at an optical path length of 1-m. In 1992, Mirkamkov *et al.* used a nitrogen (UV) laser to stimulate fluorescence from cotton. In 1992, Rosema *et al.* used a Xenon-chloride excimer laser (308-nm at 80-mJ, with 15-ns pulses) and a dye laser operating at 480-nm. In 1994, Gunther *et al.* used a Nd-YAG laser (355-nm) with a 30-m optical path length to induce fluorescence from an ensemble of leaves in an oak tree. The 30-cm spot size diameter at target was achieved by using a beam expander with divergence of 10-mrad and total laser energy was 35-mJ.

In 1994, Cecchi *et al.* used an excimer laser with XeCl gas mix (308-nm, 80-mJ) and a dye laser (480-nm, 7-mJ). In 1994, Krajicek and Vrbova used a XeCl (308-nm, 50-Hz, 80-mJ, 15-ns pulses) to induce fluorescence from common European plants. The non-lambertian spectral brightness was on the order of  $0.01 \text{ W m}^{-2} \text{ sr}^{-1} \text{ nm}^{-1}$  at 740-nm. In 1994, Subhash and Mohanan used a HeNe laser (632.8-nm, 2-mW) to study red chlorophyll fluorescence in rice. In 1994, Bonji *et al.* used a nitrogen laser (337-nm, 20-

Hz, 30- $\mu$ J per pulse with 3-ns pulses) to induce fluorescence from cut plant samples in petri dishes. In 1994, Stober *et al.* used a pulsed nitrogen laser (377-nm, 10-Hz, 2.5-mJ with 10-ns pulses) to induce fluorescence in wheat, soybean, and tobacco. The integration time of the gateable detector was 100-ms per single scan with a gating time of 160-ns. In 1997, Corp *et al.* used a 280-nm excitation source to induce a UV fluorescence band in soybean in addition to blue and red fluorescent bands. In 1998, Saito *et al.* used a pulsed Nd:YAG laser (355-nm, 7-Hz, 0.2-mJ with 10-ns pulses) to induce fluorescence in excised leaves from seven types of trees. *Figure 4.2* depicts the 1998 Saito *et al.* experimental set-up for laser induced fluorescence of a plant leaf. In this configuration, the filter location after the right angle mirror eliminated residual light at 532-nm from the 3<sup>rd</sup> harmonic crystal. The filter in front of the fiber optic eliminated scattered laser radiation of 355-nm from the leaf sample surface.

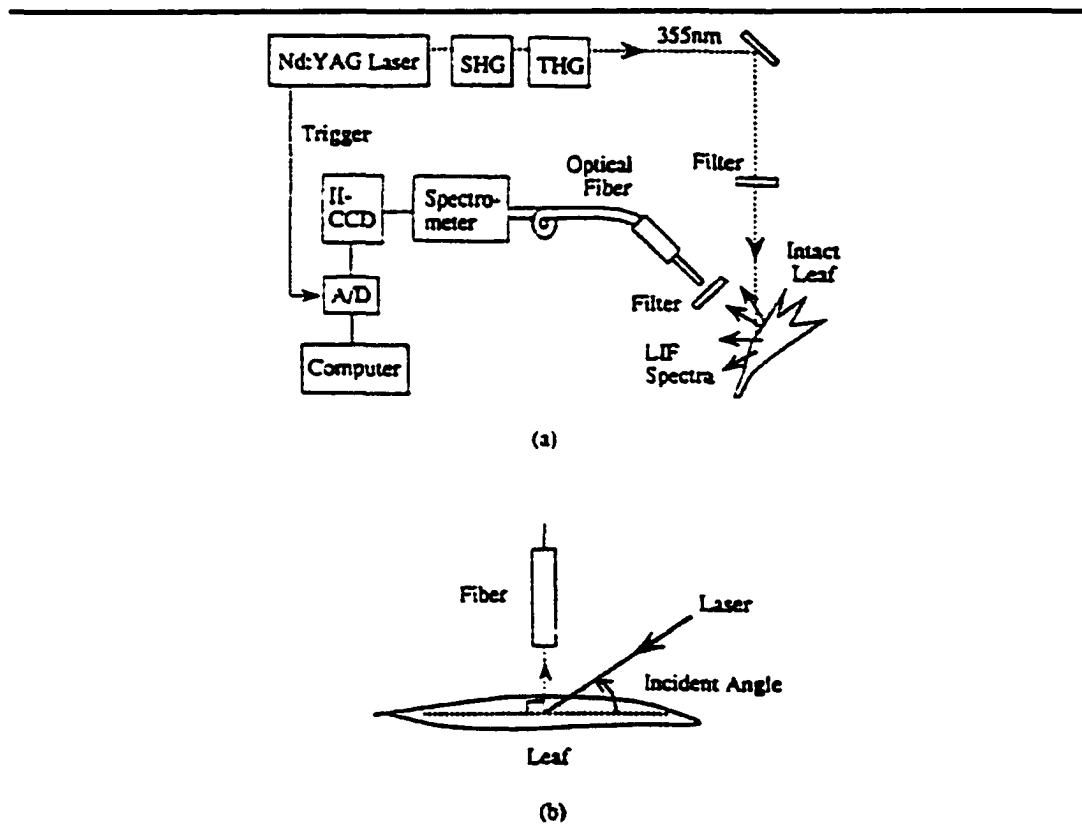


**Figure 4.2)** Laboratory configuration for Saito et al. (1998) LIF experiments. **a)** experimental setup and **b)** configuration of leaf, laser beam, and fiber.

#### 4.2 Instrumentation for Optical Spectroscopy

Spectrometers are monochromators with a fixed slit in the focal plane (Skoog and Leary, 1992). Monochromators are designed for spectral scanning; that is, they are designed to vary radiation wavelength over a considerable range. Monochromators for ultraviolet, visible, and infrared radiation are all similar in mechanical construction in the sense that they

employ slits, lenses, mirrors, windows, and gratings or prisms (Skoog and Leary, 1992). Gratings and prisms are the two types of dispersing elements generally found in monochromators. Historically, most monochromators were nonlinear prism instruments dispersing shorter wavelengths to a greater degree than longer ones. Presently most all commercial monochromators are based upon reflection gratings that disperse radiation linearly. The spectrometer used in this study (Ocean Optics S2000) uses this type of dispersing element. A block diagram of the hardware is shown in *Figure 4.3*.

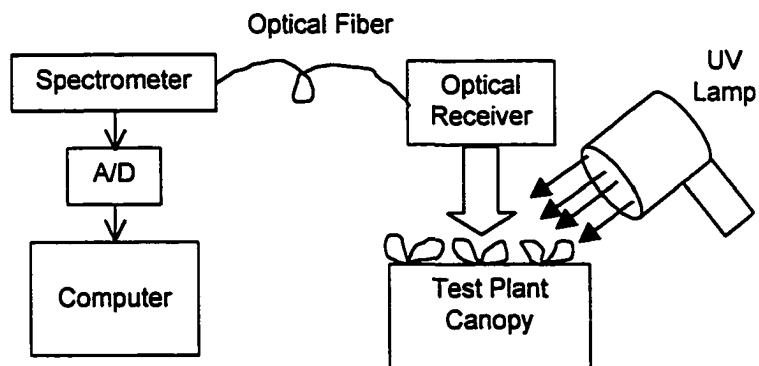


**Figure 4.3.)** Block diagram of experimental hardware configuration

---

The fiber optic spectrometer is a miniature, commercial diffraction grating instrument. Each channel in the spectrometer is configured with a user specified grating fixed in place by the manufacturer. For systems with

multiple gratings, they are configured as a master channel plus multiple slave channels and a single grating is specified for each spectrometer channel.

Grating selection involves a trade-off on optimum wavelength range, optical resolution, and signal level. The dispersion of a grating is determined by the density of the grating's ruled or holographically etched grooves. The greater the groove density (lines/mm) the higher the optical resolution that results, but the more truncated the spectral range.

Spectral range is determined from the dispersion of the radiation across the linear Charged Couple Device (CCD) detector array, and resolution depends on the relative size of the illuminated pixels in the linear array. The path length of the optical bench, the length of the array, and the asymmetry of the optical bench determine the spectral range and resolution of the instrument. A greater spectral range for a specific channel results in greater bandwidth but the trade off is a lesser groove density and thus poorer optical resolution.

Optical resolution, generally measured as Full Width Half Maximum (FWHM), of a monochromatic source depends on the groove density (lines/mm) of the grating and the size of the entrance optics (optical fiber or slit width). Again there are important trade-offs: 1) resolution increases with an increase in the groove density of the grating, but at the expense of spectral range and signal strength; and 2) resolution increases as the slit width or fiber diameter decreases, but at the expense of signal strength.

The approximate optical resolution in nm (FWHM) can be calculated as follows:

**1) Dispersion (nm/pixel) = Spectral Range of the Grating ÷ Number of Detector Elements**

**2) Resolution (in pixels) = value from slit size (see below)**

Typical pixel resolution by slit size/fiber diameter

- 5 micron slit = ~3.0 pixels
- 10 micron slit = 3.2 pixels
- 25 micron slit = 4.2 pixels
- 50 micron slit = 6.5 pixels
- 100 micron slit = 12.0 pixels
- 200 micron slit = 24.0 pixels

**3) Optical Resolution (in nm) = Dispersion (nm/pixel value from #1) x Resolution (pixels value from #2)**

The four-channel spectrometer used in this study has the following grating arrangement: The Master channel spectral range was 200 nm, spanning 800 to 1000 nm, and used a 100 micron slit width with a cylindrical lens placed on detector to increase light collection efficiency. The number of detector elements for the instrument was 2048 per channel. This



arrangement resulted in an optical resolution of  $200 \text{ nm} \div 2048 \text{ elements} = 0.098 \text{ nm/pixel} \times 12.0 \text{ pixels} = 1.2 \text{ nm (FWHM)}$ .

Slave 1 channel spectral range was 200 nm, spanning 610 to 810 nm, and used a 100 micron slit width with cylindrical lens on the detector. This arrangement resulted in the same optical resolution of  $200 \text{ nm} \div 2048 \text{ elements} = 0.098 \text{ nm/pixel} \times 12.0 \text{ pixels} = 1.2 \text{ nm (FWHM)}$ .

Slave 2 channel spectral range was 300 nm, spanning 375 to 675 nm, and used a 100 micron slit width with a cylindrical lens on the detector. This arrangement resulted in  $300 \text{ nm} \div 2048 \text{ elements} = 0.15 \text{ nm/pixel} \times 12.0 \text{ pixels} = 1.76 \text{ nm (FWHM)}$ .

Slave 3 channel spectral range was 150 nm, spanning 250 to 400 nm, and used a 25 micron slit width with a cylindrical lens on detector. This resulted in an optical resolution of  $150 \text{ nm} \div 2048 \text{ elements} = 0.073 \text{ nm/pixel} \times 4.2 \text{ pixels} = 0.31 \text{ nm (FWHM)}$ .

### **4.3 Optical Receiver**

The purpose of the optical receiver is to collect as much light as possible from the emitter and transfer it efficiently to the detector. In this design it was desired to use a large front lens to focus a large target area onto a small fiber optic at a short distance to maximize the radiant flux onto the receiver. The amount of energy gathered by the optical receiver is

directly proportional to the area of the front lens, i.e. entrance pupil. The larger clear aperture leads to a larger cone of rays from the emitter being collected. In this case, the light collected by the optical receiver must be relayed to a 1-mm optical fiber which interfaces with the system spectrometer.

Many factors were taken into consideration in the design of the optical receiver used for this project. Perhaps the most important design criteria are the conservation of power throughput at each element for the overall system. This mandates that the design is optimized by maintaining the product of area times solid angle at each component. For example, the radiant flux arriving at the receiver is proportional to the solid angle and area of the emitter (Hecht, 1990; Moller, 1988). In this specific application, there is a large emitter area and small receiver area, and the radiant flux (power) for the system is given by the following equation (Moller, 1988):

$$P = L da' (\pi \sin^2 \beta')$$

Where:  $P$  = radiant flux, power (W)

$L$  = radiance ( $W/m^2sr$ )

$da'$  = area of receiver ( $m^2$ )

$\beta'$  = angle between center of receiver and extreme edge of emitter with respect to the central axis between the two (degrees)

The emitter's largest spot size diameter was 15 mm (6-in) at a distance of 750 mm (2.5-ft) from the receiver forming a  $5.71^\circ$  cone. A 1.5 mm aspheric

lens ( $f=5.00$  mm,  $NA=0.15$ ) is used in front of the 1 mm fiber resulting in a receiver area of  $1.77$  mm<sup>2</sup>. Radiance is considered constant for the system, so it is the product of  $da' (\pi \sin^2\beta') = 0.055$  mm<sup>2</sup> should be conserved throughout the design. The area of the fiber optic ( $da'$ ) is the limiting factor for the elements of this optical system. For efficient capture of the convergent ray cone, the fiber's numerical aperture (NA) should be compatible with the receiver's  $f/D$  ratio, and the NA of the fiber usually imposes a lower limit on the  $f/D$  ratio (Jenness, 1997). Although a larger solid angle obtained with a larger diameter front lens in the optical receiver would have brought more power to the receiver, the diameter and focal length of the receiver lens are strictly limited by the numerical aperture of the fiber optic.

Large targets require small solid angles, i.e. must be very far away from the front lens of the receiver like with a telescope. Small lenses or fibers require very large solid angles to be compatible with large targets. However, the NA of the fiber determines the maximum solid angle through which light will enter. A design having a large target area and using a large lens to focus light onto a small fiber defies the conservation described. The limitations imposed by the conservation of signal through an optical system limit the sensitivity of most optical instruments. Perhaps the answer lies within the development of new fiber optic materials and "photon funnels". The design was optimized, however; the initial desired target size had to be reduced,

distance to target increased, receiver front end lens diameter reduced, and fiber optic diameter increased to the values described herein.

#### **4.4 Results of Plant Stress Measurements**

Chappelle, et al. (1984a) evaluated LIF as a means of remotely detecting plant stress and found that potassium deficiency in corn caused increase in fluorescent bands at 690 and 740nm; water stress in soybeans increased fluorescent bands at 440, 525, 690, and 740-nm; inhibition of photosynthesis in soybeans by 3-(3-4-dichlorophenyl)-1-1-dimethyl urea (DCMU) increased fluorescent bands at 690 and 740-nm; and chlorosis in senescent soybeans decreased fluorescent bands at 690 and 740-nm.

Chappelle and Williams (1987) evaluated LIF correlation to nitrogen, phosphorus, potassium, calcium, magnesium, sulfur and iron deficiency in corn (120 plants per group). *Figure 4.4* shows the effect of nutrient deficiencies on LIF intensity at 440 and 685-nm. LIF intensity at 440-nm was significantly (CI =95%) different from the control for cases of deficiency in nitrogen, phosphorus, potassium, and iron. Differences for LIF intensity at 685-nm were also observable for cases of deficiency in nitrogen, phosphorus, potassium, and iron. Data were taken from a single leaf, and the leaf angle was fixed to maintain a constant reproducible geometry of the leaf surface

relative to the laser beam and detector system, thus minimizing changes in fluorescent scatter.

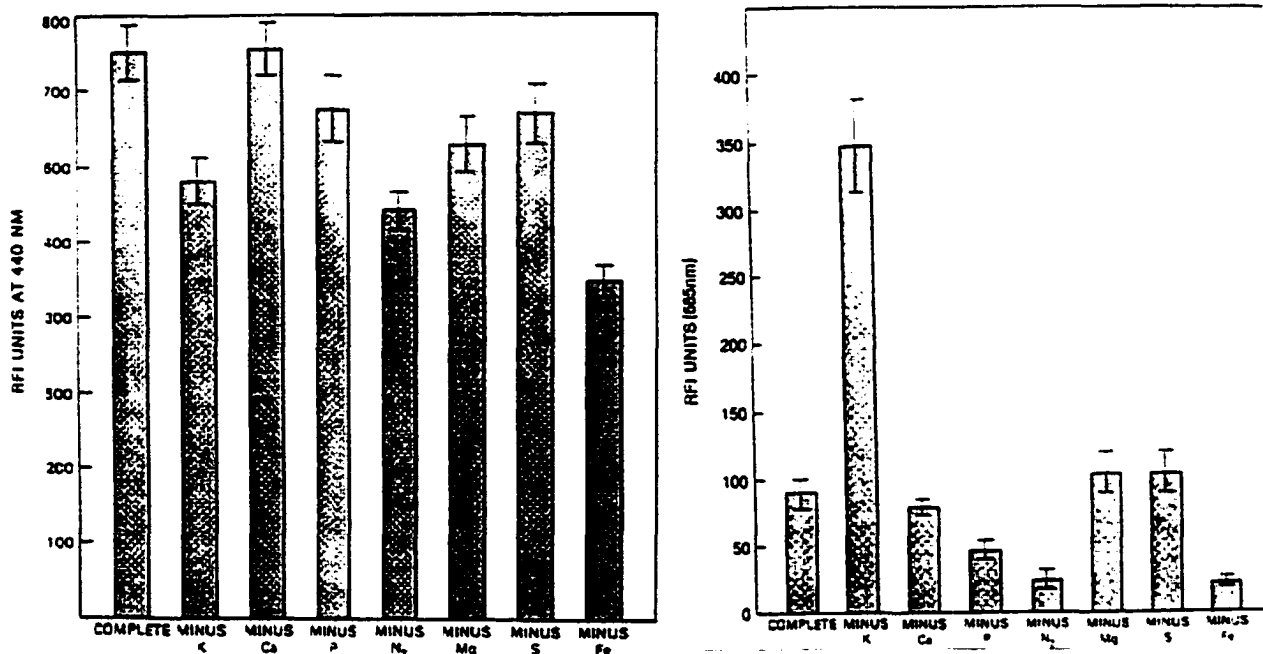


**Figure 4.4)** Effect of nutrient deficiencies on 8-week old corn plants a) LIF intensity at 440-nm and b) LIF intensity at 685-nm (Chappelle and Williams, © 1987 IEEE).

Rosema *et al.* (1992) conducted far range LIF studies on Douglas fir. From an experimental point of view, the measurements on whole plants or small trees appeared problematic and did not give satisfactory results. The main cause was believed to be variable leaf orientation and shadowing. Small displacements of the plants could give almost 2-fold increase of fluorescence. However, Spearman rank correlation tests showed significant

correlation between LIF and air pollution. It was found that the peak fluorescence ratio, 685/720-nm, was less variable and could possibly compensate for variations in canopy structure (Rosema *et al.*, 1992).

Methy, *et al.* (1994) simulated canopy fluorescence for two levels of measurement, leaf and canopy. The model consisted of three components: 1.) Fluorescent signal received by the sensor, 2.) Background reflection in the sensor direction of the downward emitted fluorescence, and 3.) Fluorescence from the background reflection of the laser exciting radiation. The model was used to simulate the peak fluorescence ratio, 690/730-nm, in soybean as a ratio of leaf area index (LAI) before and during drought stress. Due to a higher chlorophyll content, the unstressed canopy had the lowest ratio (Methy, *et al.* 1994).

Gunther, *et al.* (1994) monitored the daily cycle of LIF for healthy and excised canopy clusters of an evergreen oak. For the excitation of the leaf fluorescence, a tripled air-cooled Nd-YAG laser (Spectra Physics, DCR11) was used. The diameter of the laser spot at the target was 30-cm while the total laser energy was 35-mJ per pulse. Fluorescent peaks at 440, 685, and 730-nm were recorded as a function of time. As global irradiation (sunlight) decreased in the afternoon, all fluorescent signals increased. Carbon fixation rate data indicated that chlorophyll fluorescence increased with a decreasing rate of carbon fixation. The fluorescence ratio 685/730-nm was nearly independent (correlation coefficient = 0.552) of ambient light in contrast to the

blue-red ratio, 440/685-nm, which decreased with decreasing light (correlation coefficient = 0.976). LIF data from a cut branch showed that fluorescent intensity decreased with decreasing light and absolute intensity was strongly reduced in comparison to the healthy branch. However, the average fluorescence ratio, 685/730-nm for the stressed branch (0.30) was similar for the unstressed branch (0.35) demonstrating that the use of fluorescence ratios to predict stress is still not completely understood, and perhaps more than two spectral points are required to determine specific plant physiological conditions.

## **5. Artificial Neural Networks (ANN's)**

The use of artificial neural network has been employed to provide a decision process to determine the biological response to nutrient concentration. An artificial neural network is a numerical model consisting of a series of simple interconnected processing units often called nodes or neurons. The architecture, function, and interaction of the artificial neurons are based on structure and behavior of biological neurons in the brain. The input signal to an ANN node is likened to the dendrites of a biological neuron. Multiple inputs are allowed; however, like biological neurons, nodes have only one output; its biological counterpart being the axon.

**A neural network consists of four main parts:**

1. Processing units  $\{u_j\}$ , where each  $u_j$  has a certain activation level  $a_j(t)$  at any point in time.
2. Weighted interconnections between the various processing units that determine how the activation of one unit leads to input for another unit.
3. An activation rule which acts on the set of input signals at a unit to produce a new output signal, or activation.
4. Optionally, a learning rule that specifies how to adjust the weights for a given input/output pair (Russell, 1996).

The processing ability of an ANN is in the weights and biases associated with each node that are either defined by the network user and/or "learned" by the network in an iterative training process. The inherent flexibility in their parallel processing and learning abilities make ANN's powerful multipurpose tools. ANN's can be designed to perform prediction, classification, data association, data conceptualization, and data filtering functions. Popular application areas for ANN's currently include: agriculture, chemistry, economics, finance, games, gambling, imaging, industry, materials science, medicine, music, oceanography, physics, robotics, voice synthesis, and weather forecasting. The research described herein employed an ANN for the association of reflectance and fluorescence spectra with canopy nutrient status for the development of an automated monitoring system.



## **5.1 History of Artificial Neural Networks**

### **5.1.1 Bain's Concept of Memory**

The first ANN was presented by Alexander Bain (1818 - 1903) from the United Kingdom in his 1873 book entitled *"Mind and Body, The Theories of Their Relation"*. During Bain's lifetime, the true extent of the interlocking fibers of the brain was first fully realized and appreciated by scientists. Bain first described memory as a set of nerve currents weaker than that produced by the original stimulus (Olmsted, 1998).

"If we suppose the sound of a bell striking the ear, and then ceasing, there is a certain continuing impression of a feebler kind, the idea or memory of the note of the bell; and it would take some very good reason to deter us from the obvious inference that the continuing impression is the persisting (although reduced) nerve currents from the past - the remembrance of the former sound of the bell" (Bain, 1873).

Recalling a specific memory requires an association be formed with some other memory, sensation, or motor action by neural stimulus, growth, or transformation (Wilkes and Wade 1997). "For every act of memory, every exercise of bodily aptitude, every habit recollection, train of ideas, there is a specific grouping, or coordination, of sensations and movements, by virtue of specific growths in cell junctions" (Bain, 1873). Bain applied these general

ideas in a more concrete fashion suggesting an early form of threshold logic using linear relationships to represent ideas. However, Bain realized that if his theory of simple linear "idea functions" were true, then every possible association or grouping would have to be "hardwired" into the brain which he deemed impractical due to the infinite number of possibilities and permutations.

In order to reduce this degree of "electrical hardwiring" in the brain, Bain suggested more flexible stepped signal attenuation network by drawing upon the newly established electrical induction principles of the extraordinary intellect, Michael Faraday (1791-1867):

"... a more energetic current necessarily takes a more extended sweep, and affects a number of cells and fibers that are left quiescent under a feebler current. The cells being viewed as crossings - where a current in one circuit induces a current in an adjoining circuit - there is, at each crossing, a certain resistance to overcome, and the feebler current is sooner exhausted and stops short of the distance reached by the stronger" (Bain, 1873).

Not until the dawn of computer age in 1943 were brain theorists, McCulloch and Pitts, of equivalent caliber to be found who went beyond generalities to actual network drawings (Olmsted, 1998). Even now the "hardwiring" implied by multi-valued logic based neural networks is not readily

accepted despite the failure of more diffuse forms of neural networks to accurately simulate artificial intelligence. It appears that Bain was on the right track. He simply did not have powerful enough tools like a Pentium® III processor, 512MB of RDRAM, and multi-dimensional multi-valued logic algorithms with which to form higher order network groupings and perform complex network simulations.

### 5.1.2 The First Logic Circuits

In 1938, N. Rashevsky proposed that the brain could be organized around binary logic operations since action potentials could be viewed as binary 1 (true) values (Rashevsky, 1938). Rashevsky presented the circuit shown in *Figure 5.1* showing how a binary logic EXCLUSIVE OR operation could be implemented using addition and subtraction operations.

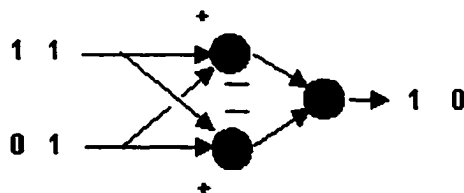


Figure 5.1.) Rashevsky's binary logic operation, EXCLUSIVE OR (Rashevsky, 1938; Olmsted, 1998).

---

In 1943 McCulloch and Pitts realized that the natural consequence of the standard neuron model's threshold in combination with binary action potentials produced another type of logic called threshold logic. Since each action potential pulse is an all or nothing binary event, a threshold value of 2 defines an AND operation as shown in *Figure 5.2*. Likewise, a threshold value of 1 defines an INCLUSIVE OR operation since only one action potential on either line is sufficient to produce an output (Olmsted, 1998).

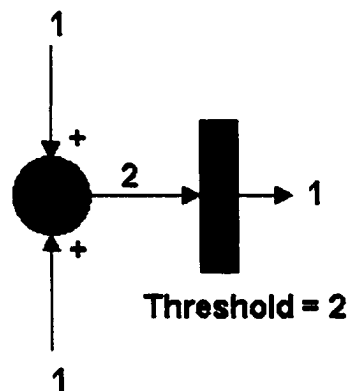


Figure 5.2.) McCulloch and Pitts's (1943) threshold logic circuit for an AND operation (Olmsted, 1998).

---

Threshold logic was expanded spatially by adding more input lines so that the output of the summation node would become analog since this seemed to fit in more with the standard neuron model (Olmsted, 1998). The existence of analog values allowed node operations to become adaptive

using multiplication factors called weights. However, rarely if ever do modifications to a single parameter fully characterize the distribution (the pattern) of an operation's input. Some ambiguity is almost always present, yet this ambiguity can be beneficial in neural networks because it allows neural networks to work with partial knowledge even though this ambiguity could never be precisely defined as it is in a classification hierarchy (Olmsted, 1998).

The achievement of adaptability in the neural networks of this time came at the cost of losing the logical decision making resolution. By 1963 this split theoretical neuroscientists into the separate groupings of neural network researchers and artificial intelligence researchers (Olmsted, 1998).

The 1963 paper by R.O. Winder seems to have been the last major paper which still attempted to combine the weight based and mathematical neural network approach with the logical artificial intelligence approach, but it used mathematical techniques to find the desired weights of a network instead of learning them. The result was that the neural network researchers continued to develop parameter based classifier circuits while the artificial intelligence researchers expanded and abstracted the binary logic approach to form propositional and prepositional logics (Olmsted, 1998).

### 5.1.3 Perceptron and ADELIN

In 1957, Frank Rosenblatt at Cornell developed Perceptron, a hardware neural net for character recognition. This type of network using unsupervised learning is called an auto-learning network or a pattern regularity detector. The original Perceptron attempted to describe the format that information was stored or remembered and to describe how this information influenced recognition and behavior. The original Perceptron circuit shown in *Figure 5.3* consisted of many convergent type subcircuits feeding into a gate comparator (Rosenblatt, 1958).

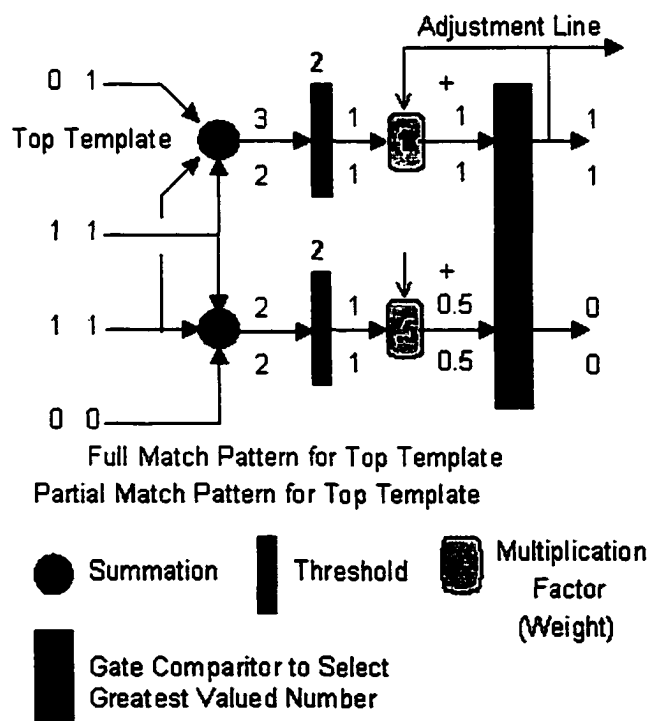


**Figure 5.3.)** Rosenblatt's (1958) original Perceptron circuit (Olmsted, 1998).

A convergent subcircuit is characterized by several input lines feeding into some central operation or series of operations. In this case the central operation is a summation node connected to a threshold unit which in turn connects to a multiplication factor (weight). Rosenblatt called these subcircuits "A" units for association units. Each received a certain number of binary (0 or 1) positive inputs and a lesser number of negative (subtractive) inputs connected in a random manner. If the sum of these inputs exceeded the threshold value then the threshold would produce an output value of 1. This value was then modified by the weight valued between 0 and 1 which Rosenblatt called the *value* of the "A" unit.

The output of each convergent subcircuit was next sent to a subcircuit called in this web site a "gate comparator" which selected its largest input value, passed it on and fed it back to that subcircuit's weight to increment it by a certain amount. In this way the most used template would increase its transmission efficiency in conformity to the Hebb learning rule (Rosenblatt, 1960; Olmsted, 1998).

In 1959, Widrow and Hoff at Stanford developed ADALINE for adaptive control of noise on telephone lines. ADALINE could recognize binary patterns which enabled it to predict the next bit in a flowing stream of bits. This was the first time a convergent type of subcircuit having weights before the

summation node was used to formally classify patterns (Widrow and Hoff, 1960; Olmsted, 1998).

A more successful procedure was found by Widrow in 1962 and was called the Widrow-Hoff learning rule or the Delta learning rule. It is based on the realization that the greatest sources of the error are from the active lines. Consequently, the Widrow-Hoff learning rule changes the value of each weight in proportion to its pre-weight line value (in this case 1 or 0) according to the following rule (Widrow, 1962; Olmsted, 1998):

$\text{Weight Change} = (\text{Pre-Weight Line Value}) * (\text{Error} / (\text{Number of Inputs}))$ .

In 1962, Rosenblatt revised his original Perceptron with ADALINE features. The adaptive multiplication factors (weights) were placed before the summation node like ADALINE instead of after the node as in the original Perceptron. In addition, all convergent subcircuits now share a common set of inputs instead of having randomly connected inputs (although the initial values of the weights may be randomized which would effectively accomplish the same thing). These changes allowed the input pattern to dispense with the binary line signal requirement in favor of more realistic analog signals which could represent the frequency of an action potential pulse or the ionic charge on a neuron (Rosenblatt, 1962; Olmsted, 1998). Rosenblatt summed up perceptrons in this passage from his 1962 book:

"Perceptrons are not intended to serve as detailed copies of any actual nervous system. They're simplified networks, designed to permit the



study of lawful relationships between the organization of a nerve net, the organization of its environment, and the 'psychological' performances of which it is capable. Perceptrons might actually correspond to parts of more extended networks and biological systems; in this case, the results obtained will be directly applicable. More likely they represent extreme simplifications of the central nervous system, in which some properties are exaggerated and others suppressed. In this case, successive perturbation and refinements of the system may yield a closer approximation (Rosenblatt, 1962)."

In 1972, James Anderson and Teuvo Kohonen independently described models for association networks. Anderson proposed a multiplicative function of activity in pre- and postsynaptic cells that generated an interactive memory process (Anderson, 1972). Kohonen also sought to model an interactive memory process (Kohonen, 1972). Both of their models made use of matrix mathematics which basically resulted in an array of analog ADALINE circuits.

#### 5.1.4 Multilayered Backpropagation Association Networks

With the development of multiple layered neural networks, the best way to extend the Widrow-Hoff (Delta) rule to multiple layers was given much

attention. In 1986, three independent groups of researchers: 1.) Y. Le Cun  
 2.) D. Parker 3.) D. Rumelhart, G. Hinton, and R. Williams devised essentially  
 the same idea, which came to be called the backpropagation network for the  
 way it distributes pattern recognition errors throughout the network.

The basic repeatable unit used in the backpropagation network as described  
 by Rumelhart, Hinton, and Williams is shown in *Figure 5.4*.

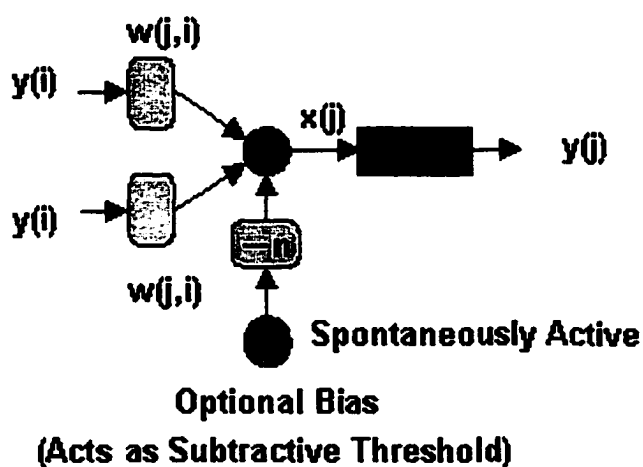


Figure 5.4.) The basic backpropagation node (Olmsted, 1998).

---

The weights, represented by  $w(j,i)$ , can be any positive or negative  
 value but they start out as small, randomly chosen numbers. The function  
 (funct.) is generally used to keep the output of the convergent circuit 1 or less.  
 The error is the difference between the desired output and the actual output.

The strategy used in back-propagation is to determine and use the error contribution made by each *pathway* through the network. In a three layered network the learning rule for each layer is (Olmsted, 1998):

$$\Delta Wt. Value_{i-1} = (Const.)*(Error)*(\Delta Value_{i-1})*(pre-Wt. Value)*(Wt._{i-1})$$

$$\Delta Wt. Value_i = (Const.)*(Error)*(\Delta Value_{i-1})*(\Delta Value_i)*(pre-Wt. Value)*(Wt._{i-1})*( Wt._i)$$

$$\Delta Wt. Value_{i+1} = (Const.)*(Error)*(\Delta Value_{i-1})*(\Delta Value_i)*(\Delta Value_{i+1})*(pre-Wt. Value)*(Wt._{i-1})*( Wt._i)*(Wt._{i+1})$$

Properly trained backpropagation networks tend to give reasonable answers when presented with inputs that they have never seen. Typically, a new input will lead to an output similar to the correct output for input vectors used in training that are similar to the new input being presented. This generalization property makes it possible to train a network on a representative set of input/target pairs and get good results without training the network on all possible input/output pairs (Demuth and Beal, 1998).

## **5.2 Neural Network Operation**

The basis for all neural networks is the Hebb's Rule which states that changes in synaptic strengths are proportional to neuron activation (Hebb, 1949). There are various forms of learning for each specific type of neural net

work. For example, Grossberg learning involves self-training and self-organization that allows the net to adapt to changes in input data over time (Grossberg, 1982). While Kohonen's learning law consists of a two-layer network with content addressable associative memory for unsupervised learning (Kohonen, 1984).

In unsupervised learning, networks are self-learning and weight adjustments are not from comparison with known output values. Based on the input patterns, only weights from the "winning" node or nodes are modified.

In supervised learning, networks are trained on given outputs. Input vectors are fed into the net and weights are adjusted by the training algorithm to achieve a desired output for the training data. Corrections based on actual and desired output are computed for each training cycle or epoch. If the calculated error is within a given tolerance the training stops, otherwise training continues until this condition is met. Final weights are then established and the net is ready to be run on new sets of input data.

Backpropagation is a form of supervised learning where input vectors are fed into the model and error is computed from the difference between predicted and actual outputs. This error is then used to adjust the output layer weights, the hidden layer weights and finally the input layer weights. These steps are then repeated in this order until the desired accuracy level is achieved, hence the term backpropagation.

When designing a neural network there is a trade off between training speed and weight quality. If the network is too simple and fast, the weights may not be very effective for new data, i.e. the weight quality is poor. If it is too complex and/or slow, the network may memorize the training data and not predict well for new data, i.e. generalization is poor. This is why when designing an ANN, the number of nodes and hidden layers must usually be determined by trial and error.

Although there are several equations in ANN literature for determining the number of hidden layers in a model, none appear to be based on any well defined theory or singularly convincing logic argument. The soundest practice seems to be to simply start with no hidden layers and then add one layer at a time until the desired accuracy is achieved.

Trial and error must also be applied to determine the number of nodes per layer. The output layer must contain the same number of nodes as desired outputs, and an interesting rule of thumb is to decrease the number of nodes by 50% in a feedforward fashion. For example, if a two-hidden layer NN has a five element output vector, the output layer must have five nodes, the second hidden layer might have ten nodes and the first hidden layer might have twenty nodes.

Another important design consideration is the activation function to be used by the nodes in each layer. Three popular transfer functions are the hard limit transfer function, linear transfer functions, and log-sigmoid transfer

functions. The activation function is sometimes called a "transfer" function, and activation functions with a bounded range are often called "squashing" functions, such as the commonly used tanh (hyperbolic tangent) and logistic functions. If a unit does not transform its net input, it is said to have an "identity" or "linear" activation function (Sarle, 1997).

The hard limit transfer function is the type of function used by the Perceptron. The output of the neuron is either 0 if the net input argument is less than 0 or 1 if the input is greater or equal to 0. This type of transfer function is useful for NN's that perform simple classification decisions.

Linear transfer functions are useful for modeling linear distributions. This type of function is also commonly used in an output layer when the desired target values are outside of the range of squashing functions.

The log-sigmoid transfer function is also called standard sigmoid (or logistic) function, and it is:

$$y = 1 / (1 + \exp (- D * x))$$

where: y = final value of the neuron

D = sharpness or gain of the neuron

x = the input to the neuron

The log-sigmoid function takes any input between positive and negative infinity and produces an output in the range of 0 to 1. This transfer function is commonly used in backpropagation networks, in part because it is

differentiable (Demuth and Beale, 1998). The log-sigmoid transfer function is also ideal for training sets involving the prediction of Boolean vector outputs.

### **5.3 Neural Network Terminology**

In order to clarify the neural net operation and design, agreement on terminology is necessary. The terms neural network, NN, and artificial neural network, ANN, are used interchangeably; however, ANN is perhaps the superior term because it is less ambiguous. There seems to be no term in the ANN literature for the set of all cases to which you wish to generalize. Statisticians call this set the "population." There also does not seem to be a consistent term in the ANN literature for the set of cases that are known, i.e. available for training and evaluating an ANN. Statisticians call this set the "sample," and the sample is usually a subset of the population, as entire populations are rarely known in real world situations. Neurobiologists usually mean something entirely different by "population," apparently some collection of neurons, and their term "sample," usually refers to a biological subunit or specimen from a larger segment, mass, or sometimes the entire organism. In this document, however, the terms "population" and "sample" will be used strictly in the statistical sense in an attempt to avoid confusion.

The terms "validation" and "test" are unfortunately often the source of inordinate confusion. In ANN methodology, the sample set consisting of input and corresponding output data is often subdivided into "training", "validation",

and "test" sets. The distinctions among these sample subsets are crucial, but the terms "validation" and "test" sets are often used incorrectly. The training set is composed of examples used for learning; that is to fit the parameters [i.e., weights] of the classifier Ripley (1996). The validation set is composed of examples used to tune the parameters [i.e., architecture, not weights] of a classifier, for example to choose the number of hidden units in a neural network (Ripley, 1996). The test set is composed of examples used only to assess the performance [generalization] of a fully-specified classifier (Ripley, 1996).

The following explains the source of much of the confusion between training and validation sets. Some training methods such as "early stopping" require a validation set be used in training the network. Early stopping is a technique for improving network generalization. As described by Demuth and Beale (1998), the sample set is subdivided into three subsets: training, validation, and test sets. The training set is used to compute the gradient and update the network weights and biases. The error on the validation set is calculated and monitored during the training process to determine when to stop updating the weights and biases. For example, the validation error normally decreases during the initial phase of training along with the training set error. However, when the network begins to overfit the data, i.e. memorize noise, the error on the validation set will rise. When the validation error increases for a specified number of iterations, the training is stopped,



and the weights and biases at the minimum of the validation error are returned. Since this procedure itself can overfit the validation set, the performance of the selected network is confirmed by measuring its performance on the third independent sample subset, the test set. Other NN training methods such as maximum likelihood do not inherently require a validation set so the training set for maximum likelihood might encompass both the training and validation sets for early stopping (Sarle, 1997).

The crucial point is that the test set is not used to choose among two or more networks. The error on the test set simply provides an unbiased estimate of the NN generalization error. Any data set that is used to choose the best of two or more networks is by definition a validation set.

#### ***5.4 Prediction of specific nutrient levels in vegetation***

Neural networks have recently been reported as an effective processing technique for multi-spectral and hyper-spectral for agricultural applications (Tumbo et al., 2000, Wilkerson et al., 1999, Yang et al., 1998, Lee and Slaughter, 1998, and Stone, 1994). ANN's have also been successfully implemented to predict nutrient status in plants (Tumbo et al., 2000 and Wilkerson, et al., 1999).

Yang et al. (1998) implemented a neural network to distinguish weeds from corn plants using pixel color indexes. The accuracy rate of image recognition was 90 to 100% for corn and 60 to 70% weeds. Lee and

Slaughter (1998) used a neural network model to distinguish weeds from tomato. The model correctly identified 38.9% of tomato cotyledons, 37.5% true tomato leaves, and 85.7% weeds. Stone (1994) used a neural network with optical sensor data to identify weeds with 92% accuracy.

Tumbo et al. (2000) used a backpropagation neural network model with inputs of 201 bands of reflectance data from corn and solar background data to predict chlorophyll level. The model correlation to the testing set was  $r^2 = 0.92$  and correlation to an independent validation set was  $r^2 = 0.91$ .

Wilkerson et al. (1999) used a supervised multilayer feedforward neural network trained with a backpropagation algorithm to predict nitrogen deficiency in corn using four spectral bands and growth stage as the input parameters. Under the conditions of 50% data for training and 50% for testing, the average diagnosing accuracy rate ranged from 95 to 99% with an average of 96.8%. In general, the more data used for training, the better the model performed. The diagnostic accuracy rate averaged 94% with 50% data for training and 50% for testing when growth stage was eliminated as an input parameter to the model.

## **6. Hypothesis and Objectives**

### **6.1 Hypothesis**

Remote sensing of plant canopies with multiple leaves and random orientation will provide NASA and other CEA (Controlled Environment

Agriculture) users with a rugged, reliable and automated method for monitoring specific nutrient stresses. Specifically, a fiber optic spectrometer is a useful tool for remote analysis of nutrient deficiency of hydroponic lettuce, 'Ostinata' canopies as the representative crop. Reflectance data will provide generalized stress information for monitoring concentration of primary plant pigment, and fluorescence spectra correlates to specific changes in nitrogen and phosphate fertilization regiments. It is also hypothesized that canopy element grid size information gained will provide necessary specifications for design and fabrication of a self-monitoring growth chamber. Monitoring of plant growth by remote sensing can advance capability of early detection of successful crop growth important for future crop growth in space.

## **6.2 Objectives**

The primary goal of this research was to develop a robust and automated technique for monitoring crop nutrient stress in controlled environments. The specific objectives of this research are:

- 1.) Investigate the spectral information in reflectance, and fluorescence, or a combination of both to predict specific nutrient stresses.
- 2.) Design an optical receiver to maximize signal collection for the largest possible FOV over the shortest distance to target.
- 3.) Determine importance of spatial resolution on predictions using reflectance and fluorescence.

- 4.) Develop rugged and automated techniques for remote monitoring of plant health that can be used for applications to agriculture and for more critical space based plant growth.

## **7. Methodology**

### **7.1 Lettuce Cultivation**

*Lactuca sativa*, 'Ostinata', (lettuce) was cultivated hydroponically in a plant growth chamber to maturity (35-days) using a standing aerated nutrient solution method. The entire test was replicated for a total of two complete growth cycles of one lettuce variety.

The specific elements investigated were two macro-nutrients, nitrogen and phosphorous. There were two sets of test groups and a set of control groups as shown in *Table 7.1*. Test plants expressing specific nutrient stresses were cultivated hydroponically using 5% and 25% of the concentration recommended for optimal growth for each nutrient. Each set (2) of the three nutrient groups, nitrogen deficiency, phosphorous deficiency, and control group, has four replications for a total of 24-hydroponic trays (2x3x4). Data were collected every other day through days 12-34 of the growth cycle. One of the two nutrient control groups was sampled less frequently, every 4 days rather than every 2, to assess sensitivity of the lettuce crop to UV excitation, e.g. bleaching associated with ultra violet radiation used for the fluorescence measurements.

Production began with seeding Oasis Wedge (Smithers-Oasis USA; Kent, Ohio) growing medium on day one. The medium had a small amount of 1-1-1 (N, P, K) to serve as a plant starter, and pH of the medium was in the 5.5-6.5 range.

---

**Table 7.1.)** Experimental design for hydroponic lettuce cultivation.

	N	P	Sample #
<b>Group 1</b>	5%	100%	1-4
	25%	100%	5-8
<b>Group 2</b>	100%	5%	9-12
	100%	25%	13-16
<b>nutrient controls</b>	100%	100%	17-20
<b>UV exposure controls</b>	100%	100%	21-24

---

Tap water was tested to find the concentration of each nutrient present in the water supply and nutrient solution was adjusted accordingly. Control group solutions were prepared in accordance with Cornell's CEA Hydroponic Lettuce Production Handbook (Wells, 1995), *Table 7.2*, and were added 24-

hours after seeding. Tap water concentrations for Cl, Mg, and Cu were higher than what was required for lettuce production, however; compared to values for hydroponic Hoaglands solution (Weiler and Sailus, 1996) all values were within an acceptable range avoiding toxicity. On day 5 seedlings were selected based on uniformity of size and expansion of their first true leaf. Seedlings which had unacceptable growth were discarded. After final seedling selection on day 10, the test nutrient solutions were added as shown in *Table 7.1*. Detailed information concerning the chemical composition of all nutrient solutions is provided in Appendix A. *Figure 7.1* shows the aerated hydroponic cultivation setup used in this study.

---

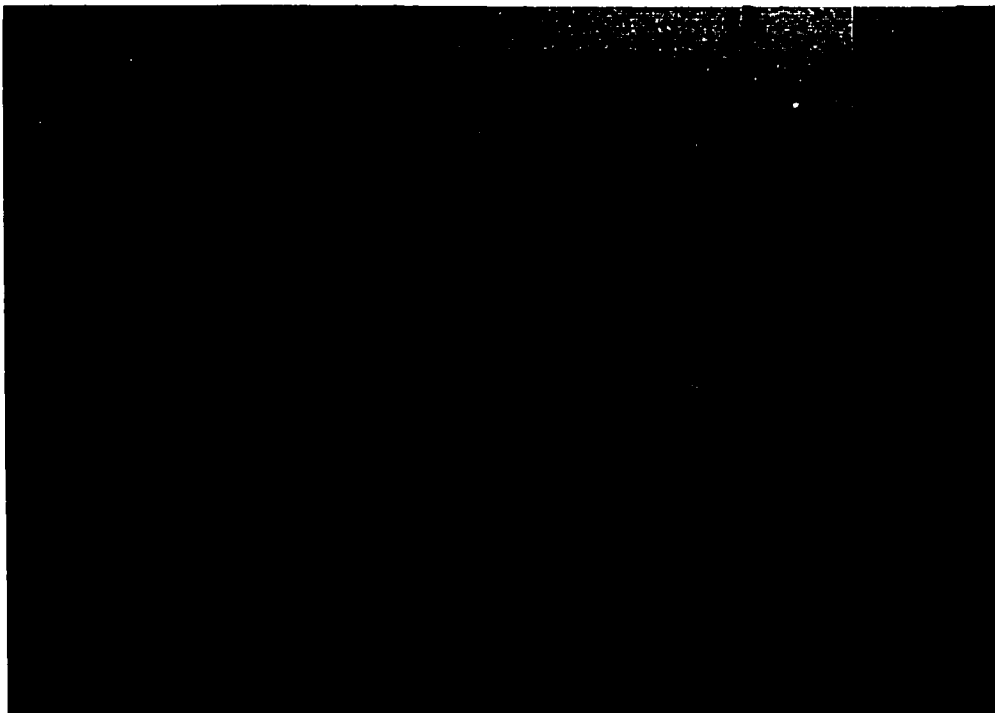


**Figure 7.1.)** Experimental setup for hydroponic cultivation of test plants.

---

**Table 7.2.)** Control nutrient solution (Wells, 1995) and tap water concentrations.

<b>--- Hydroponic Nutrient Solution and Tap Water ---</b>			
<b>mM</b>	<b>Required Nutrient Conc. (mM)</b>	<b>Tap Water Conc. (mM)</b>	<b>Final Conc. Added (mM)</b>
<b>N</b>	8.90	0.087	8.81
<b>P<sup>**</sup></b>	1.00	0.012	0.988
<b>K<sup>***</sup></b>	5.50	0.030	5.47
<b>Ca<sup>***</sup></b>	2.10	0.714	1.39
<b>Mg<sup>***</sup></b>	1.00	2.61	0.00
<b>S<sup>****</sup></b>	1.10	0.212	0.888
<b>μM</b>	<b>μM</b>	<b>μM</b>	<b>μM</b>
<b>Fe<sup>***</sup></b>	16.8	0.322	16.5
<b>Mn<sup>***</sup></b>	2.50	0.091	2.41
<b>B</b>	15.0	--	15.0
<b>Zn<sup>***</sup></b>	2.00	0.535	1.46
<b>Cu<sup>***</sup></b>	0.40	1.02	0.00
<b>Mo</b>	0.30	--	0.30
<b>Cl<sup>****</sup></b>	0.00	645	0.00

\*Total N tested using ion chromatography, automated phenate method, cadmium reduction, and the persulfate method.

\*\*Total P tested using ascorbic acid method.

\*\*\*K, Ca, Mg, Fe, Mn, Zn, and Cu tested using atomic absorption spectrometric method.

\*\*\*\*S and Cl tested using ion chromatography.

All trays were emptied and refilled with fresh nutrient solution every other day during the crop growth cycle to maintain a reasonably consistent concentrations of fresh fertilizer.

The light source in the plant growth chamber was from cool white fluorescent (CWF) lamps. The lamps were configured for a uniform distribution of light over the entire growing area. The light intensity was approximately  $250\text{-}\mu\text{mole m}^{-2} \text{ s}^{-1}$  (Quantum meter, QMSS-EL, Apogee Instruments) and the photoperiod was 24-hours.

Temperature was kept between 20 and 30° C. Nutrient solution pH was maintained between 5.6 to 6.0 (pH Meter, Hanna Series, Sigma), and electrical conductivity was maintained between 1000 to 1750  $\mu\text{S cm}^{-1}$  (Conductivity Meter, Hanna Series, Sigma). Records for light intensity, temperature, relative humidity, pH, and electrical conductivity are included in Appendix A. Seedling spacing within each tray was 769-plants  $\text{m}^{-2}$ . On day 13 spacing was increased to 192 plants  $\text{m}^{-2}$ .

Trays were placed in the growth chamber using a randomized complete block design based on random number generated using MATLAB software. Counting each of the two control groups as individual treatments, there were six treatments replicated four times. Table 7.3 illustrates the randomized block design used for the experiment.



---

**Table 7.3)** Experimental layout using randomized block design. 100%N/P UV had 100% of all nutrients and was tested as frequently as the nutrient stress groups. 100%N/P -UV had 100% nutrients, but was tested at one half the rate as the other groups therefore was exposed to one half the amount of UV.

I	100% N/P UV	25% P	100% N/P -UV	25% N	5% N	5% P
II	5% N	100% N/P UV	25% N	25% P	5% P	100% N/P -UV
III	25% P	100% N/P -UV	100% N/P UV	5% P	25% N	5% N
IV	5% P	5% N	25% N	100% N/P UV	100% N/P -UV	25% P

## **7.2 Electromagnetic Radiation and Optics**

### **7.2.1 Electromagnetic Radiation Units**

Many different terms and units are used to describe light or radiation.

Type of unit used is most often a function of the specific application and specific branch of science or engineering involved in the area of investigation.

A brief summary of the units describing electromagnetic radiation supports the research methodology described herein that is associated with lighting, optics, and irradiance.

There are two main categories in the quantization of electromagnetic radiation, radiometric units and photometric units. Any electromagnetic radiation can be described using radiometric units. These units describe the energy or power that is either emitted from a source or that arrives at a surface.

Photometric units are useable only for visible radiation; and these units describe the response elicited in the human eye. While photometric units are more often used in the lighting and photographic industry, photometric units are not generally the most appropriate units to completely describe radiation used in scientific studies. For example, two lasers that have identical power output at different wavelengths, 300-nm and 600-nm, will have the same radiance in radiometric units, but in photometric units the luminance of the 300-nm laser would be zero because the human eye does not detect 300-nm radiation.

The recommended radiometric SI units are the following (Grossweiner, 1989):

#### **BASIC UNITS**

Energy: Joule (J), amount of radiation

Power: Watt (W), flux (time rate of energy transfer)

Excitance: Watt meter<sup>-2</sup> (W m<sup>-2</sup>), flux per unit area leaving a small plane surface (by emission or reflection)

#### **SOURCE UNITS**

**Intensity: Watt steradian<sup>-1</sup> (W sr<sup>-1</sup>), flux emitted into a unit solid angle**

**Radiance: Watt meter<sup>-2</sup> steradian<sup>-1</sup> (W m<sup>-2</sup> sr<sup>-1</sup>), flux in a given direction per unit solid angle and per unit area (normal to direction of propagation)**

#### **TARGET INCIDENCE UNITS**

**Irradiance: Watt meter<sup>-2</sup> (W m<sup>-2</sup>), flux per unit area incident on a small plane surface**

**Exposure: Joule meter<sup>-2</sup> (J m<sup>-2</sup>), energy per unit area incident on one side of a small plane surface**

The American Society for Horticulture Science's Growth Chambers and Controlled Environments Working Group has recommended the use of quantum flux density as the primary method for reporting radiation (Thimijan and Heins, 1983). For many purposes in plant studies, it is important to know the photon flux or quantum flux density. For instance, the rate of photosynthesis depends on the rate of absorption of photons not on the rate of absorption of energy. The photons that are photosynthetically useful fall within the 400 to 700-nm range. This is referred to as photosynthetically active radiation (PAR) or the photosynthetic photon flux density (PPFD). PAR is reported by plant scientists as  $\mu\text{Einstein s}^{-1} \text{ m}^{-2}$  ( $\mu\text{E s}^{-1} \text{ m}^{-2}$ ) or more commonly as  $\mu\text{mol s}^{-1} \text{ m}^{-2}$  where both notations represent the same unit. Since plant growers are interested in spectral quality as well as quantity; therefore, the  $\mu\text{mol s}^{-1} \text{ m}^{-2}$  unit takes into consideration photon numbers.

Photons at different wavelengths have different energies. Thus, one must know the number of photons per unit wavelength and the energy per photon at each wavelength to calculate total energy as described by quantum flux density. This problem of unit uniformity between engineering and plant science disciplines causes difficulty in communication between groups. Plant growers and other scientists require conversion into similar units to promote and facilitate interdisciplinary studies.

It is possible to convert from PAR to the SI unit of radiant flux per unit detector area, irradiance ( $\text{W m}^{-2}$ ), if the wavelength interval and the generic source of its spectral content is known. Also a corresponding conversion constant may be implemented to simplify the conversion process:

$$\text{W} \cdot \text{m}^{-2} = \frac{\mu\text{mol} \cdot \text{s}^{-1} \text{m}^{-2}}{\text{Const.}}$$

A comprehensive list of the mixed conversion quantum to radiometric constants is published in Thimijan and Heins, 1983. These conversion constants are a function of the 400 to 700-nm spectral range for specific light sources and have the unit,  $\mu\text{mol s}^{-1} \text{W}^{-1}$ .

### 7.2.2 Reflectance Light Source

A white light excitation source, GE tungsten 250-W, 3200°K spotlight, was used as the light source to generate reflectance spectra. Given the temperature rating of the lamp, spectral output as a function of wavelength is

given by Planck's law, see *Figure 7.2*. Planck's law for solving the intensity of blackbody radiation is given by the equation:

$$I(\lambda, T) = \frac{2\pi hc^2}{\lambda^5 \left( e^{\frac{hc}{\lambda kT}} - 1 \right)}$$

Where:  $I$  = Intensity  
 $\lambda$  = wavelength (m)  
 $h$  = Planck's constant,  $6.626 \times 10^{-34}$  J s  
 $c$  = speed of light,  $3 \times 10^8$  m s $^{-1}$   
 $k$  = Boltzmann's constant,  $1.381 \times 10^{-23}$  J K $^{-1}$   
 $T$  = Temperature (K)

The corresponding spectral output for the lamp is presented in *Figure 7.2*.

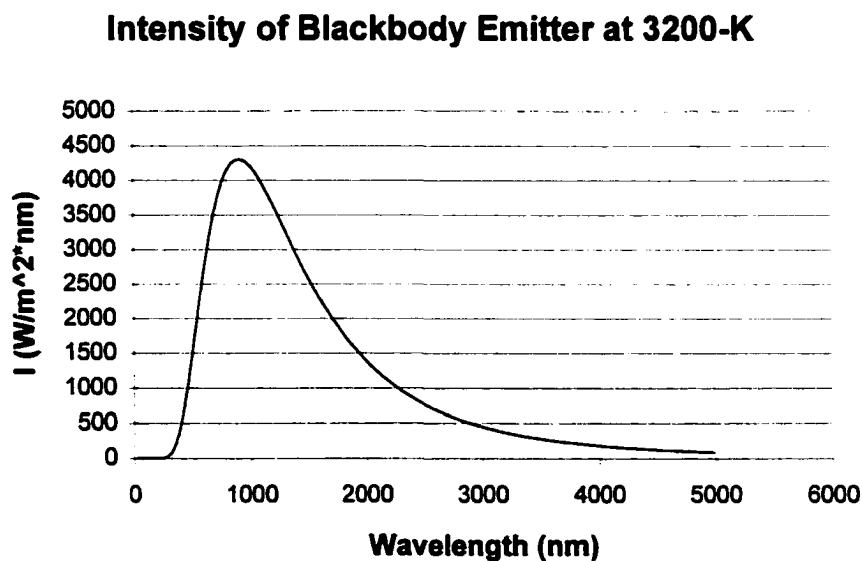


**Figure 7.2.)** Intensity of a blackbody emitter at 3200K using Planck's Law.

---

To generate a relative reflectance curve of the 3200 K light source, a 99% reflectance Spectralon diffuse reflectance standard was used (Labsphere Certified Reflectance Standard). The effect of illuminating the crop canopy with a 250-W incandescent spotlight was assumed to be negligible compared to the intensity of growing conditions in the chamber.

### 7.2.3 Fluorescence Excitation Source

In this literature review, the majority of papers cited used UV lasers as the excitation source for LIF of plant leaves. UV excitation is required to achieve fluorescent emission in blue, green, and red spectral regions. The exact optical power used as the excitation source was found to be highly variable in the literature with a median value of 9-mJ.

A medium intensity UV spotlight fitted with a 100-W Xenon lamp was used as the fluorescence excitation source. The lamp was fitted with a broad band visible filter and provided high purity UV light with a peak wavelength at 365-nm. At a distance of 38-cm (15-in) the output at 365-nm was  $5.7\text{-mW cm}^{-2}$  ( $57\text{ W m}^{-2}$ ) (Oriel GoldiLux UV Meter GUV-0L). Total lamp output in the UVA range, 315 to 400-nm, was  $4.7\text{-mW cm}^{-2}$  ( $47\text{ W m}^{-2}$ ) at a distance of 30-cm (12-in) yielding a spot size of approximately 33-cm (13-in). This is similar to the experimental setup used by Norikane and Kurata (1999) who used a 200-W halogen lamp with a low pass filter to achieve an irradiance of  $50\text{ W m}^{-2}$

over a 2.0-cm spot (0.8-in) at the plant canopy surface to monitor fluorescent emission from free standing tomato plants. Differences in fluorescence kinetics were observed for free standing tomato plants compared to previous drought stress studies conducted on plant leaves that were clamped to a sample plate.

#### 7.2.4 Plant Angle

All test plants in this study were free standing and expressed natural random growth patterns. For the NN study, plant angle measured with respect to the downward viewing optical receiver was  $0^\circ$  from zenith. As a separate test to investigate differences in fluorescence and reflectance as a function of plant angle a single plant was held parallel ( $90^\circ$ ), diagonally ( $45^\circ$ ), and perpendicular ( $0^\circ$ ) with respect to the optical receiver. The top of the plant was oriented toward the excitation light source, and root oriented away from the light source as the plant was rotated during the test.

#### 7.2.5 Optical Receiver

It is desired to compare signals from 15-cm, 7.5-cm, and 3.75-cm diameter target sizes. Light collection by the fiber optic spectrometer was concentrated *via* a custom built optical receiver from a 15-cm (6-in) diameter target at a distance of 76-cm (2.5-ft), a 7.5-cm (3.0-in) diameter target at 38-cm (16-in), and a 3.75-cm (1.5-in) diameter target at 19-cm (7.5-in).

The objective of the optical receiver design was to maximize the irradiance ( $\text{W}/\text{m}^2$ ) incident upon the detector. This was necessary because the emitted fluorescent signals are relatively weak, and detecting minute differences among the inherently weak fluorescent signals as a function of test group could be problematic, especially given other obscuring factors such as noise.

Optical design software package, ZEMAX® (Focus Software, Inc.; Tucson, Arizona), was used to determine the efficiency of the receiver and the exact spacing of the system components. A ray diagram (*Figure 7.3*) was generated for the given conditions: three fields specified at the following coordinates: (+75 mm, 1200 mm), (0 mm, 1200 mm), and (-75 mm, 1200 mm) from the first lens. The two points (75, 1200) and (-75, 1200) form the cones of light traced out by the extreme light cones from object to image. These are the cones that are most difficult to center over the relatively short distance of 1200 mm. It is quite simple to focus the center cone of light on the detector but not the extreme cones. The fraction of enclosed energy plot (*Figure 7.4*) shows the efficiency of the receiver for collecting light from each field. The center field is always efficiently collected for this design, whereas the extreme fields are the fields of primary interest in designing the receiver. For the final design selected, the collection efficiency approaches 100% at a radial distance of 140- $\mu\text{m}$  from the centroid. This means the total radiant energy of the aperture is enclosed within a 280- $\mu\text{m}$  region. The spot diagram



(Figure 7.5) shows the physical location of each 280- $\mu\text{m}$  circular region associated with each of the three fields. The center field could be captured entirely by a 280- $\mu\text{m}$  fiber optic. However, the center of the cone from +75-mm extreme field is at -0.394-mm, while the center of the cone from the -75-mm extreme field is at +0.394-mm. Therefore, enclosing all three cones requires a fiber of  $(0.14\text{-mm} + 0.394\text{-mm} + 0.394\text{-mm} + 0.14\text{-mm}) = 1.068\text{-mm}$ . As the maximum fiber optic diameter available is only 1-mm, there is a slight amount of vignetting occurring at the fiber interface. The receiver design has been fully optimized to maximize field of view and optical throughput over the shortest distance to the target as possible. The fiber captures 100% of the signal from the center field and 87.7% of each extreme fields for a total of 91.8% entering the fiber.

The following are the final design specifications used to build the optical receiver for this experiment.

Fiber Optic:

Fiber optic radius,  $r_{fo} = 0.5\text{-mm}$

Fiber optic Numerical Aperture,  $NA = 0.22$

Maximum half angle,  $\Theta_{\text{Max}} = 12.7^\circ$

Objective Lens:

Lens radius,  $r_{oL} = 0.75\text{-mm}$

Lens focal length,  $f_o = 5.00\text{-mm}$

Radius of curvature,  $R_1 = 2.945$

Radius of curvature,  $R_2 = -19.922$

Numerical Aperture,  $NA = 0.55$

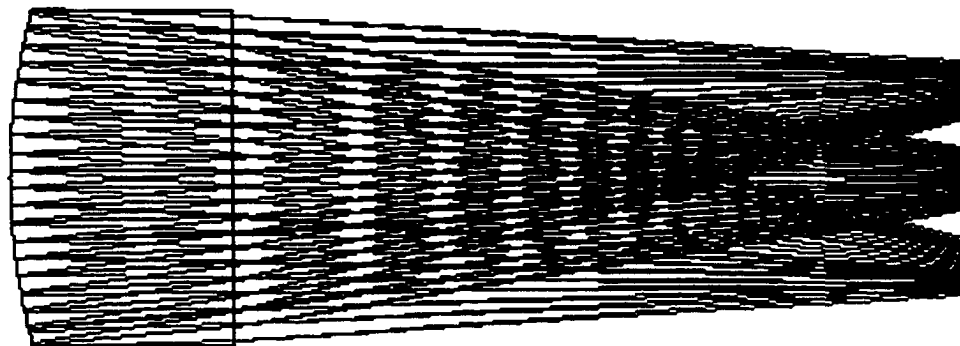
Maximum half angle,  $\text{Theta Max} = 33.4^\circ$

Distances:

Back of lens to front of fiber =  $3.32\text{-mm}$

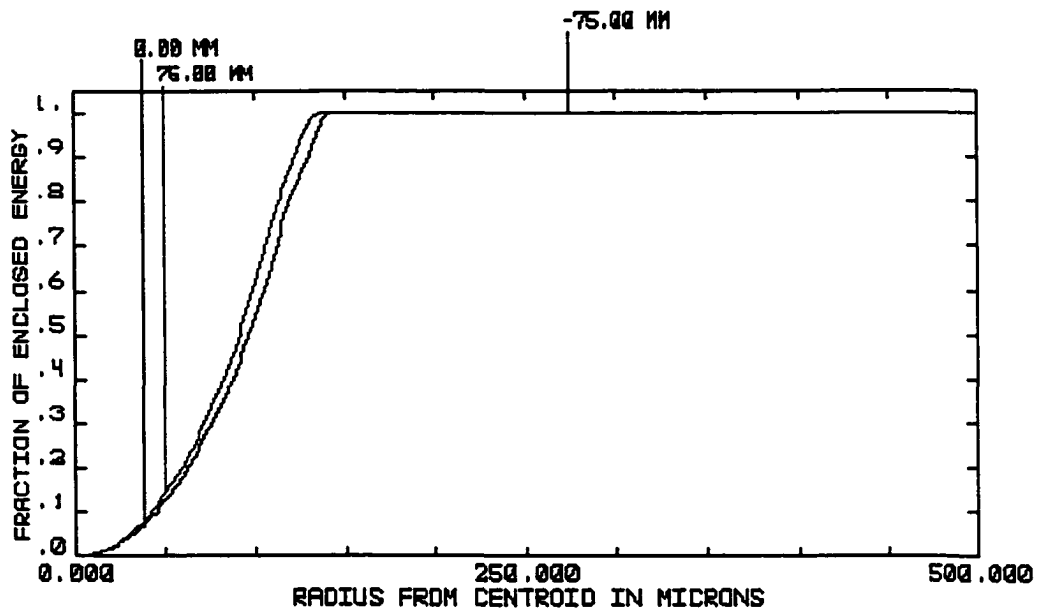
Target to front lens =  $750\text{-mm}$ ,  $375\text{-mm}$ , and  $187.5\text{-mm}$

Radial field of view at target =  $75\text{-mm}$ ,  $37.5\text{-mm}$ , and  $18.8\text{-mm}$



LAYOUT	
1.5-MM LENS FOCUSED ON A FIBER THU MAY 4 2000 TOTAL LENGTH: 4.32000 MM	
	D:\ZEMAX\SAMPLES\SEARS16.ZMX CONFIGURATION 1 OF 1

**Figure 7.3.)** Ray diagram of optical receiver focusing lens onto 1-mm diameter fiber optic




---

GEOMETRIC ENCIRCLED ENERGY

---

1.5-MM LENS FOCUSED ON A FIBER  
 THU MAY 4 2000  
 WAVELENGTH: POLYCHROMATIC  
 DATA HAS BEEN SCALED BY DIFFRACTION LIMIT.

C:\ZEMAX\SAMPLES\SEARS16.ZMX  
 CONFIGURATION 1 OF 1

**Figure 7.4.)** Enclosed energy diagram for optical receiver

---

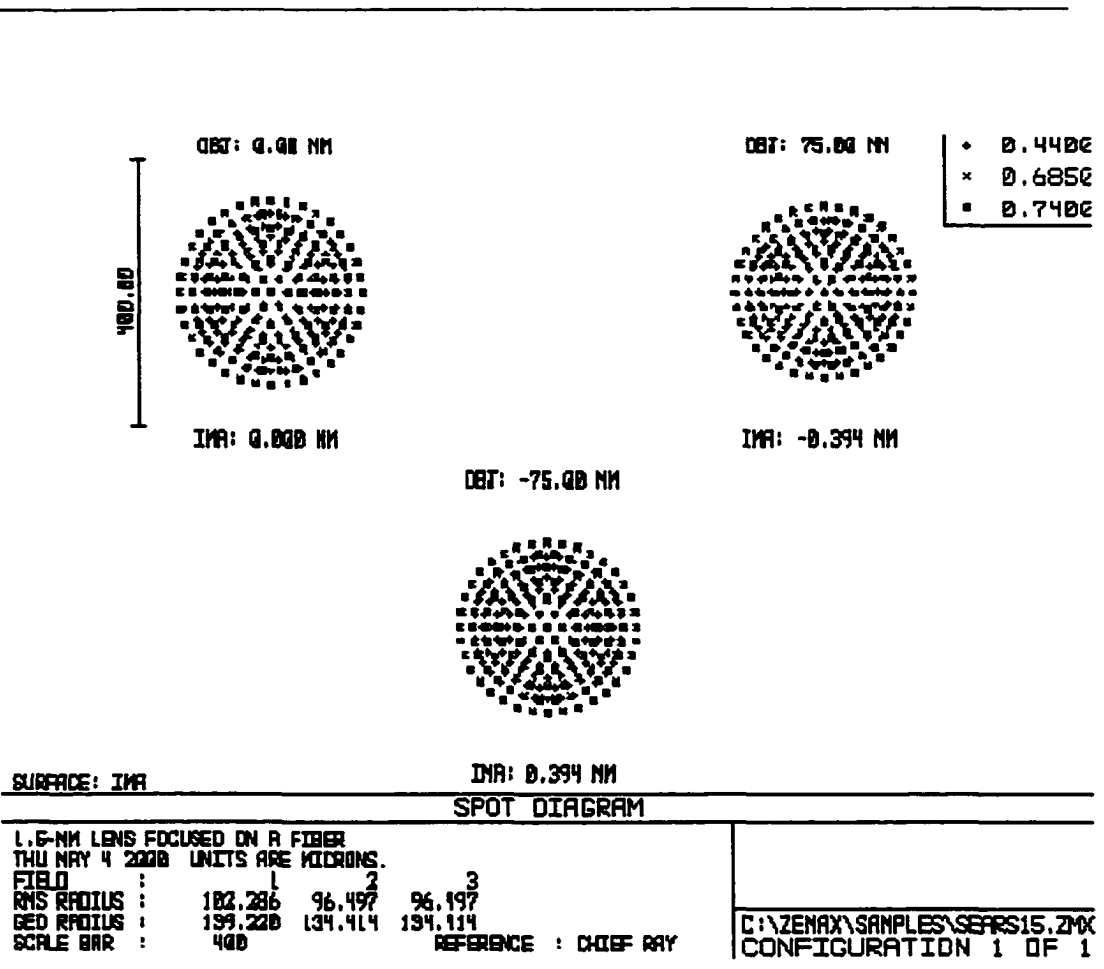


Figure 7.5.) Spot diagram for optical receiver

### **7.3 Data Analysis**

Data analysis focused on answering the following questions: a.) Does the test itself introduce a bias? b.) Does reflectance spectra enable remote nutrient deficiency detection and classification? c.) Does the addition of fluorescence spectra improve stress detection and classification? And d.) What are the effects of spatial and spectral resolution on stress detection?

The first three questions addressed the first primary objective of the study, to investigate the spectral information in reflectance, fluorescence, or a combination of both to predict specific nutrient stresses. The fourth question relates to the second research objective, determining importance of spatial resolution. All four questions were answered using artificial neural networks to process the spectral information collected during experimentation.

Designing the ANN consisted of: 1.) Arranging neurons in various layers; 2.) Deciding the way neurons receive input and produce output; 3.) Selecting a specific training algorithm to allow the network to learn the appropriate values of connection weights based on training data set; and 4.) Using the trained network to process spectral input from a validation set to assess model performance.

The general procedure for determining network architecture for this study was determined as follows. Begin with a network consisting of an input

vector and an output layer. An input vector is connected to each neuron input through a weight matrix. A layer of a network includes the combination of the weights, the multiplication and summing operations, the bias, and the transfer function. A layer that produces network output is called an output layer. All other layers are called hidden layers. The weight matrices connected to inputs is called the input weights and the weight matrices coming from layer outputs is called layer weights.

The number of neurons in the NN layers was set by the number of elements in the input vector and the number of elements in the output layer respectively. A single hidden layer was added. The number of nodes in the hidden layer were varied *via* trial and error while monitoring the network classification performance associated with both the training and validation data sets. Additional hidden layers were added to examine the effect of implementing a larger net; however, in this study a single hidden layer was found to be sufficient for all cases.

MATLAB® (The Math Works Inc.; Natick, MA) with the Neural Network Toolbox was used to create, train, and use the ANN. This ANN was built as a supervised multilayer feedforward network and trained with a backpropagation algorithm. Logistic sigmoid functions were used as the transfer functions throughout the ANN because their output range is zero or one, and they are ideal transfer functions for networks trained on Boolean vectors.

For the smaller networks, COLORBLOCK and 10-nm NN, an automated regularization training algorithm was implemented to improve model generalization. The weights and biases in this training algorithm were assumed to be random variables with specified distributions. The regularization parameters were related to the unknown variances and estimated using statistics in a procedure known as Bayesian regularization (Forsese and Hagan, 1997).

The one step secant training algorithm was implemented for the larger networks, 1-nm NN and 0.1-nm NN, due to insufficiency of computer memory to perform automated regularization training on the larger NN's. The one step secant algorithm does not store the complete Hessian matrix. It assumes that at each iteration the previous Hessian was the identity matrix which allows for the new search direction to be calculated without computing a matrix inverse.

### 7.3.1 Test Bias

The first question addressed was whether the test itself created a bias. The effect of illuminating the crop canopy with a 250-W incandescent spotlight was assumed to be negligible compared to the intensity of growing conditions in the chamber. However, the effect of exposure to the UV spotlight (100-W Xenon lamp) on the test plants was unknown. For each of the two growth cycles, one set of nutrient controls was tested twice as often as the other, these are referred to as the UV and the -UV groups respectively.



The same neural network architecture was used in the following tests as that designed to detect the presence of nutrient stress. The model was presented with both UV and -UV input vectors. If the model could differentiate between the two cases, then a certain degree of bias was present due to the UV illumination. Conversely, if the model was unable to differentiate between the two cases, it could be assumed that the test itself did not introduce any measurable stress conditions in the test crop.

### 7.3.2 Reflectance Spectra

Model input consisted of one temporal parameter, the day of the growth cycle that data were collected, and reflectance spectra from the three optical channels ranging from 370-nm to 1030-nm. An average of three scans was used per specimen to create each input vector. Model output was a five element classification vector for one of five nutrient regimes: 100%N/P, 25%N, 25%P, 5%N, or 5%P. Model performance was validated using spectral information gathered from the second complete growth cycle.

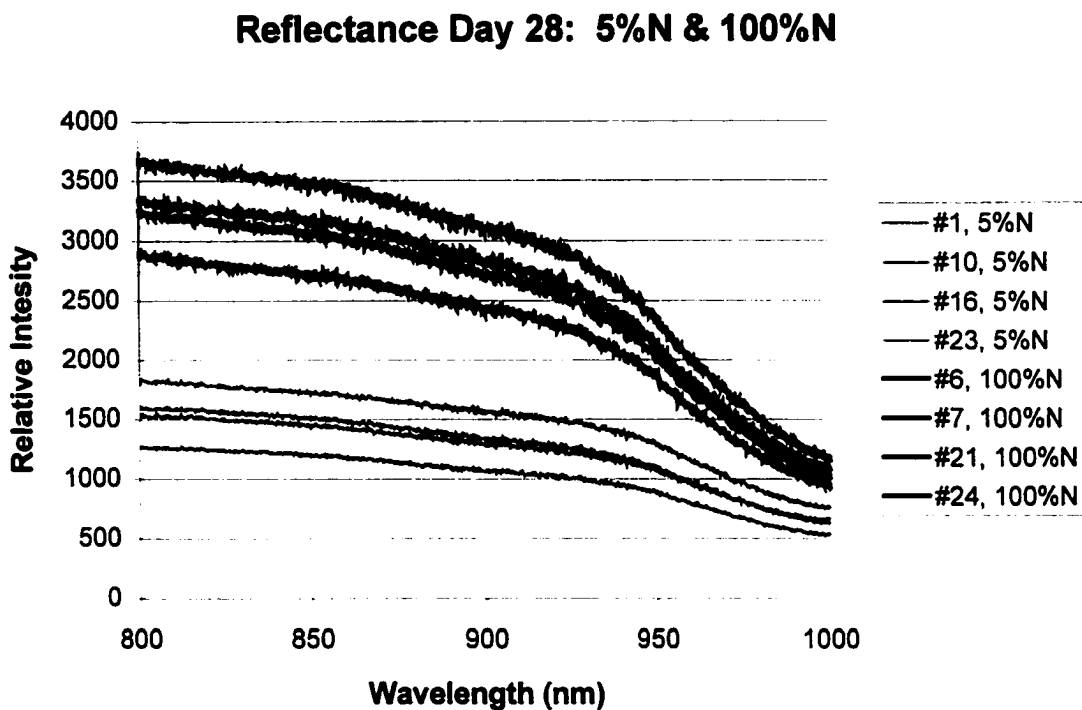
*Figures 7.6a, 7.6b, and 7.6c* show medium spot size ( $D = 7.5\text{-cm}$ ) reflectance spectra for the 5%N and 100%N/P nutrient cases on Day 28 of the growth cycle during Test 1. *Figures 7.8a, 7.8b, and 7.8c* show medium spot size reflectance spectra for the 5%N and 100%N/P cases on Day 32 of Test 1. *Figures 7.6a, 7.6b, 7.8a, and 7.8b* illustrate broadband differences in the red and NIR bands. The 5%N case reflectance from 700 to 1000-nm is

approximately half that of the scattering from the control group in this range. Reflectivity in this range is mainly attributed to plant cell structure and the amount of air between spongy mesophyll in the leaf tissue. Leaves that are small contain less air and scattered less infrared. Accordingly the leaves of the 5%N test group were visibly much smaller than the controls.

*Figure 7.8a* contains an interesting anomaly in the reflectance spectra for the spectrometer master channel. A plot of the raw data for medium FOV on Day 32 (*Figure 7.10*) shows that one of the three scans is much different than the other two. Further investigation of the raw spectra for Channel 1 reflectance spectra unearthed similar outliers; however, for different specimens of test plant suggesting experimental error rather than an actual biological signature. It is believed that the outlier spectra is signal coming directly from the of the lamp rather than scattered back from the canopy. Although each input vector is a result of the average of three scans the outlier remains pronounced as demonstrated in *Figure 7.8a*. Luckily, the frequency of such outliers was found to be approximately one in six hundred scans so the integrity of the neural network training and predictions were not believed to be compromised by this occurrence. However, to safeguard against such outliers, the number of replications should be increased and a data-processing subroutine should be written and implemented to check for a certain degree of variation in each spectral scan. Those having higher than

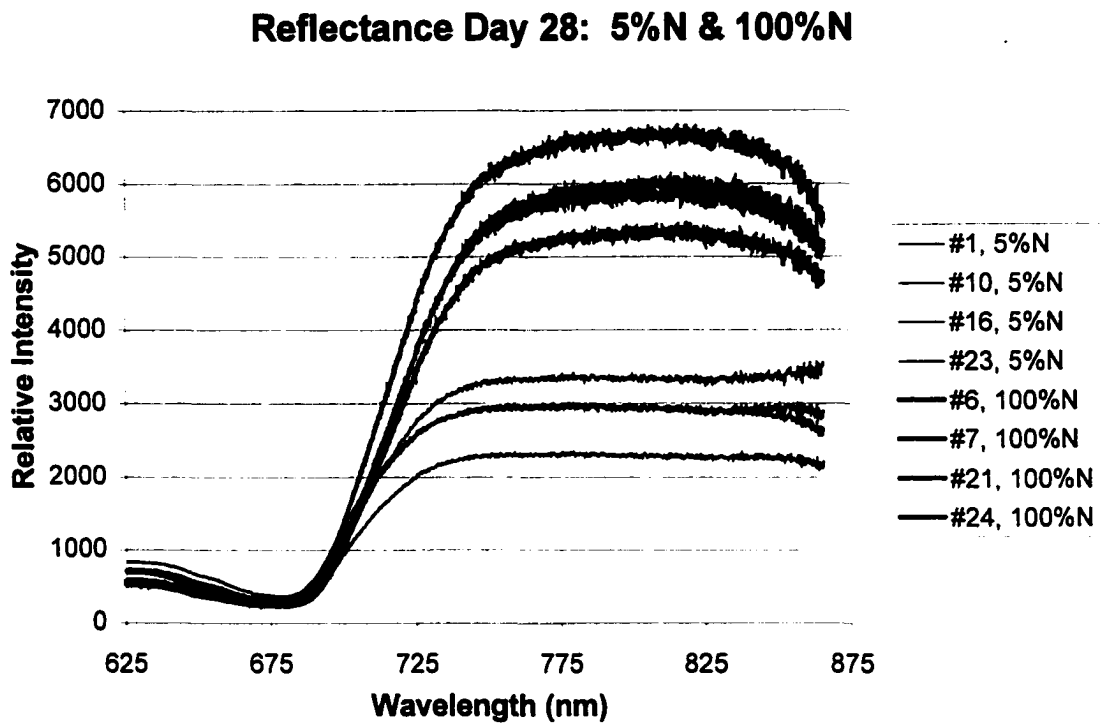
acceptable variation could then be deleted from the neural network training and testing.

Another problem is apparent in reflectance spectra associated with spectrometer channel two. During the growth cycle of the test plant, there was a visible difference between some of the groups with respect to greenness of the plants. The controls were visibly darker green while 5%N plants were visibly more yellowish green; however this difference in spectral quality was not consistently represented in the reflectance data. Figures 7.7 and 7.9 show plots of the blue:green, yellow:green, and red:green color ratios for reflectance data on Day 28 and Day 32 of Test 1. Values for colors are taken as the summation of specific points collected by spectrometer channel two. Blue is the summation of points at 475-nm. Green is the summation of points at 510-nm. Yellow is the summation of points in the 570-nm range. Red is the summation of points in the 650-nm range. The two plots of the blue:green, yellow:green, and red:green ratios in *Figures 7.7* and *7.9* support the inconsistency of spectral quality in the visible range that is demonstrated in *Figures 7.6c* and *7.8c*. This level of inconstancy was unexpected as a reliable measure of greenness was believed to be paramount for classification of nutrient deficiency.



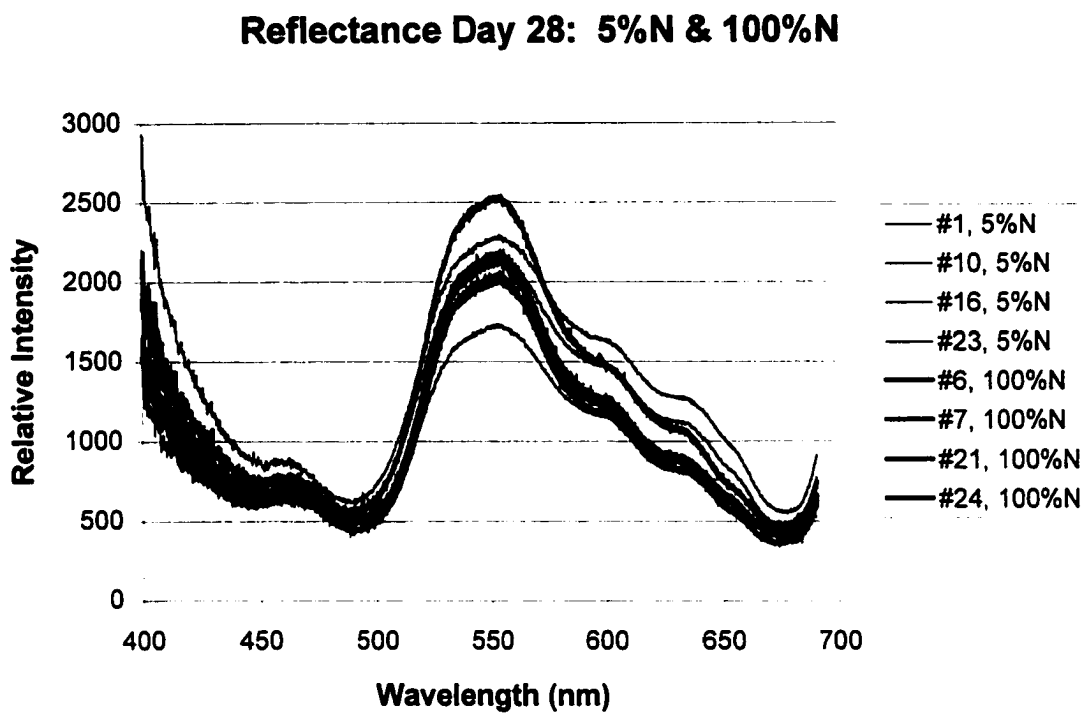
a.)

**Figure 7.6a.)** Reflectance spectra of medium spot size on Test Day 28 of Test 1. Spectrometer Channel 1, 800 to 1000-nm.



b.)

**Figure 7.6b.)** Reflectance spectra of medium spot size on Test Day 28 of Test 1. Spectrometer Channel 2, 625 to 865-nm.



c.)

**Figure 7.6c.)** Reflectance spectra of medium spot size on Test Day 28 of Test 1. Spectrometer Channel 3, 400 to 690-nm.

---

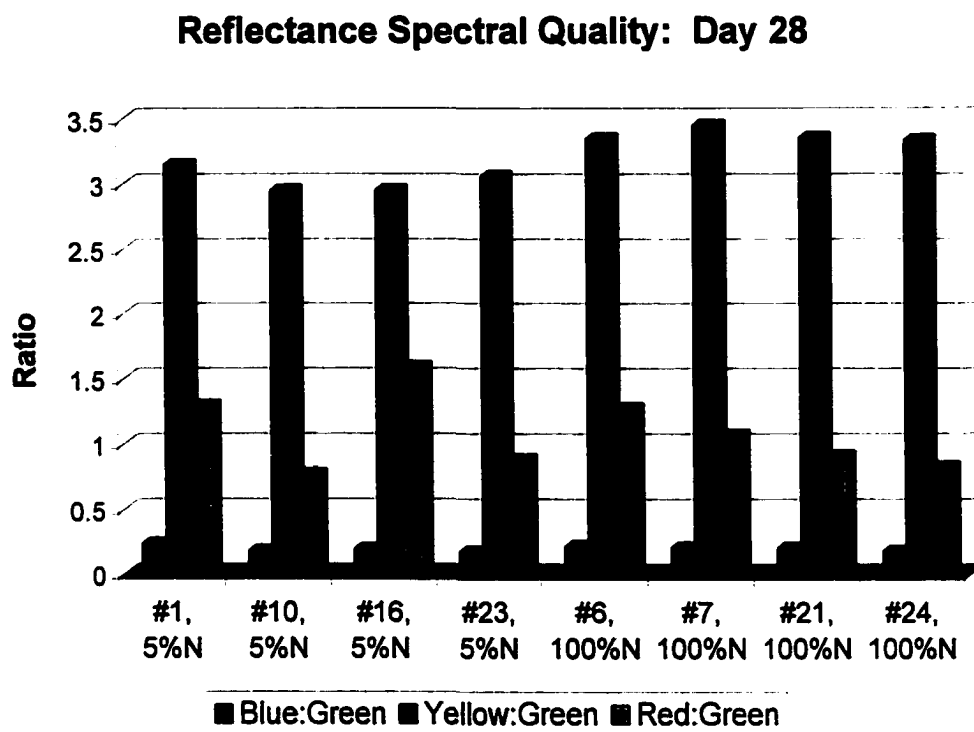
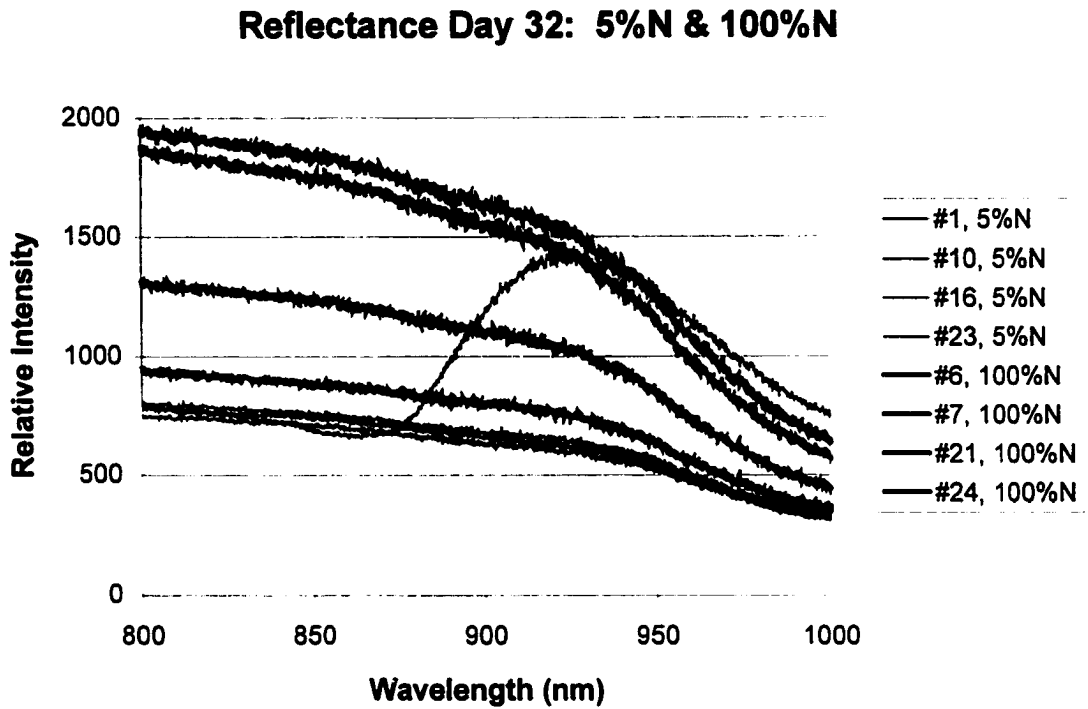


**Figure 7.7.)** Spectral quality for medium spot size FOV on Day 28 of Test 1.

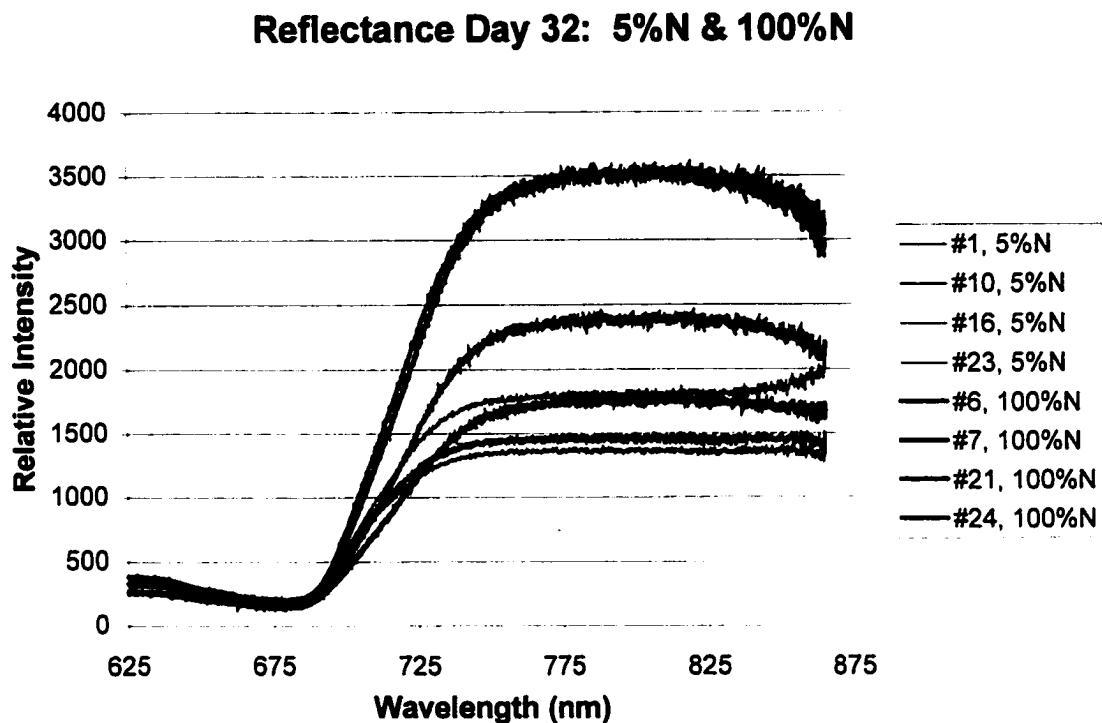
---



a.)

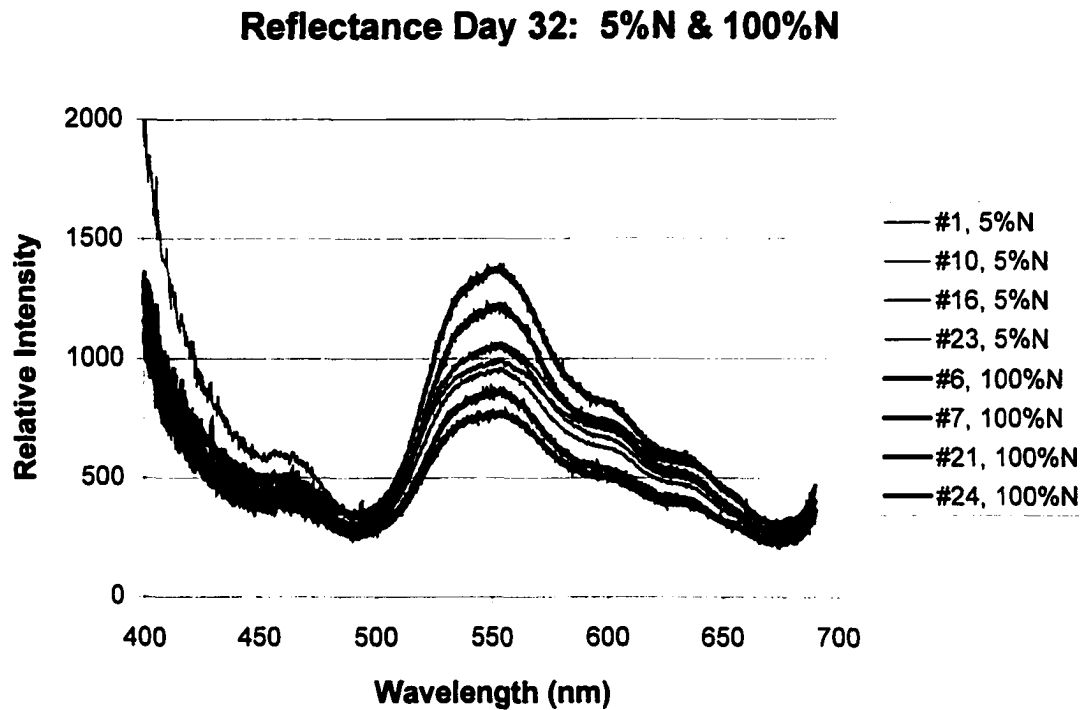
**Figure 7.8a.)** Reflectance spectra of medium spot size on Test Day 32 of Test 1. Spectrometer Channel 1, 800 to 1000-nm.





b.)

**Figure 7.8b.)** Reflectance spectra of medium spot size on Test Day 32 of Test 1. Spectrometer Channel 2, 625 to 865-nm.



c.)

**Figure 7.8c.)** Reflectance spectra of medium spot size on Test Day 32 of Test 1. Spectrometer Channel 3, 400 to 690-nm.

---

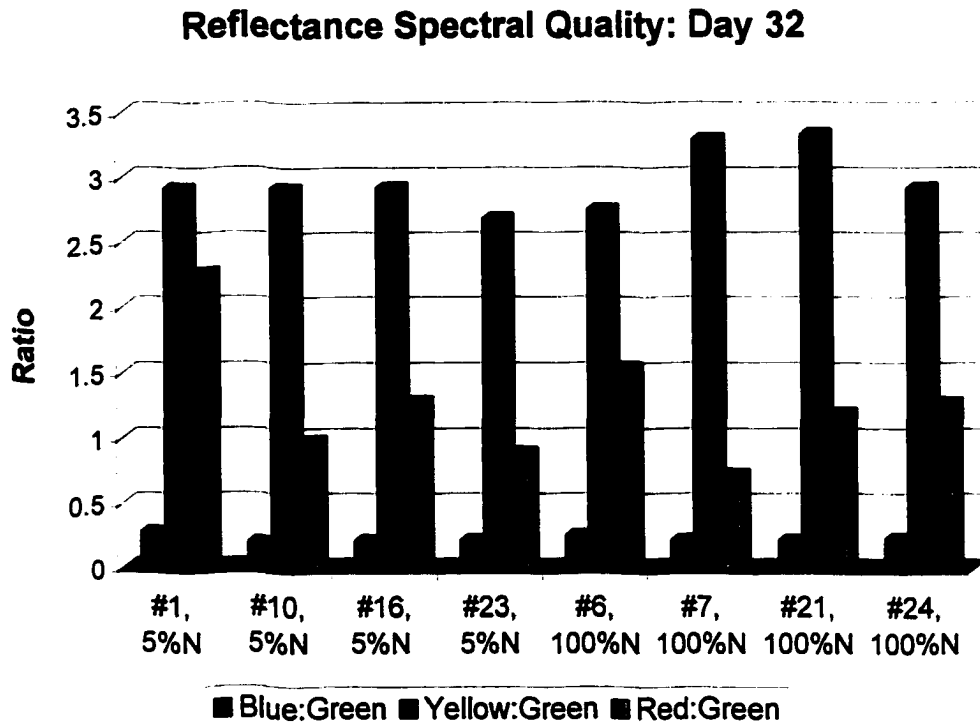


**Figure 7.9.)** Spectral quality for medium spot size FOV on Day 32 of Test 1.

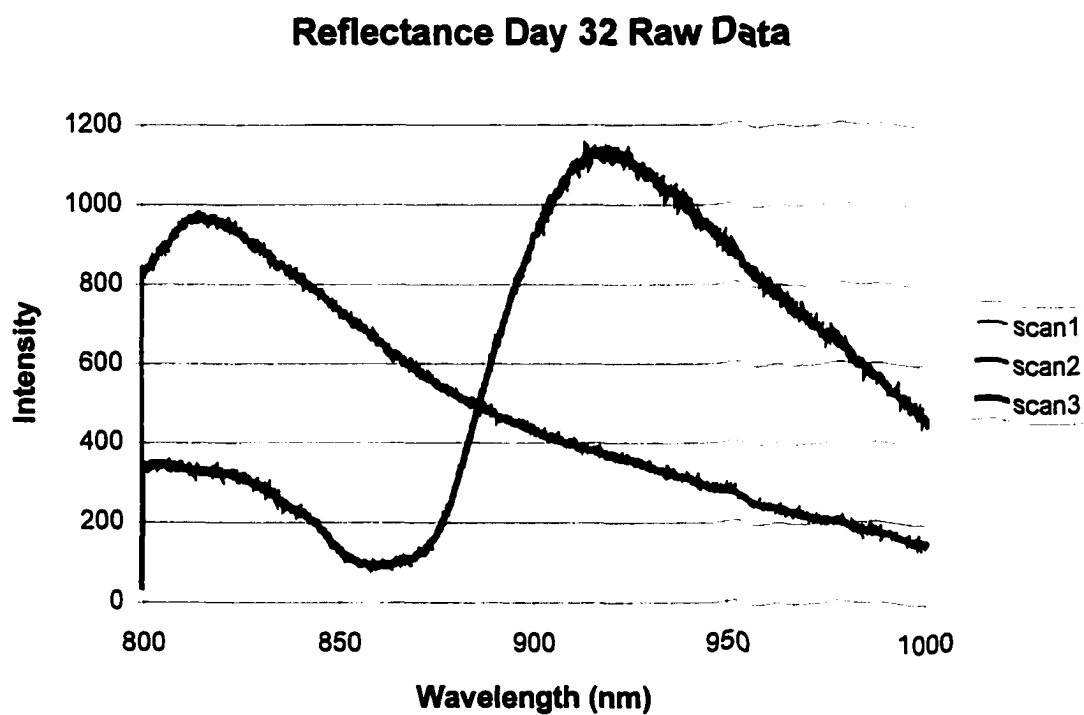


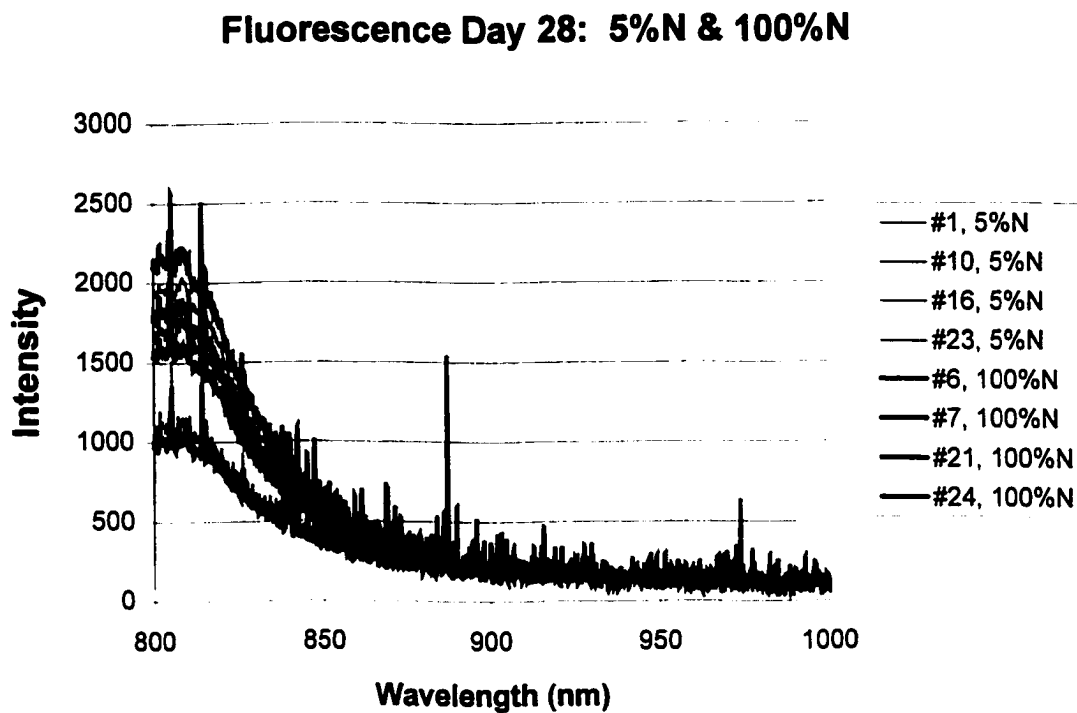
**Figure 7.10.)** Raw data of spectrometer Channel 1 for reflectance of medium FOV on Day 32 of Test 1.

---

### 7.3.3 Fluorescence Spectra

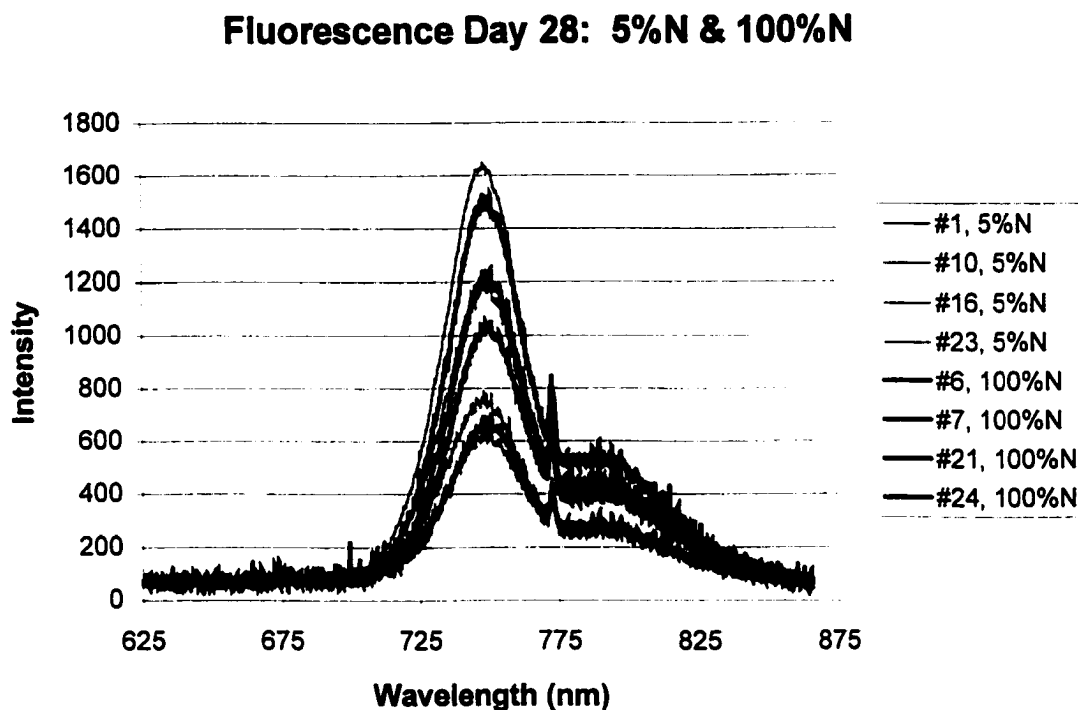
Model input included one temporal parameter, the day of the growth cycle, and fluorescence spectra from 370-nm to 1030-nm. An average of three scans was used to create each input vector. Model output was a five element classification vector for one of five nutrient regimes: 100%N/P, 25%N, 25%P, 5%N, or 5%P. Model performance was validated for comparison using spectral information gathered from the second complete growth cycle.

*Figures 7.11a, 7.11b, and 7.11c* show fluorescence spectra from medium size spot sizes on Day 28 of Test 1. *Figures 7.12a, 7.12b, and 7.12c* show fluorescence spectra from medium size spot sizes on Day 32 of Test 1. Data for day 32 shows a clear distinction between the controls and 5%N for three of the four specimens, but fluorescence spectra was fairly inconsistent with respect to classification based on relative intensity. Based on output from the spectrometer Channel 1 and Channel 2, the fluorescent emission was greater for the controls than for the 5%N case. The greatest fluorescent peaks at 750-nm and 800-nm were also associated with the controls. This is possibly due to the larger leaf area index of the control plants compared to the extreme, 5%, nitrogen treatment. Fluorescence data from spectrometer Channel 3 was found to be of little value as the biological spectral signatures were overlapping and obscured by noise.



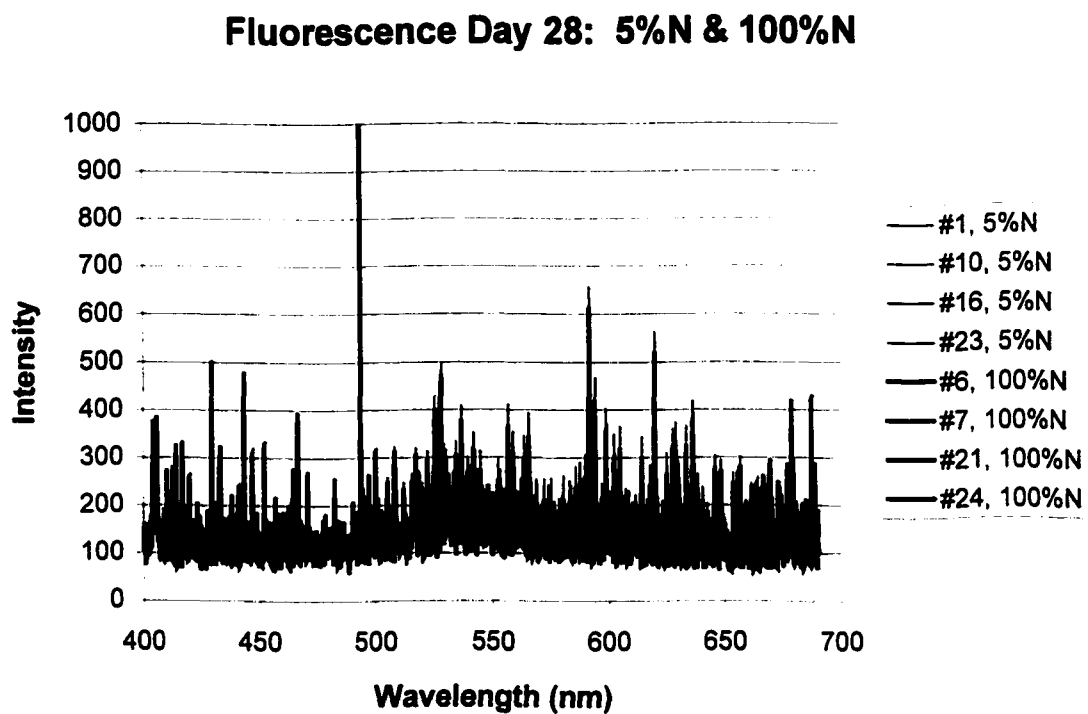
a.)

**Figure 7.11a.)** Fluorescence spectra of medium spot size on Test Day 28 of Test 1. Spectrometer Channel 1, 800 to 1000-nm.



b.)

**Figure 7.11b.)** Fluorescence spectra of medium spot size on Test Day 28 of Test 1. Spectrometer Channel 2, 625 to 865-nm.

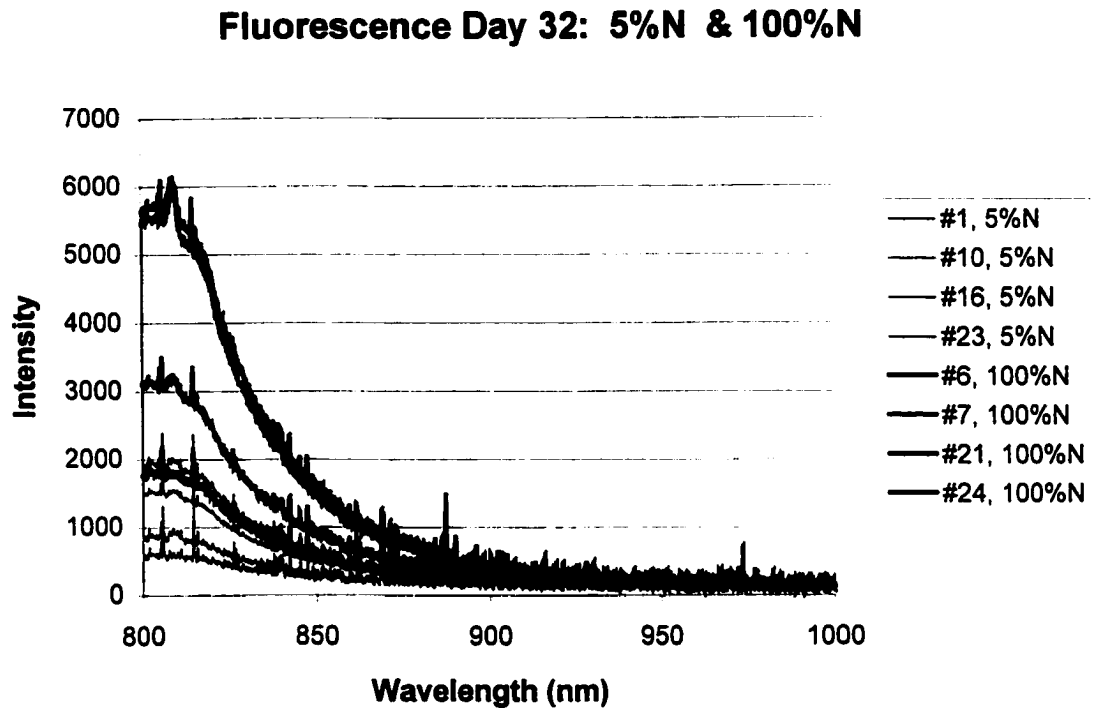


c.)

**Figure 7.11c.)** Fluorescence spectra of medium spot size on Test Day 28 of Test 1. Spectrometer Channel 3, 400 to 690-nm.

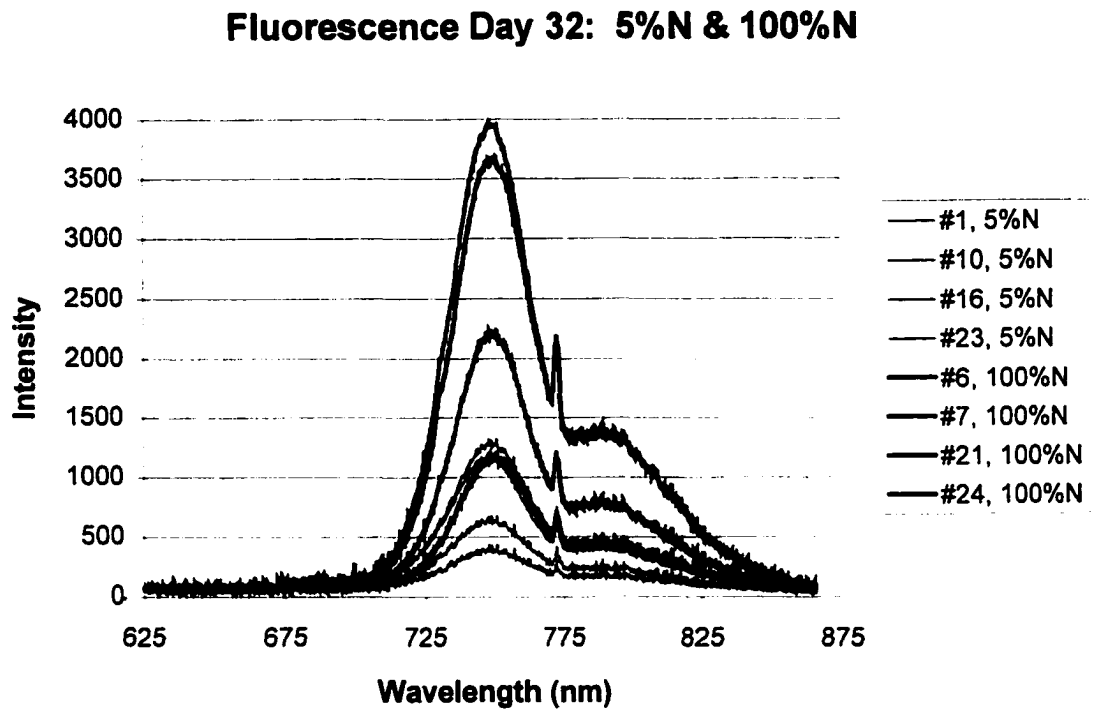
---





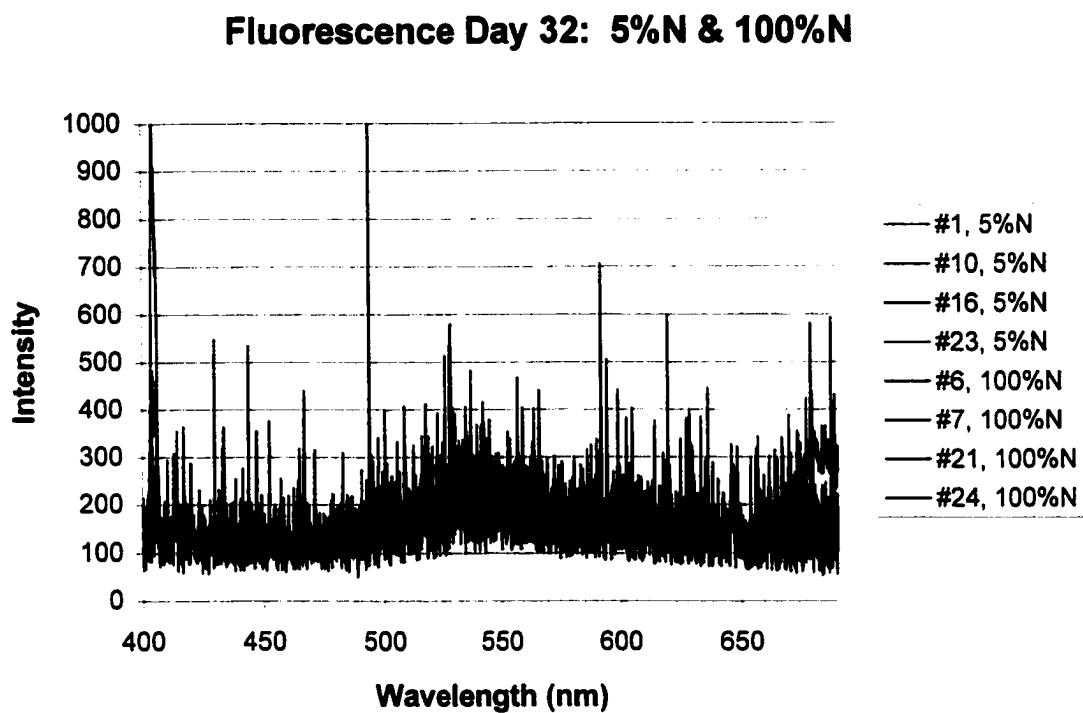
a.)

**Figure 7.12a.)** Fluorescence spectra of medium spot size on Test Day 32 of Test 1. Spectrometer Channel 1, 800 to 1000-nm.



b.)

**Figure 7.12b.)** Fluorescence spectra of medium spot size on Test Day 32 of Test 1. Spectrometer Channel 2, 625 to 865-nm.



c.)

**Figure 7.12c.)** Fluorescence spectra of medium spot size on Test Day 32 of Test 1. Spectrometer Channel 3, 400 to 690-nm.

---

### 7.3.4 Combination of Reflectance and Fluorescence Spectra

Model input included one temporal parameter, reflectance spectra (370-nm to 1030-nm), and fluorescence spectra (370-nm to 1030-nm). An average of three scans was used to construct each spectral input vector. Since this combination of input represented the most complex network used in this study, NN architecture was designed for this case and then used for the other cases as well. Output consisted of a five element classification vector. Model performance was validated by comparison using spectral information gathered from the second complete growth cycle.

The spectral wavelengths found to be most important in information content for reflectance were the broadband red and near infrared regions, 700 to 1 000-nm. For fluorescence the most significant regions were found to be between 700 and 850-nm. Sensitivity of the spectrometer Channel 3, visible light, is believed to be partially responsible for the inconsistency of the majority of the spectral quality information for blue, yellow, and green reflectance and fluorescence. Perhaps more importantly, however, are the effects of canopy structure and leaf angle which were found to obscure the more subtle differences in spectral quality as a function of nutrient condition. Nitrogen deficiency was expected to be associated with yellowing and phosphorous deficiency with darker green leaves. The effects of canopy structure and leaf angle are addressed in more detail in Section 8.

### 7.3.5 Spatial Resolution

Spatial resolution was examined by collecting spectra at three different distances from the canopy during experimentation. Small, 3.75-cm (1.5-in), Medium, 7.5-cm (3.0-in), and Large, 15-cm (6-in), diameter spot sizes were accomplished by varying distance to the target. Distances of 19-cm (7.5-in), 38-cm (15-in), and 76-cm (30-in) were used to achieve the small, medium and large diameter spots, respectively. Spectrometer integration time was adjusted according to distances to target.

For reflectance data, the integration times were 38-ms, 75-ms, and 150-ms for the closest, middle, and farthest ranges, respectively. For fluorescence data, the integration times were also set as a function of each of the three spectrometer channels. For Channel 1 (796-1 030nm), integration times were: 2 500-ms, 5 000-ms, and 10 000-ms for the closest, middle, and farthest ranges, respectively. For Channel 2 (604-865nm), integration times were: 625-ms, 1 250-ms, and 2 500-ms for the closest, middle, and farthest ranges. For Channel 3 (370-690nm), integration times were also: 2 500-ms, 5 000-ms, and 10 000-ms for closest, middle, and farthest ranges, respectively.

### 7.3.6 Spectral Resolution

The effect of spectral resolution was determined by creating four models with varying levels of resolution in the input spectra. The types of

ANN's created represent ultra low-resolution, medium resolution, high resolution and ultra high systems

For the ultra low resolution neural net, COLORBLOCK, spectral information was divided into five broad spectral bands: UV (370-399nm), blue (400-499nm), green (500-599nm), red (600-699nm), and NIR (700-1030nm). These broad spectral bands were selected by assigning 100-nm blocks for blue, green, and red and creating single blocks for all UV and all NIR data. A single value was calculated for each band by taking the summation across the spectral range of the band. The input vector was normalized to have zero mean and unity standard deviation. One temporal parameter and five spectral bands provided COLORBLOCK with a six element input vector for both the reflectance and the fluorescence neural networks. An eleven element input vector was the input for COLORBLOCK when trained with both reflectance and fluorescence bands of spectra.

The medium resolution model, 10-nm NN, was created using input spectra with 10-nm resolution. Each spectrometer channel collected 2 048 data points totaling 6 144 points for all three channels (370-nm to 1 030-nm). These points were summed into blocks of 100 points or 21 blocks per channel. For three channels this yielded 63 input points. Including growth cycle day, reflectance model input consisted of a 64 element vector for each specimen. Input to the 10-nm NN fluorescence model was a 64 x 1 column

vector for each specimen. Input to the 10-nmNN using both reflectance and fluorescence data consisted of a 127 x 1 input vector for each specimen.

The high resolution model, 1-nm NN, was created using input spectra with 1-nm resolution. Each spectrometer channel collected 2 048 data points totaling 6 144 points for all three channels (370-nm to 1030-nm). These points were summed into blocks of 10 points or 205 blocks per channel. For three channels this yielded 615 input points. Including growth cycle day, reflectance model input consisted of a 616 element vector for each specimen. Input to the 1-nm NN fluorescence model was a 616 x 1 column vector for each specimen. Input to the 1-nmNN using both reflectance and fluorescence data consisted of a 1 231 x 1 input vector for each specimen.

The ultra high-resolution neural net, 0.1-nm NN, was trained using detailed spectrum ( $\Delta\lambda\approx 0.1\text{nm}$ ). Each spectrometer channel collected 2 048 data points totaling 6 144 points for all three channels (370-nm to 1030-nm). Including growth cycle day, reflectance model input consisted of a 6 145 element vector for each specimen. Input to the 0.1-nm NN fluorescence model was a 6 145 x 1 column vector for each specimen. The input to the 0.1-nm NN net trained on both reflectance and fluorescence spectra was a 12 289 x 1 column vector for each specimen. For a single test there were 20 specimens analyzed for twelve days creating a 12 289 x 240 input matrix for the 0.1-nm NN temporal, reflectance, fluorescence NN.

## 8. Results and Conclusions

### 8.1 Plant Cultivation

On Day 36 of the growth cycle, all test plants were harvested and weighed. *Figure 8.1* shows the effect of the different nutrient regimes on average fresh mass of the test plants.

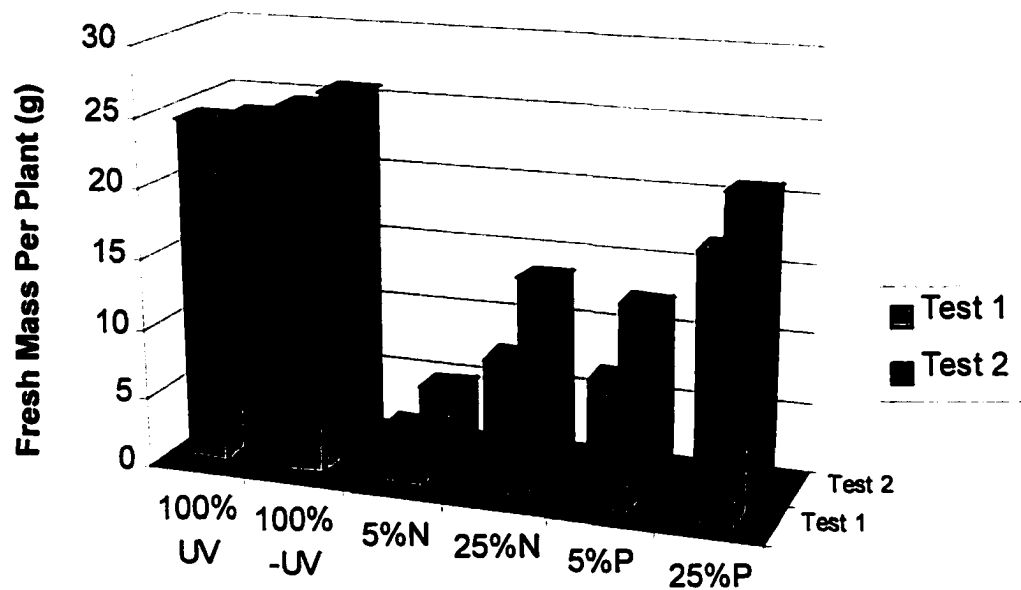


**Figure 8.1.)** Effect of nutrient deficiency on average fresh mass.

Nutrient deficiency symptoms in plants are the expression of metabolic disorders resulting from an insufficient supply of an essential element. These



disorders are, in turn, related to the roles played by essential elements in normal plant metabolism and function (Taiz and Zeiger, 1991). The experimental data trend is the same for both Tests 1 and 2 in that nutrient controls were the largest plants averaging 23 to 26-g per plant. The next largest plants were 25%P, averaging 18 to 20-g per plant. The 25%N and 5%P were approximately the same size between 9 and 14-g, and the 5%N regime resulted in dramatically small sizes, <5-g per plant. Plant size, structure, and color was expected to be correlated with nitrogen and phosphorous availability. Nitrogen is a constituent of amino acids, amides, proteins, nucleic acids, nucleotides, coenzymes, and hexosamines. Phosphorous is a component of sugar phosphates, nucleic acids, nucleotides, coenzymes, phospholipids, and phytic acid. Since nitrogen is associated with many plant cell components, such as amino acids and nucleic acids, it is not surprising that a characteristic deficiency symptom is stunted growth. Phosphorous has a key role in reactions in which ATP is involved (Taiz and Zeiger, 1991). Since phosphorous is an integral component of a number of the sugar phosphates used in respiration and photosynthesis and of the phospholipids making up plant membranes, plants deficient in this nutrient were expected to be smaller as well.

A paired two sample t-Test for means was performed to determine if sample means were significantly different. These results are shown in *Table 8.1*. For Test 1 there were significant differences, two tailed p-values <0.05,

among all test conditions except UV and -UV controls and between 25%N and 5%P nutrient treatments. Results were the same for Test 2, with the addition of no significant difference occurring between 25%P nutrient regime and the UV nutrient control. A comparison between Test 1 and Test 2 showed there to be no significant difference between 100% UV, between 100% -UV, or between the 25% P groups. However, average plant size was significantly different for the 5%N, 25%N, and 5%P nutrient regimes. Fresh mass results may have more clearly represented nutrient status if pH had been held more constant and overcrowding conditions had been more fully ameliorated.

Based on fresh mass values and visual inspection, distinguishing between control groups and 25%P was difficult. Similarly distinguishing between the 25%N and 5%P based on plant size, shape, and color was also difficult. This is most likely due to the recommended concentration of phosphorous and nitrogen being greatly exaggerated by the hydroponic growers manual (Wells, 1995). The only clearly visible differentiable groups of test plants were the controls and the 5%N nutrient conditions.

Differences in color, i.e. visible light scattering, were expected to be more readily correlated with nitrogen and phosphorous deficiency. In many plants the first symptom of nitrogen deficiency is chlorosis (yellowing of the leaves), especially in the older leaves which become completely yellow and then fall off the plant. Younger leaves may not show these symptoms initially

because nitrogen can be mobilized from older leaves (Taiz and Zeiger, 1991).

Often the first symptom of phosphorous deficiency is stunted growth with a dark green coloration in the leaves, however this was not seen in the test plant, *Lactuca Sativa*, 'Ostinata', cultivated for this particular study.

**Table 8.1.) Paired two sample t-Test for means, 2-tailed p-values, where values <0.05 are considered significantly different.**

Test 1	100% -UV 26.08-g	100% UV 24.78-g	5%N 4.13-g	25%N 9.87-g	5%P 9.18-g	25%P 18.76
100% -UV	—					
100% UV	0.459	—				
5%N	0.001	0.000	—			
25%N	0.002	0.001	0.009	—		
5%P	0.001	0.000	0.002	0.371	—	
25%P	0.022	0.005	0.001	0.021	0.007	—

Test 2	100% -UV 25.78-g	100% UV 23.53-g	5%N 4.80-g	25%N 13.56-g	5%P 12.34-g	25%P 20.82-g
100% -UV	—					
100% UV	0.234	—				
5%N	0.000	0.000	—			
25%N	0.000	0.005	0.002	—		
5%P	0.001	0.002	0.000	0.278	—	
25%P	0.041	0.368	0.003	0.020	0.024	—

Test 1 -vs- Test 2

Case	p-value
100% -UV	0.728
100% UV	0.329
5%N	0.024
25%N	0.030
5%P	0.004
25%P	0.258

## **8.2 Test Bias**

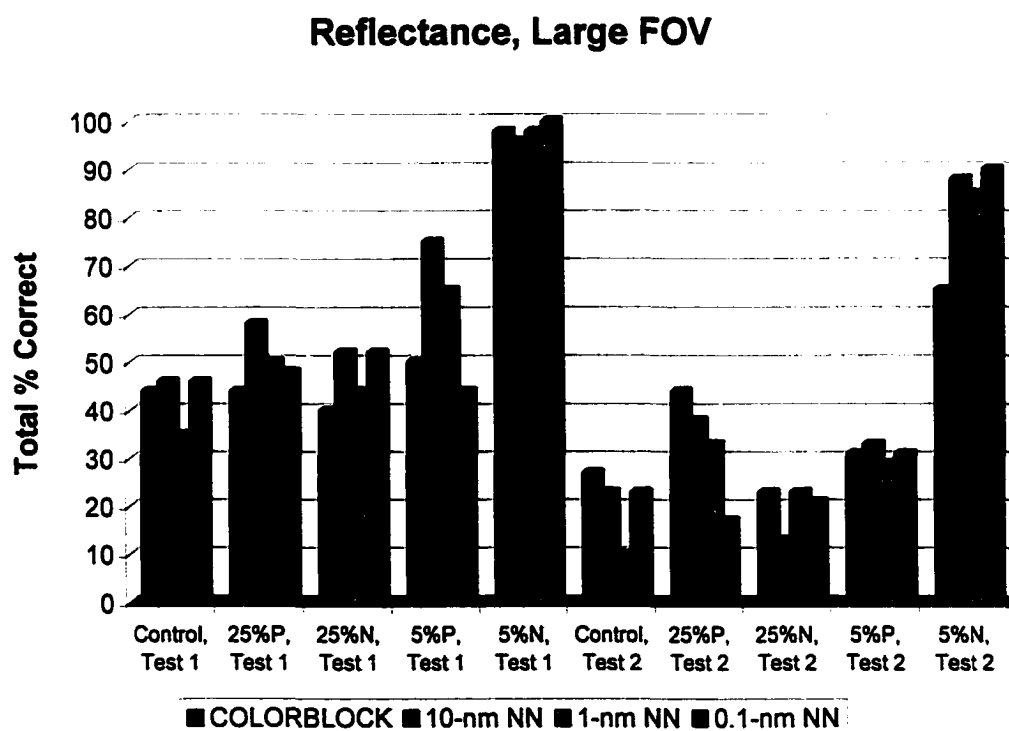
Although average fresh mass for -UV plants was slightly higher (1-g and 2-g) than the UV plants this difference was not found to be statistically significant. The reason for a slight difference in mass could be attributed to random differences or to the removal of the plants from the hydroponic bay during testing. Over the course of the entire test this amounted to approximately three additional hours or 0.3% of the total growth cycle, that the -UV group spent in the nutrient bath versus the UV group.

The COLORBLOCK neural network trained on -UV versus UV vectors was unable to differentiate. COLORBLOCK consistently gave equal weight to both elements in the two-element classification output vector. Specifically, for all days and all specimens the output classification vector was [0.5, 0.5]. Therefore it was assumed that the test itself imposed no bias.

## **8.3 Neural Net Output**

*Figures 8.2, 8.3, and 8.4* show the neural network classification results for all four modes of input vector resolution. Results are plotted as a function of the optical receiver field of view: Large, Medium, and Small. The Large field of view collected spectra from 3.4 plants, Medium from 0.8 plants, and Small from 0.2 plants. In general the Medium spot size was associated with the best validation classification results, although the differences between the

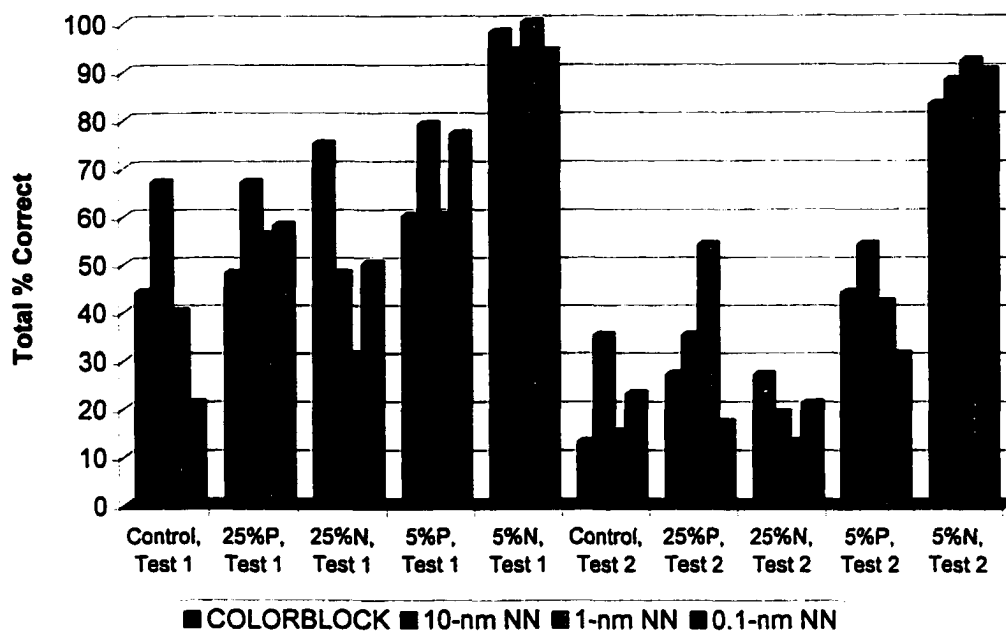
Large and Medium spot sizes were minimal. This represents the trade off associated with increased signal and elevated noise gained over longer integration times and greater distances from canopy to optical receiver. The Small , 0.2, spot size was generally associated with poorer model classification results especially for the cases where both reflectance and fluorescence spectra were implemented as the network input vector.



a.)

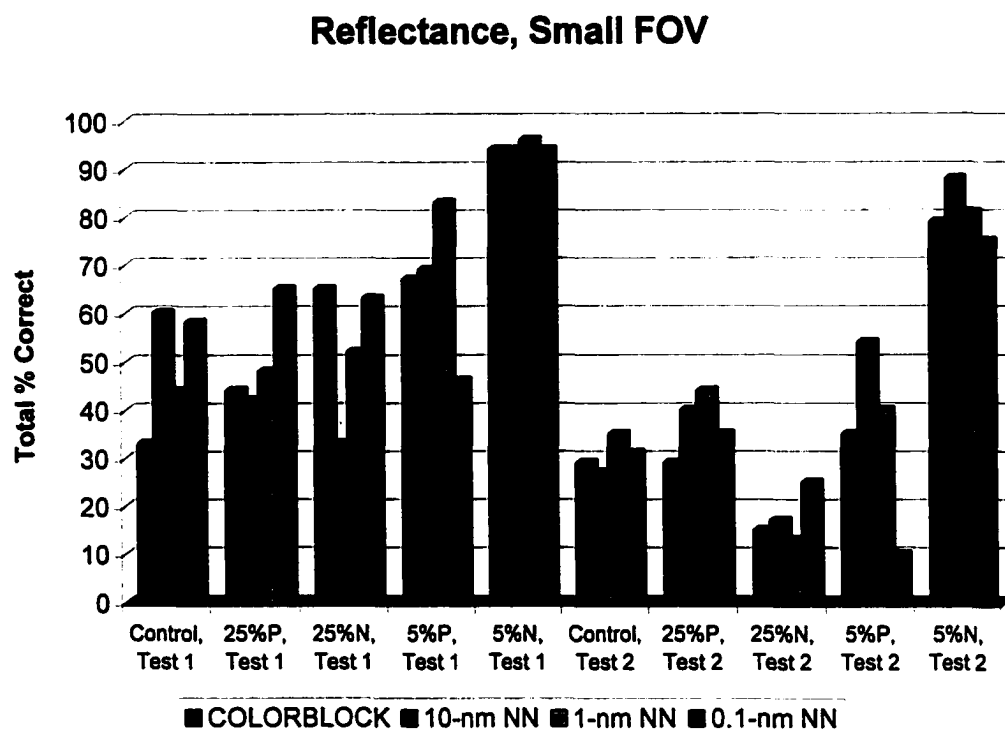
**Figure 8.2a.)** Results of neural networks using reflectance spectra as input vector for Large Field Of View (FOV), Diameter = 15-cm.

### Reflectance, Medium FOV



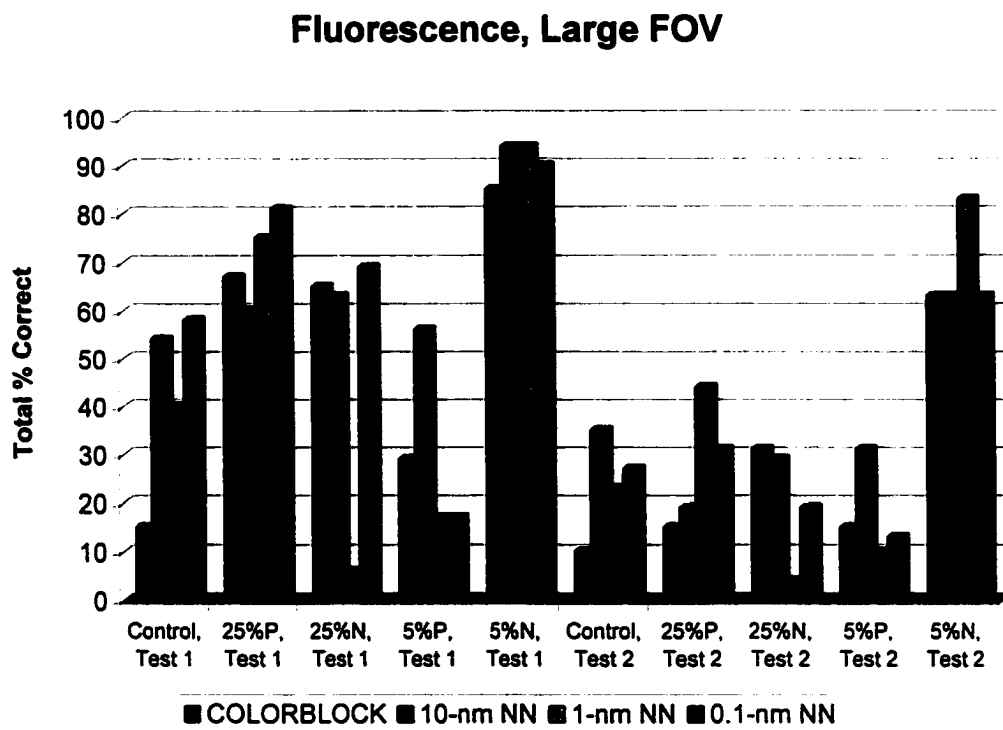
b.)

**Figure 8.2b.)** Results of neural networks using reflectance spectra as input vector for Medium Field Of View (FOV), Diameter = 7.5-cm.



c.)

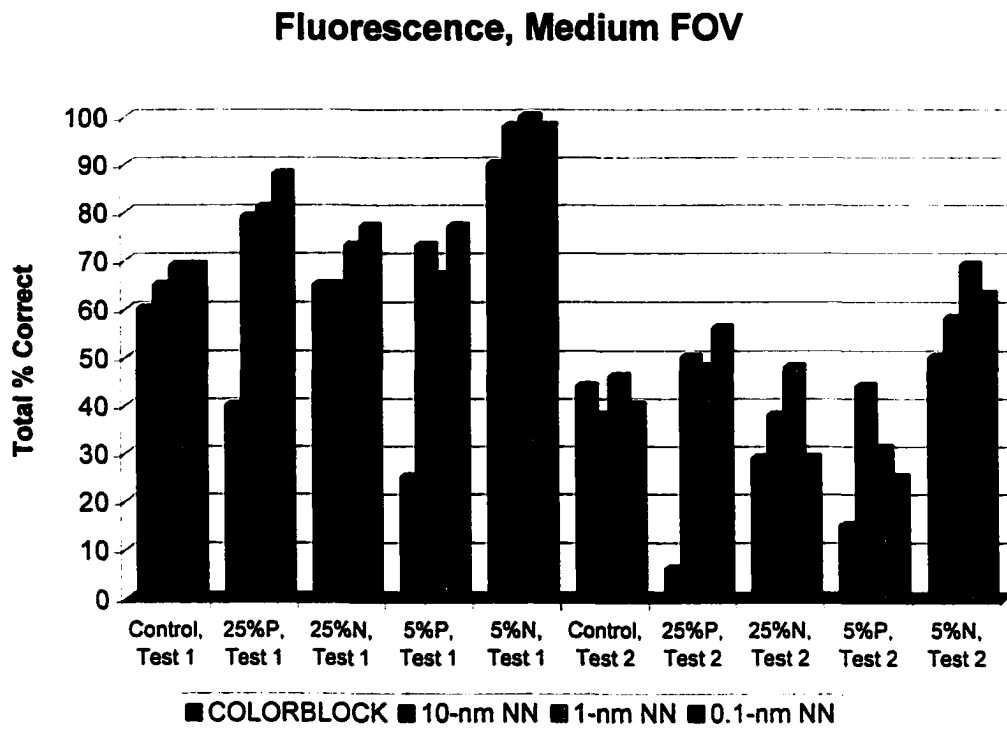
**Figure 8.2c.)** Results of neural networks using reflectance spectra as input vector for Small Field Of View (FOV), Diameter = 3.75-cm.



a.)

**Figure 8.3a.)** Results of neural networks using fluorescence spectra as input vector for Large Field Of View (FOV), Diameter = 15-cm.

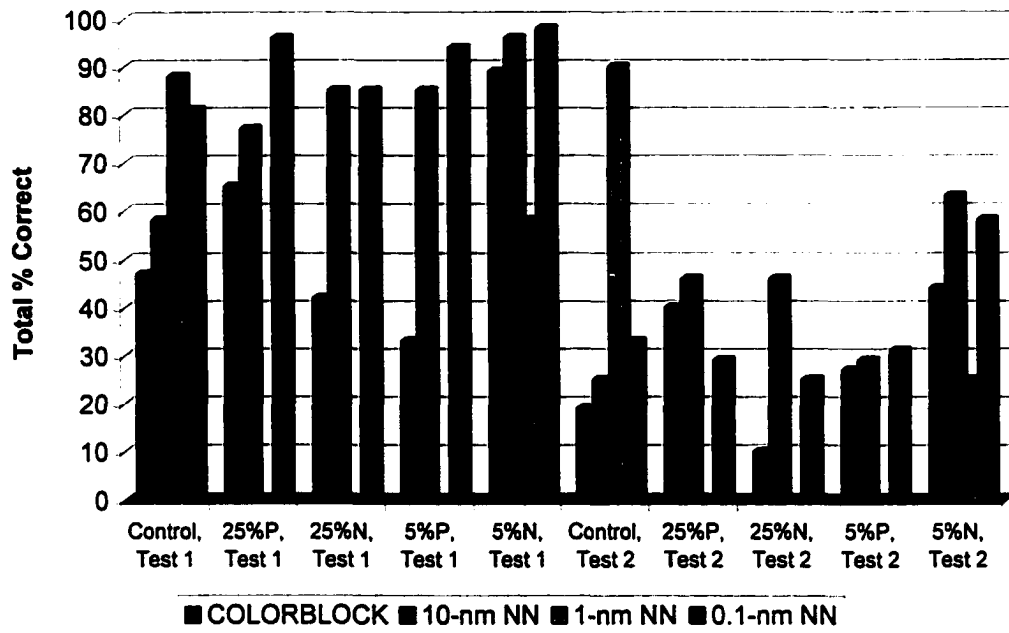




b.)

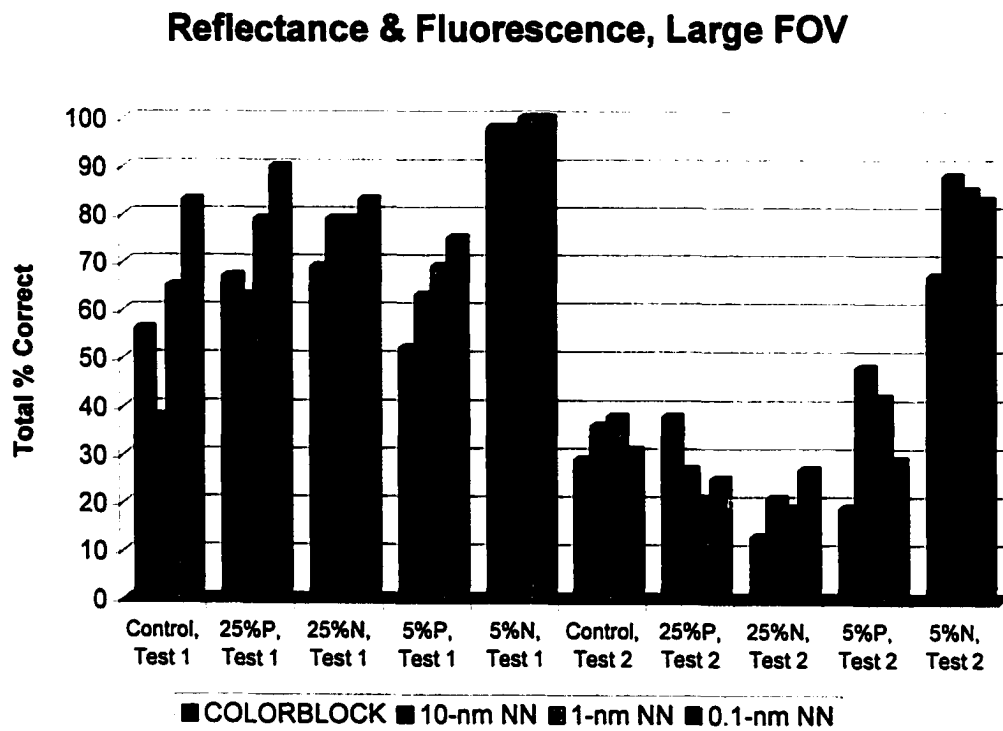
**Figure 8.3b.)** Results of neural networks using fluorescence spectra as input vector for Medium Field Of View (FOV), Diameter = 7.5-cm.

### Fluorescence, Small FOV



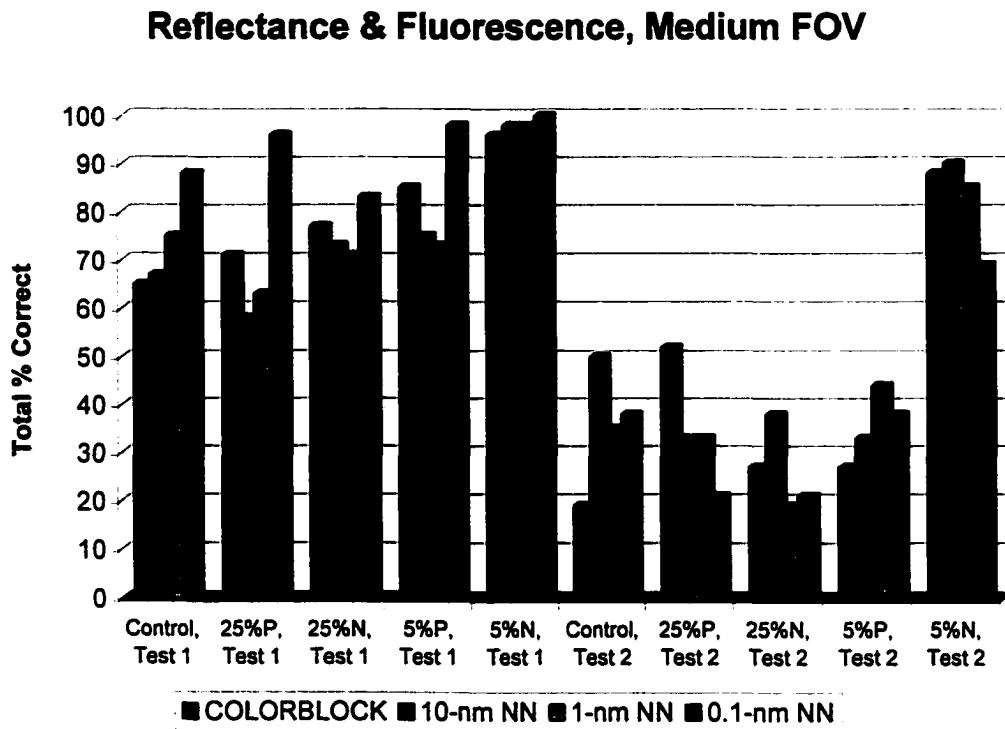
c.)

**Figure 8.3c.)** Results of neural networks using fluorescence spectra as input vector for Small Field Of View (FOV), Diameter = 3.75-cm.



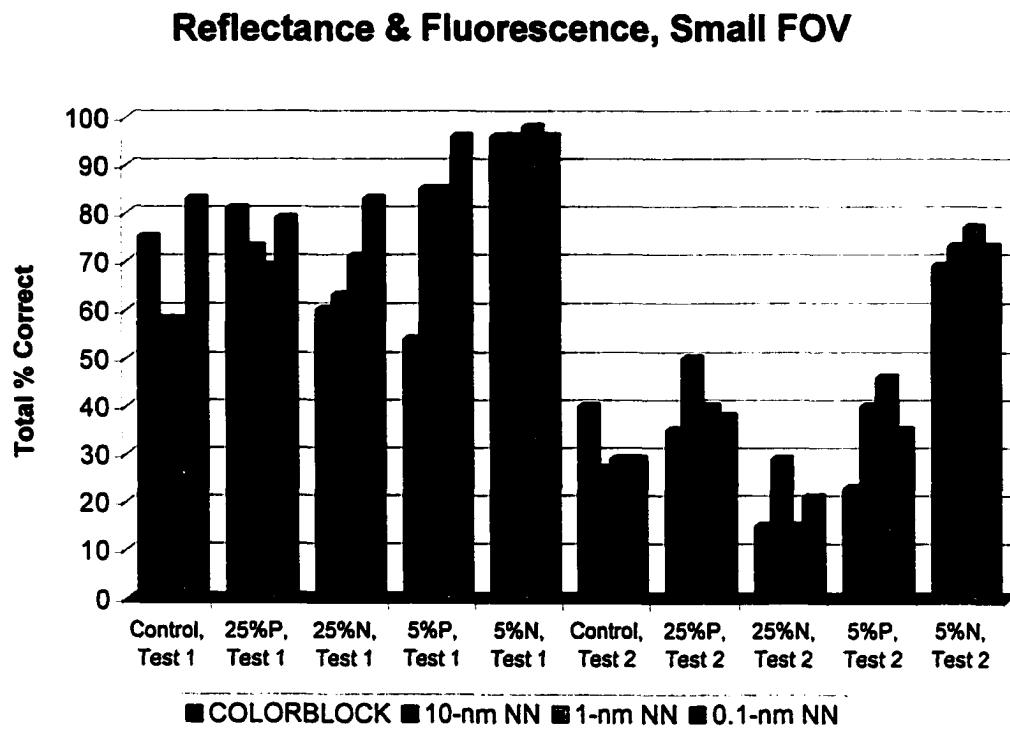
a.)

**Figure 8.4a.)** Results of neural networks using both reflectance and fluorescence spectra as input vector for Large Field Of View (FOV), Diameter = 15-cm.



b.)

**Figure 8.4b.)** Results of neural networks using both reflectance and fluorescence spectra as input vector for Medium Field Of View (FOV), Diameter = 7.5-cm.



c.)

**Figure 8.4c.)** Results of neural networks using both reflectance and fluorescence spectra as input vector for Small Field Of View (FOV), Diameter = 3.75-cm.

In general, reflectance spectra resulted in better model classification than fluorescence spectra. Adding fluorescence spectra to reflectance spectra in the input vector did not enhance model performance as expected. Spectral resolution of the input vector was not found to be highly significant in this study which was also an unexpected result. A spectral resolution of 10-nm was found to be adequate and even out performed all the others for Small FOV cases and cases where both reflectance and fluorescence were used to create the model input vector.

### 8.3.1 COLORBLOCK

Classification performance for COLORBLOCK NN is provided in *Figures 8.2, 8.3, and 8.4* and detailed classification results are included in Appendix B. Model performance was evaluated by comparing classification results to the target values for each of the five nutrient cases, 100%, 25%N, 5%N, 25%P, and 5%P. The case assigned the largest value by the model was given a value of "1" and the other cases given values of "0". The model output value was then compared to the Boolean vector representing the corresponding target value. Total Percent (%) Correct Per Case was determined by calculating the percentage of target values correctly predicted by the NN for each nutrient class over all twelve test days of the study. Four repetitions of each case tested over twelve days for an average of 48 vectors

per case per test. Since there were five different nutrient regimes, a score of 20% for each case implies that the network was unable to differentiate this case from the others.

Percent (%) Correct Per Case Per Day was calculated in a similar fashion and are included in the Appendices. Four repetitions of each nutrient case were tested for an average of 4 vectors per case per day for each test.

Total % Correct and Sum Square Error are also included in the Appendices. Total % Correct represents how many target values were correctly predicted for the entire test. Four repetitions of 5 classes over 12 days yielded an average over 240 output vectors per test. Sum Square Error is the summation of the difference of the raw model output vectors compared to the target Boolean vectors.

The NN trained on reflectance data performed better than the NN trained on fluorescence data; however, adding fluorescence information to the reflectance model did improve classification. In all cases, network performance was much better for the training set than the validation set. As ample precautions were taken to not "over fit" the data during network training, it is believed that this discrepancy is indicative of the physical differences between the two tests as shown by the fresh mass of the test plants and perhaps limitations in generalization imposed by training the NN on extremely broad band data. When trained in this fashion, the network

classifies extreme nitrogen deficiency well, 88%, but does not distinguish moderate nitrogen deficiency or phosphate deficiency from the controls.

The field of view was found to be related to model performance. The NN trained on fluorescence data predicted extreme nitrogen deficiency best, 63%, for spectra collected over the large FOV 15-cm (6-in). The medium spot size, 7.5-cm (3-in) was associated with the best classification of extreme nitrogen deficiency, 88% and 83%, for NN's trained with both reflectance and fluorescence data and for the NN trained on reflectance spectra respectively.

For the network trained with both reflectance and fluorescence spectra, extreme nitrogen deficiency was predicted correctly 50% for test days 12 and 14, and between 75% and 100% for all the remaining test days. As the nutrient test itself began on test day 10, this demonstrates that the COLORBLOCK NN can be used to monitor and identify early stress conditions for extreme nitrogen deficiency.

### 8.3.2 The 10-nm NN

Classification performance for the 10-nm NN is provided in *Figures 8.2, 8.3, and 8.4* and detailed classification results are included in Appendix C. Model performance was evaluated by comparing classification results to the target values for each of the five nutrient cases, 100%, 25%N, 5%N, 25%P, and 5%P. The case assigned the largest value by the model was given a value of "1" and the other cases given values of "0". The model output value



was then compared to the Boolean vector representing the corresponding target value. The NN trained on reflectance data predicted the 5%N case better than the NN trained on fluorescence data; however, adding fluorescence information to the reflectance model improved classification by 2% for Medium FOV and reduced percent classified correctly by 15% for the Small FOV. In all cases network performance was much better for the training set than the validation set. The model classified extreme nitrogen deficiency well, 90%, but does not distinguish moderate nitrogen deficiency or phosphate deficiency from the controls.

Field of view was related to model performance. The medium spot size, 7.5-cm (3-in) was associated with the best classification of extreme nitrogen deficiency, 90% and 88%, for NN's trained with both reflectance and fluorescence data and for the NN trained on reflectance spectra respectively.

For the network trained with Medium FOV, reflectance and fluorescence spectra, extreme nitrogen deficiency was predicted correctly 100% for test all days except Days 14, 18, 26, 30 and 32 when it was predicted correctly for three of the four 5%N specimens. As the nutrient test ran from Days 10 to 36, this demonstrates that the 10-nm NN can be used to monitor and identify early stress conditions for extreme nitrogen deficiency.

### 8.3.3 The 1-nm NN

Classification performance for the 1-nm NN is provided in *Figures 8.2, 8.3, and 8.4* and detailed classification results are included in Appendix D. Model performance was evaluated by comparing classification results to the target values for each of the five nutrient cases, 100%, 25%N, 5%N, 25%P, and 5%P. The case assigned the largest value by the model was given a value of "1" and the other cases given values of "0". The model output value was then compared to the Boolean vector representing the corresponding target value. Total Percent (%) Correct Per Case was determined as described for the COLORBLOCK NN. Since there were five different nutrient regimes, a score of 20% for each case implies that the network was unable to differentiate this case from the others.

The 1-nm NN trained on reflectance data predicted 5%N better than the NN trained on fluorescence data, and adding fluorescence information to the reflectance model did not improve classification. In all cases network performance was much better for the training set than the validation set. The network classified extreme nitrogen deficiency well, 92%, but did not distinguish moderate nitrogen deficiency or phosphate deficiency from the controls.

Field of view was found to be related to model performance. The 1-nm NN trained on fluorescence data predicted extreme nitrogen deficiency best, 83%, for spectra collected over the large FOV 15-cm (6-in). The medium spot size, 7.5-cm (3-in) was associated with the best classification of extreme

nitrogen deficiency, 85% and 92%, for NN's trained with both reflectance and fluorescence data and for the NN trained on reflectance spectra respectively.

For the network trained with Medium FOV reflectance spectra, extreme nitrogen deficiency was predicted correctly 50% for test day 14, correctly 75% for test days 16 and 32, and correctly 100% for all the remaining test days. As the nutrient test began on test day 10, this demonstrates that the 1-nm NN can be used to monitor and identify early stress conditions for extreme nitrogen deficiency.

#### 8.3.4 The 0.1-nm NN

Classification performance for 0.1-nm NN is provided in *Figures 8.2, 8.3, and 8.4* and detailed classification results are included in Appendix E. Model performance was evaluated by comparing classification results to the target values for each of the five nutrient cases, 100%, 25%N, 5%N, 25%P, and 5%P. The case assigned the largest value by the model was given a value of "1" and the other cases given values of "0". The model output value was then compared to the Boolean vector representing the corresponding target value. Total Percent (%) Correct Per Case was determined as described above.

The 0.1-nm NN trained on reflectance data predicted 5%N better for Large and Small FOV's than the NN trained on fluorescence data. Adding fluorescence information to the reflectance model improved 5%N

classification by 8%, -6%, and 10% for Large, Medium, and Small FOV's respectively. In all cases network performance was much better for the training set than the validation set. The network classified extreme nitrogen deficiency well, 90%, but does not distinguish moderate nitrogen deficiency or phosphate deficiency from the controls.

The field of view was found to be related to model performance. The 0.1 NN trained on all three types of input vectors predicted extreme nitrogen deficiency best, 90%, 63%, and 83%, for spectra collected over the large FOV 15-cm (6-in). For the network trained with reflectance spectra, extreme nitrogen deficiency was predicted correctly 50% for test day 14, 75% for test days 26, 30, and 32, and 100% for all the remaining test days. As the nutrient test itself began on test day 10, this demonstrates that the 0.1-nm MM can also be used to monitor and identify early stress conditions for extreme nitrogen deficiency.

#### **8.4 Canopy Structure and Plant Angle**

*Figure 8.5* illustrates the manner in which the test plant was rotated for data collection. *Figures 8.6* and *8.7* show the effect of plant angle on reflectance and fluorescence spectra. The effects of plant angle and canopy structure were the least pronounced for angles of 0° and 45° from zenith in the broadband red and near infrared reflectance spectra of Channel 1 and Channel 2. For Channel 1, even the reflectance intensity at 90° is at least

75% of the intensity at  $0^\circ$  and at least 87% of the intensity at  $45^\circ$ . For Channel 2 the reflectance intensity of leaves at  $45^\circ$  angles is about 95% of the intensity of leaves at  $0^\circ$ , although the difference between  $45^\circ$  and  $90^\circ$  plant angles is approximately 50%. Reflectance intensity as a function of plant angle is also quite pronounced for Channel 3 spectra. The variability of reflectance intensity was more random with a variation of 60% between plant angles of  $45^\circ$  and  $90^\circ$ , and the reflectance intensity associated with top viewed leaves,  $0^\circ$ , falling between that of plants viewed at angles of  $45^\circ$  and  $90^\circ$ 's.

---

#### Plant Angle Experimental Configuration

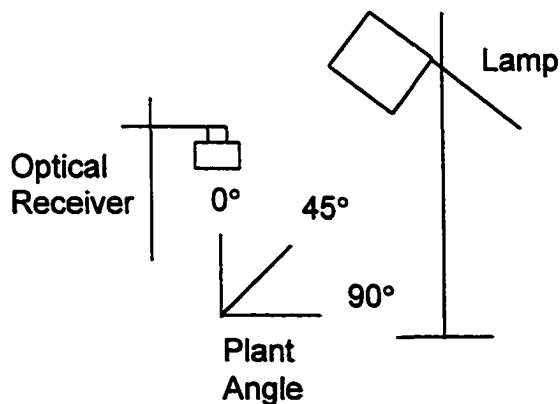
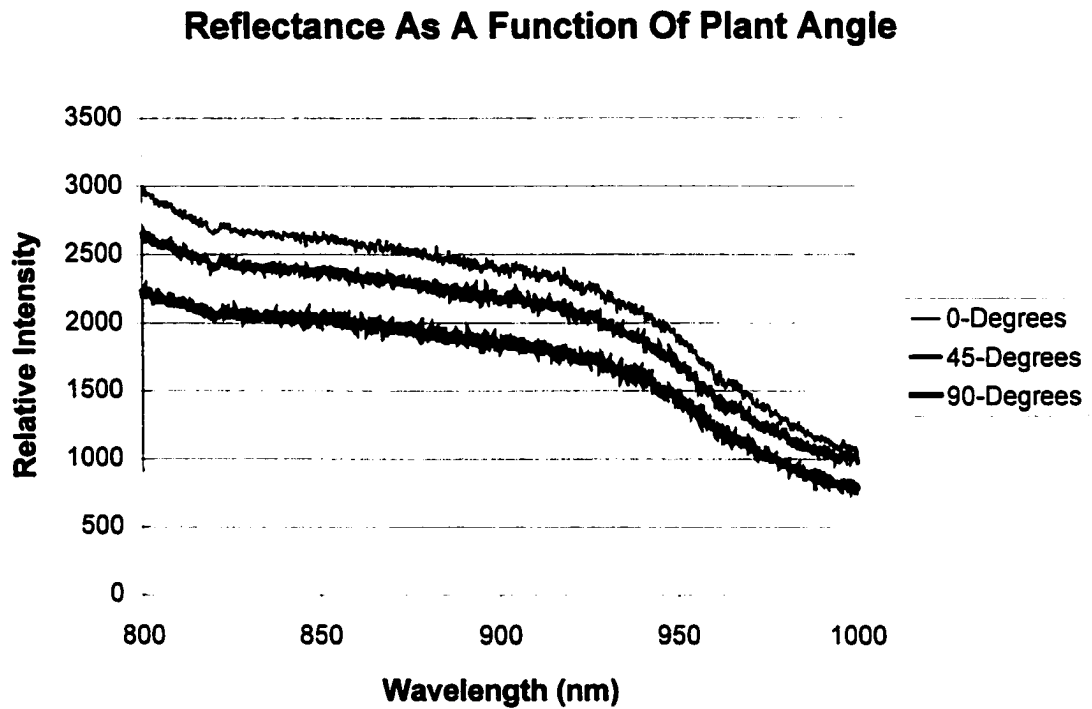


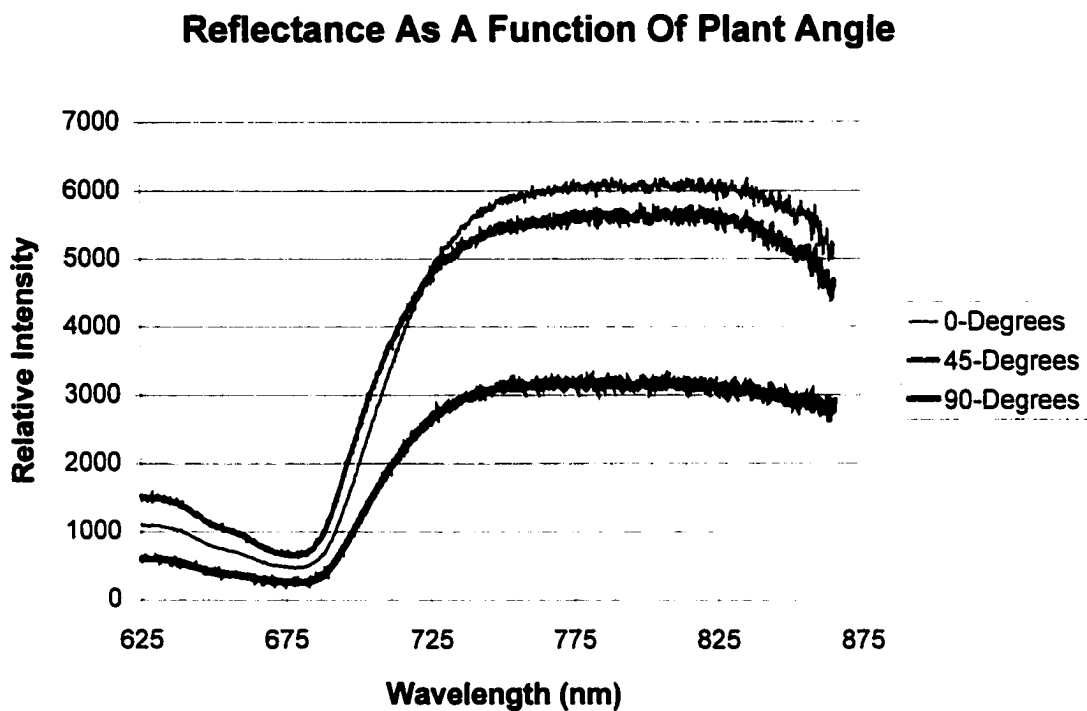
**Figure 8.5.)** Direction of rotation for plant angle experiments with respect to optical receiver zenith and lamp angled at  $45^\circ$ .

---



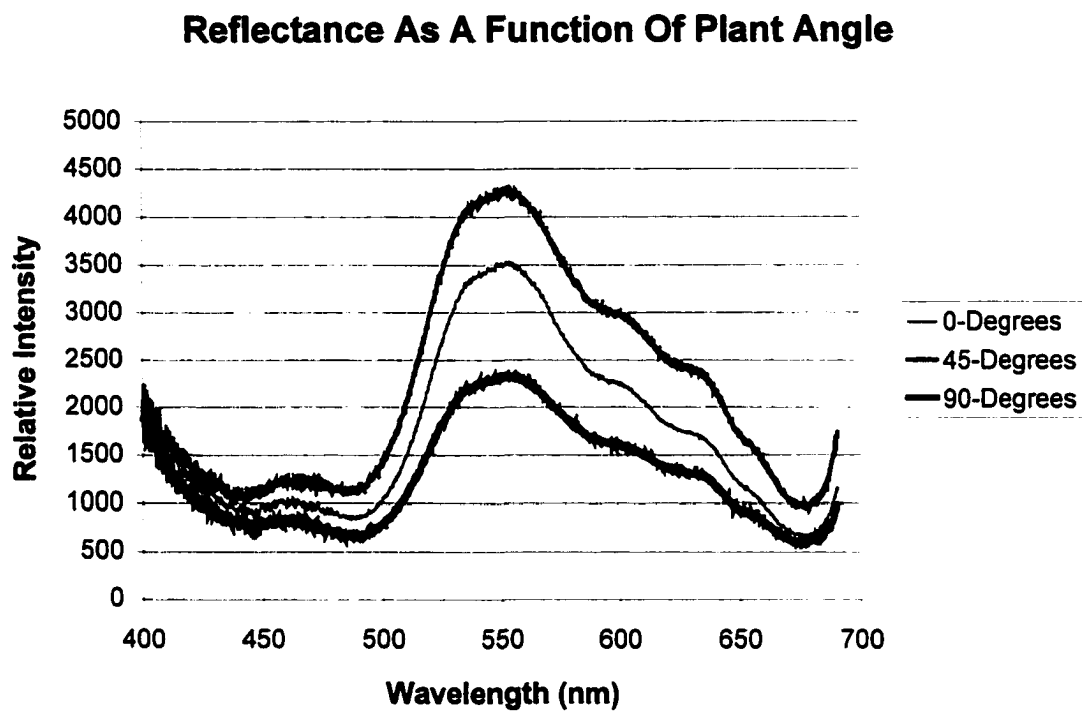
a.)

**Figure 8.6a.)** Effect of plant angle on reflectance spectra. Spectrometer Channel 1.



b.)

**Figure 8.6b.)** Effect of plant angle on reflectance spectra. Spectrometer Channel 2.

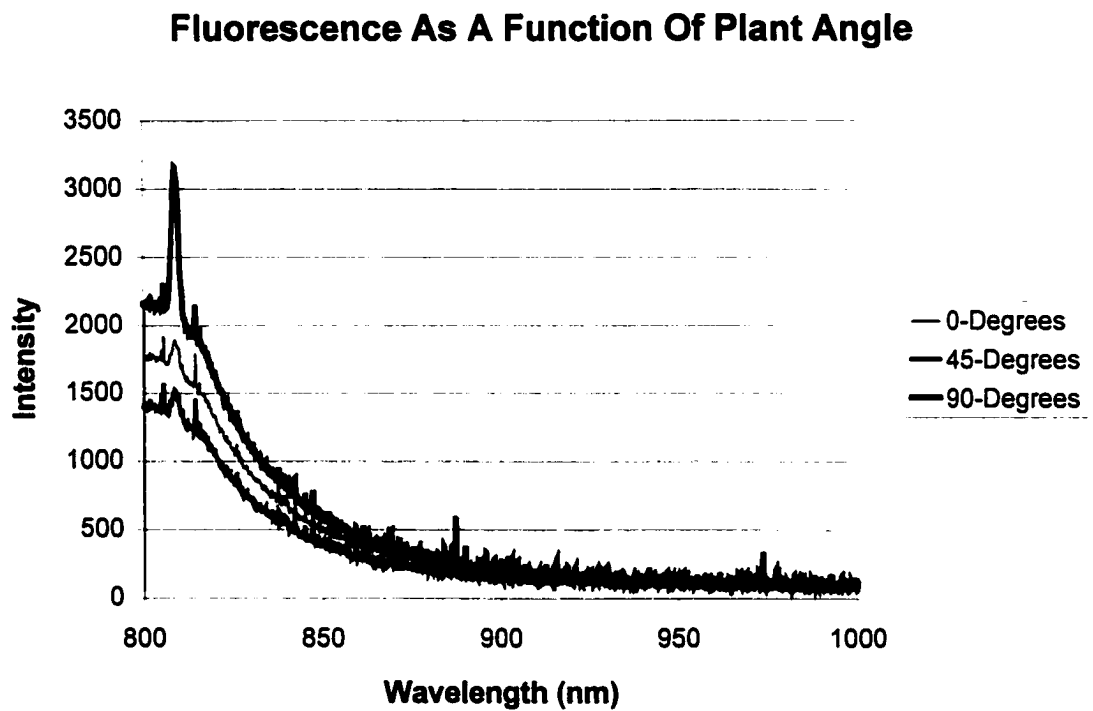


c.)

**Figure 8.6c.)** Effect of plant angle on reflectance spectra.  
Spectrometer Channel 3.

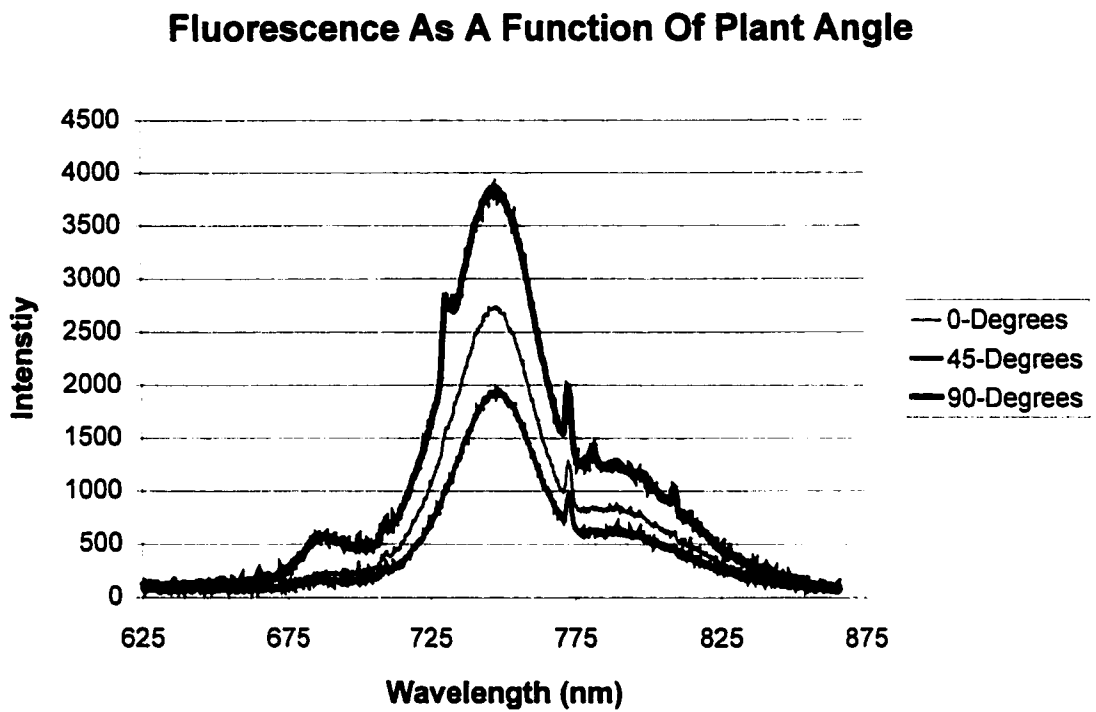
---





a.)

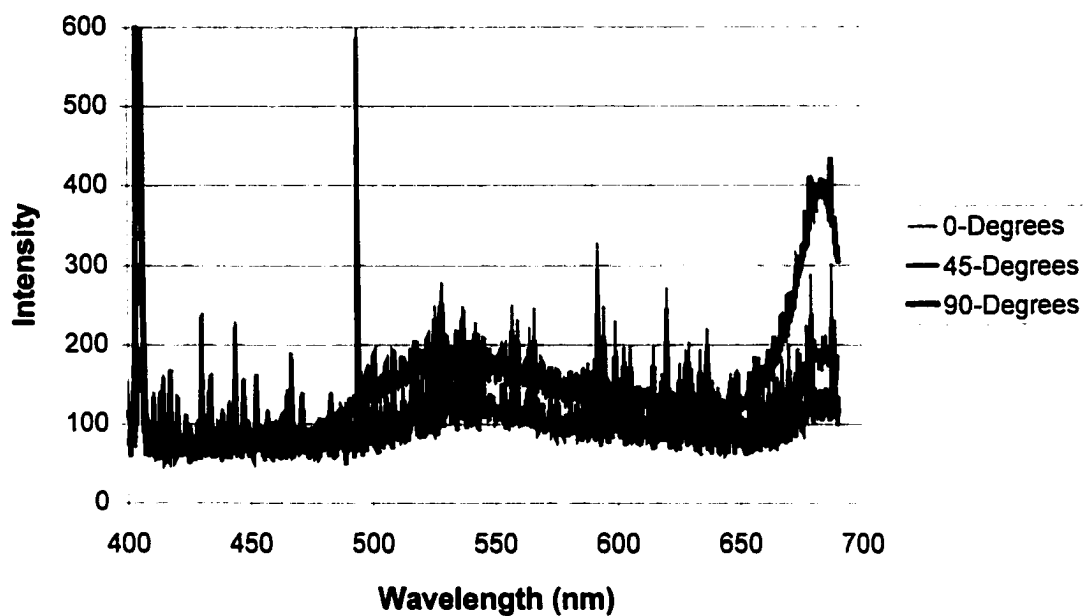
**Figure 8.7a.)** Effect of plant angle on Fluorescence spectra.  
Sectrometer Channel 1.



b.)

**Figure 8.7b.)** Effect of plant angle on Fluorescence spectra. Spectrometer Channel 2.

### Fluorescence As A Function Of Plant Angle



c.)

**Figure 8.7c.)** Effect of plant angle on Fluorescence spectra. Spectrometer Channel 3.

---

The robustness of Channels 1 and 2 with respect to leaf angle and canopy structure explain why these were the most significant wavelengths for the optical analysis of free standing plants in this study. The randomness introduced by plant angle in spectrometer Channel 3 also explains why this spectral range was not as important to network classification as it could have been otherwise, i.e. greenness index of fixed leaf or small point on single leaf.

Similarly, fluorescence spectra was also greatly inconsistent as a function of plant angle. For all three spectrometer channels, fluorescent intensity was greatest for plant angles of 90°'s. This is most likely because the underneath side of a leaf is less likely to be exposed to bright light especially of short wavelength and high energy. Thus, the underneath side of the leaf is poorly equipped to absorb and readily use the high energy photons from the UV spotlight and a greater percentage are re-released as fluorescence. For Channel 1, peak fluorescent intensity from plants at 45° angles was only 40% of the peak intensity from leaves at 90° angles with values for leaves at 0°'s falling in between. For Channel 2, peak fluorescent intensity from plants at 45° angles was only 50% of the peak intensity from plants at 90° angles with values for leaves at 0°'s falling in between. Spectra from Channel 3 was primarily obscured by noise, but the largest peaks were also associated with leaves at 90° with values approximately twice that as for leaves at 0° and 45° angles.

## **8.5 Conclusions**

Hydroponic lettuce was cultivated to express phosphorous and nitrogen deficiencies. Visual inspection, fresh mass values, and optical spectra failed to differentiate between controls and 25% P groups of lettuce. There was also difficulty discerning between 25% N and 5%P based on fresh mass, visual inspection, and optical spectra. Fresh mass results may have more clearly represented nutrient status if pH had been held more constant and overcrowding conditions had been more fully ameliorated.

Neural networks were implemented to classify reflectance and fluorescence spectra as a function of test day and field of view of the optical receiver. In general the neural networks performed well when classifying 5% N cases compared to controls, but did not classify well for 25% N, 25% P, and 5% P. Differences in color, i.e. visible light scattering, were expected to be more readily correlated with nitrogen and phosphorous deficiency. In many plants the first symptom of nitrogen deficiency is chlorosis (yellowing of the leaves), especially in the older leaves which become completely yellow and then fall off the plant. Often the first symptom of phosphorous deficiency is stunted growth with a dark green coloration in the leaves, however this was not seen in the test plant, *Lactuca Sativa*, 'Ostinata', cultivated for this particular study. This is most likely due to the recommended concentration of phosphorous and nitrogen being greatly exaggerated by the hydroponic growers manual (Wells, 1995).

The NN's were trained on input vectors created using reflectance and test day, fluorescence and test day, and reflectance, fluorescence, and test day. Four networks were created representing four levels of spectral resolution: COLORBLOCK ( $\Delta\lambda\approx 100\text{-nm}$ ), 10-nm NN, 1-nm NN, and 0.1-nm NN.

As shown in *Figure 8.8*, results from the NN validation classification demonstrated that all four types of network could be used as a remote sensing method for detecting extreme nitrogen deficiency early in the growth cycle. For the lower resolution models, COLORBLOCK and 10-nm NN, the best classification results of 5%N occurred using both reflectance and fluorescence spectra and a medium field of view. For the higher resolution models, 1-nm NN and 0.1-nm NN, 5%N specimens were classified the best using reflectance spectra without fluorescence. For the highest resolution model, 0.1-nm NN, the best classification results coincided with the largest FOV. The 10-nm resolution was found to be sufficient for classifying extreme nitrogen deficiency in freestanding hydroponic lettuce. As a result of leaf angle and canopy structure broadband reflectance intensity in the 700-nm to 1 000-nm range was found to be the most useful portion of the spectrum in this study. More subtle effects of "greenness" and fluorescence emission were thought to be obscured by canopy structure and leaf orientation.

To safeguard against outliers, the number of replications should be increased and a data-processing subroutine should be implemented to check

for a certain degree of variation in each spectral scan. Scans having higher than acceptable variation should then be deleted from the neural network training and testing. This would enhance the robustness of the system. As field of view was not as found to be as significant as originally believed, systems implementing higher repetitions over more uniformly oriented, i.e. smaller, flatter, target areas would provide for more discernible neural network input vectors.

This overall technique holds great promise for the early detection of extreme nitrogen deficiency in *Lactuca Sativa* for NASA's Advanced Life Support and terrestrial applications. However, further research is recommended using stereoscopic digital cameras to quantify leaf area index, leaf shape, and leaf orientation as well as reflectance. Given the additional information provided by stereoscopic vision systems, fluorescence emission may also prove to be a useful biological assay of freestanding vegetation.

**Table 8.2.)** Best neural network (NN) validation output for each level of spectral resolution as a function of Test Day.

<b>Test Day</b>		<b>% Correct Per Day (Percent Predicted Correctly Out of Four Repetitions)</b>			
<b>Day of Growth Cycle</b>	<b>Day of Nutrient Test</b>	<b>COLORLOCK, Medium FOV, Reflectance and Fluorescence Spectra</b>	<b>10-nm, Medium FOV, Reflectance and Fluorescence Spectra</b>	<b>1-nm, Medium FOV, Reflectance Spectra</b>	<b>0.1-nm, Large FOV, Reflectance Spectra</b>
12	2	50%	100%	100%	100%
14	4	50%	75%	50%	50%
16	6	100%	100%	75%	100%
18	8	100%	75%	100%	100%
20	10	100%	100%	100%	100%
22	12	100%	100%	100%	100%
24	14	100%	100%	100%	100%
26	16	75%	75%	100%	75%
28	18	100%	100%	100%	100%
30	20	100%	75%	100%	75%
32	22	75%	75%	75%	75%
34	24	100%	100%	100%	100%



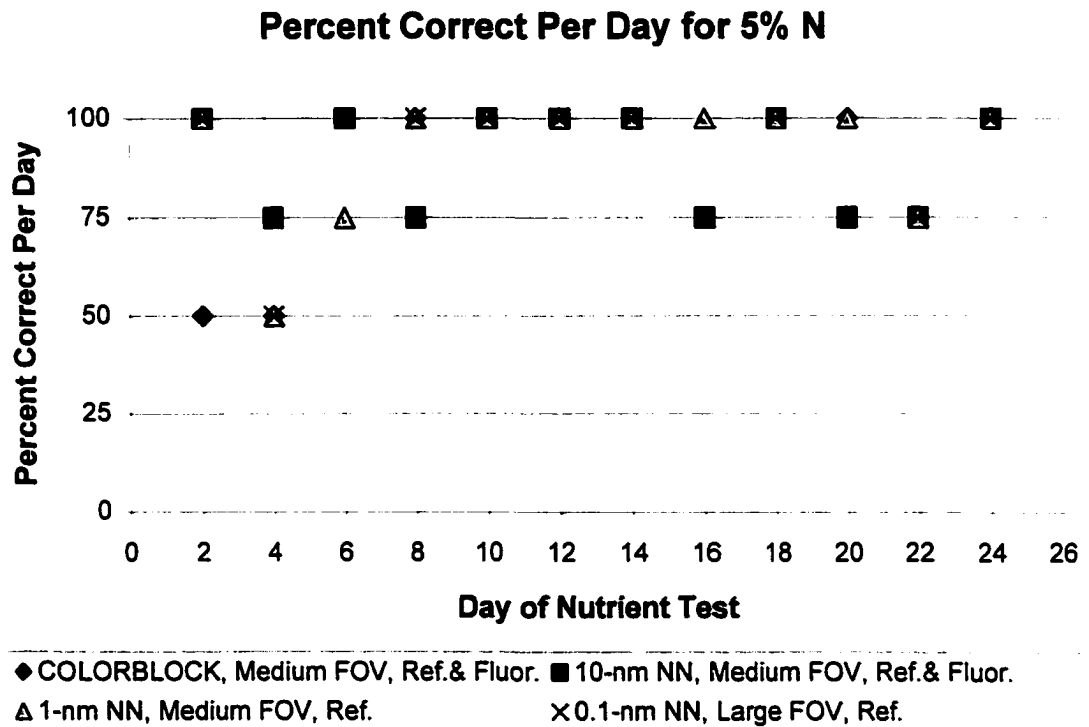


Figure 8.8.) Summary of NN validation results for classification of 5%N specimens as a function of Test Day.

---

## References

- Anderson, James A. 1972. *A simple neural network generating an interactive memory*. *Mathematical Biosciences*. Vol. 14, p. 197-220.
- Anderson, James A. and Edward Rosenfeld. 1988 Neurocomputing Foundations of Research. MIT Press, Cambridge, Massachusetts.
- Bain, A. 1873. Mind and body. The theories of their relation. London: Henry King.
- Biehl, L. L., M. E. Bauer, B. F. Robinson, C. D. Daughtry, and D. E. Pitts. 1982. *A crops and soils data base for scene radiation research*, Proceedings of 8<sup>th</sup> Symposium on Machine Processing of Remotely Sensed Data, p. 169-177.
- Bongi, G., A. Palliotti, P. Rocci, I. Moya, Y. Goulas. 1994. *Spectral characteristics and a possible topological assignment of blue green fluorescence excited by UV laser on leaves of unrelated species*. *Remote Sensing of Environment*. Vol. 47, p. 55-64.
- Brach, E. J., J. M. Molnar, and J. J. Jasmin. 1978a. *Detection of lettuce maturity and variety by remote sensing techniques*. *Journal of Agricultural Engineering and Research*. Vol. 22, p. 45-53.
- Brach, E. J., M. A. Klyne, T. Phan, and J. J. Jasmin. 1978b. *Use of laser fluorescence spectroscopy to study lettuce growth and development under controlled environment*. *Proceedings of Photographic and Optical Instrument Engineering*. Vol. 156. p. 158-164.
- Bugbee, B. G. and F. B. Salisbury. 1986. *Studies on the maximum yield of wheat for the controlled environments of space*. NASA Technical Memorandum No. 88215, Moffett Field, CA.
- Bugbee, Bruce. 1995. *Nutrient management in recirculating hydroponic culture*. 1995 Proceedings, Hydroponic Society of America, p. 15-30.

- Campbell, N. A. 1990. Biology. 2<sup>nd</sup> ed. The Benjamin Cummings Publishing Co. Inc., New York. p. 204-224.
- Campbell, J. B. 1996. Introduction to Remote Sensing. The Guilford Press. New York.
- Cecchi, G., P. Mazzinghi, L. Pantani, R. Valentini, D. Tirelli, and P. De Angelis. 1994. *Remote sensing of chlorophyll a fluorescence of vegetation canopies: 1. Near and far field measurement techniques*. Remote Sensing of the Environment. Vol. 47, p. 18-28.
- Chappelle, E. W., F. M. Wood Jr., J. E. McMurtrey III, and W. W. Newcomb. 1984a *Laser-induced fluorescence of green plants. 1: A technique for the remote detection of plant stress and species differentiation*. Applied Optics. Vol. 23, p. 134-138.
- Chappelle, E. W., J. E. McMurtrey III, F. M. Wood Jr., , and W. W. Newcomb. 1984b *Laser-induced fluorescence of green plants. 2: LIF caused by nutrient deficiencies in corn*. Applied Optics. Vol. 23, p. 139-142.
- Chappelle, E. W., F. M. Wood Jr., W. W. Newcomb, and J. E. McMurtrey III. 1985 *Laser-induced fluorescence of green plants. 3: LIF spectral signatures of five major plant types*. Applied Optics. Vol. 24, p. 74-80.
- Chappelle, E. W. and D. L. Williams. 1987. *Laser induced fluorescence (LIF) from plant foliage*. IEEE Transactions on Geoscience and Remote Sensing. Vol. GE-25, p. 726-736.
- Chappelle, E. W., J. E. McMurtrey III, and M. S. Kim. 1991. *Identification of the pigment responsible for the blue fluorescence band in the laser induced fluorescence (LIF) spectra of green plants, and the potential use of this band in remotely estimating rates of photosynthesis*. Remote Sensing of the Environment. Vol. 36, p. 213-218.

- Chappelle, E. W., M. S. Kim, and J. E. McMurtrey III. 1992. *Ratio analysis of reflectance spectra (RARS): an algorithm for the remote estimation of the concentrations of chlorophyll a, chlorophyll b, and carotenoids in soybean leaves*. *Remote Sensing of the Environment*. Vol. 39, p. 239-247.
- Colwell, Robert N. 1956. *Determining the prevalence of certain cereal crop diseases by means of aerial photography*. *Hilgardia*. Vol. 26. No. 5, p. 223-286.
- Colwell, Robert N. 1966. *Uses and limitations of multispectral remote sensing*. *Proceedings of the Fourth Symposium on Remote Sensing of the Environment*. Ann Arbor: University of Michigan.
- Corp, L. A., J. E. McMurtrey, E. W. Chappelle, C. S. Daughtry, and M. S. Kim. 1997. *UV band fluorescence (in vivo) and its implications for the remote assessment of nitrogen supply in vegetation*. *Remote Sensing of the Environment*. Vol. 61, p. 110-117.
- DeCusatis, Casimer. 1997. Handbook of Applied Photometry. American Institute of Physics Press, Woodbury, New York.
- Demuth, Howard and Mark Beal. 1998. Neural Network Toolbox For Use with MATLAB. The Math Works Inc. User's Guide Version 3.
- Elachi, Charles. 1987. Introduction to the Physics and Techniques of Remote Sensing. John Wiley & Sons, New York.
- Estes, John E. 1999. "History of remote sensing."  
<http://grouchy.geog.ucsb.edu/powerpoint/corse/ppframe.htm>. August 2000.
- Fiocco, G. and L. D. Smullin. 1963. *Detection of scattering layers in the upper atmosphere (60-140 km) by optical radar*. *Nature*. Vol. 199, p. 1275-1276.

- Foresee, F. D., and M. T. Hagan. 1997. Gauss-Newton approximation to Bayesian regularization, *Proceedings of the 1997 International Joint Conference on Neural Networks*, p. 1930-1935.
- Goel, N. S. 1982. *A review of crop canopy reflectance models, Final Report*, Contract NAS9-16505, August, 50 pp.
- Goel, N. S. and D. E. Strebel. 1983. *Inversion of vegetation canopy reflectance models for estimating agronomic variables. I. Problem definition and initial results using the Suits model*. *Remote Sensing of Environment*. Vol. 13, p. 487-507.
- Grossweiner, L.I. 1989. *The Science of Photobiology*, Ed. K.C. Smith, Plenum Publ. Co., pp. 1-45.
- Gunther, K. P., H. G. Dahn, and W. Ludeker. 1994. *Remote sensing vegetation status by laser induced fluorescence*. *Remote Sensing of Environment*. Vol. 47, p. 10-17.
- Gunther, K. P. 1990. *Vegetation stress monitoring by fluorescence*. *Remote sensing and the Earth's environment 'Proceedings of Summer School held at Alpbach, Austria, 26 July - 4 August 1989 (ESA SP-301, March 1990)*.
- Hardin, W. H. 1997. *Hyperspectral imaging: How much is hype?* *Photonics Spectra*. July, p. 82-94.
- Hecht Eugene. 1990. *Optics*. Addison-Wesley Publishing Company, Reading, Massachusetts.
- Hickman, G. D. and R. B. Moore. 1970. *Laser induced fluorescence in Rhodamine 3 and algae*. *Proceedings 13 of the Great Lakes Res. Int. Assoc. Great Lakes Res.*, p. 1-14.

- Hixon, M., et al. 1980. *Evaluation of several schemes for classification of remotely sensed data*. Photogrammetric Engineering and Remote Sensing. Vol. 46, No. 12, p. 1547-1553.
- Jacquemoud, S., F. Baret, B. Andrieu, F. M. Danson, and K. Jaggard. 1995. *Extraction of vegetation biophysical parameters by inversion of PROSPECT + SAIL models on sugar beet canopy reflectance data. Application to TM and AVIRIS sensors*. Remote Sensing of the Environment. Vol. 52, p. 163-172.
- Jenness, J., D. Lysak, and C. R. Philbrick. 1997. *Design of a lidar receiver with fiber-optic output*. Applied Optics. Vol. 36, No. 18. June 20, 1997.
- Kautsky, N and A. Hirsch. 1931. *Neue versuche zur kohlenaureassimilation (New method for scientific chlorophyll measurement)*. Naturwissenschaften 19, p. 964-967.
- Kim, H. H. 1973. *New algae mapping technique by use of an airborne laser fluorosensor*, Applied Optics. Vol. 12, p. 1454-1459.
- Kimes, D. S. and J. A. Kirchner. 1982. *Radiative transfer model for heterogeneous 3-D scenes*. Applied Optics. Vol. 21, No. 22, p. 4119-4129.
- Kohonen, Teuvo. 1972. *Correlation matrix memories*, IEEE Transaction on Computers. Vol. C-21, p. 353-359.
- Krajicek, V. and M. Vrbova. 1994. *Laser induced fluorescence spectra of plants*. Remote Sensing of Environment. Vol. 47, p. 51-54.
- Kuusk, A. 1994. *A multispectral canopy reflectance model*. Remote Sensing of Environment. Vol. 50, p. 75-82.
- Lee, W. S. and D. C. Slaughter. 1998. *Plant recognition using hardware-based neural network*. 1998 ASAE Annual International Meeting. Paper No. 983040. ASAE, 2950 Niles Rd., St. Joseph, MI 49085-9659 USA.

- Ligda, M. G. H. 1963. Proceeding of the Conference on Laser Technology, 1<sup>st</sup>. San Diego, CA. p. 63-72.
- Lillesand, T. M. and R. W. Kiefer. 1987. Remote Sensing and Image Interpretation. John Wiley & Sons, New York, p. 597-601.
- Maiman, T. H. 1960. *Stimulated optical radiation in ruby*. Nature. Vol. 187, p. 493-494.
- McClung, F. J. and R. W. Hellwarth. 1962. *Giant optical pulsations from ruby*. Journal of Applied Physics. Vol. 33, p. 828-829.
- McCulloch, W.S. and W. H. Pitts. 1943. *A logical calculus of the ideas immanent in nervous activity*, Bulletin of Mathematical Biophysics, Vol. 5, p. 115-137.
- McHenry, Lawrence, C. 1969. Garrison's History of Neurology. Charles C. Thomas Publishers Ltd. Springfield, IL.
- McMurtrey III, J. E., E. W. Chappelle, M. S. Kim, J. J. Meisinger, and L. A. Corp. 1994. *Distinguishing nitrogen fertilization levels in field corn (zea mays L.) with actively induced fluorescence and passive reflectance measurements*. Remote Sensing of the Environment. Vol. 47, p. 36-44.
- Measures, R. M. 1992. Laser Remote Sensing Fundamentals and Applications. Krieger Publishing Co. Malabar, Florida, p. 442-450.
- Methy, M., Oliosio, A., and L. Trabaud. 1994. *Chlorophyll fluorescence as a tool for management of plant resources*. Remote Sensing of Environment. Vol. 47, p 2-9.
- Mirkamilov, D. M., A. A. Mukhamedov, M. M. Mansurov, and Sh. N. Ernazarov. 1992. *Identification of the physiological condition of plants using laser-induced fluorescence spectra*. Soviet Journal of Remote Sensing. Vol. 10(1), p. 140-145.

Moller, K. D. 1988. Optics. University Science Books. Mill Valley, California.

Molzwarth, A. R. 1986. *Fluorescence lifetimes in photosynthetic systems*. Photochemistry and Photobiology. Vol. 43(6), p. 707-725.

NASA's Observatorium. 1998. "Remote sensing in history."  
[http://observe.ivv.nasa.gov/nasa/exhibits/history/history\\_0.html](http://observe.ivv.nasa.gov/nasa/exhibits/history/history_0.html).  
September, 2000.

Neu, J. T., R. S. Dummer, M. T. Beecroft, P. N. McKenna, and D. C. Robertson. 1990. *Surface Optical Property Measurements on Bark and Leaf Samples*, Smart Weapons Operability Enhancement (SWOE) Report 90-14, December, 31, 1990.

Norikane, J. H. and K. Kurata. 1999. *Fluorescence monitoring using the relative reference method on a free-standing tomato plant*. 1999 ASAE/CSAE-SCGR Annual International Meeting, Paper No. 993206. ASAE, 2950 Niles Rd., St. Joseph, MI.

Olmsted, David D. 1998. *History and Principles of Neural Networks*.  
<http://www.neurocomputing.org/history.htm>. August, 2000.

Porter, G., I. A. Synowiec, and L. I. Tredwell. 1977. *Intensity effects on the fluorescence of in vivo chlorophyll*, Biochim. Biophys. Acta. Vol. 459, p. 329-326.

Rashevsky, N. 1938. Mathematical Biophysics, University of Chicago Press, Chicago, IL.

Ripley, B. D. 1996. Pattern Recognition and Neural Networks, Cambridge: Cambridge University Press.

Rosema, A., g. Cecchi, L. Pantani, B. Radicatti, M. Romuli, P. Mazzinghi, O. Van Kooten, C. Kliffen. 1992. *Monitoring photosynthetic activity and ozone stress by laser induced fluorescence in trees*. International Journal of Remote Sensing. Vol. 13, No. 4. p. 737-751.



- Rosenblatt, F. 1958. *The Perceptron: A probabilistic model for information storage and organization in the brain*, Psychological Review, Vol. 65, p. 386-408.
- Rosenblatt, F. 1960. *Perceptron simulation experiments*, Proceedings of the IRE, Vol. 48, p. 301-309.
- Rosenblatt, F. 1962. Principles of Neurodynamics: Perceptrons and the Theory of Brain Mechanisms, Spartan books, Washington D.C.
- Rummel, John A., et al. 1998. *Advanced Life Support Program Plan; Crew and Thermal Systems Division Lyndon B. Johnson Space Center NASA*, CTSD-ADV-348 JSC 39168.
- Rumelhart, David D., Hinton Geoffrey E., and Williams, Ronald J. 1986. *Learning representations by back-propagating errors*, Nature Vol. 323, p. 533-536.
- Russell, Ingrid. 1996. "Neural Networks Module".  
[http://uhavax.hartford.edu/disk\\$userdata/faculty/compsci/www/neural-networks-definition.html](http://uhavax.hartford.edu/disk$userdata/faculty/compsci/www/neural-networks-definition.html), August 2000.
- Saito, Y., M. Kanoh, K. Hatake, T. D. Kawahara, and A. Nomura. 1998. *Investigation of laser induced fluorescence of several natural leaves for application to lidar vegetation monitoring*. Applied Optics. Vol. 37, No. 3, p. 431-437.
- Sarle, W. S., ed. 1997. *Neural Network FAQ*, periodic posting to the Usenet newsgroup comp.ai.neural-nets, URL: <ftp://ftp.sas.com/pub/neural/FAQ.html>. August 2000.
- Schawlow, A. L. and C. H. Townes, 1958. *Infrared and Optical Masers*. Physics Review. Vol. 112, p. 1940-1949.
- Schmuck, G., J. Verdebout, C. Koechler, I. Moya, and Y. Goulas. 1991. *Laser-induced time-resolved fluorescence of vegetation*. IEEE Transactions on Geoscience and Remote Sensing. Vol. 29, p. 674-678.

- Sellers, P. J., J. A. Berry, G. J. Collatz, C. B. Field, and F. G. Hall. 1992. *Canopy reflectance, photosynthesis, and transpiration. III. A reanalysis using improved leaf models and a new canopy integration scheme*. Remote Sensing of Environment. Vol. 42, p. 187-216.
- Skoog, D. A. and J. J. Leary, 1992. Principles of Instrumental Analysis. 4<sup>th</sup> ed. Saunders College Publishers, Philadelphia.
- Smith, J. A. 1982. *Role of scene radiation models in remote sensing*, Proceedings of 8<sup>th</sup> Symposium on Machine Processing of Remotely Sensed Data, p. 546-549.
- Spick, Mike. 1994. Milestones of Manned Flight. Smithmark Publishers Inc., New York.
- Stephens, G. L. 1994. Remote Sensing of the Lower Atmosphere, Oxford University Press, New York, p. 181-183.
- Stober, F., Lang, M, and H. K. Lichtenthaler. 1994. *Blue, green, and red fluorescence emission signatures of green, etiolated, and white leaves*. Remote Sensing of Environment. Vol. 47, p. 65-71.
- Stone, M. L. 1994. *Embedded neural networks in real time controls*. SAE Paper No. 941067. SAE, Warrendale, PA.
- Subhash, N. and C. N. Mohanan. 1994. *Laser-induced red chlorophyll fluorescence signatures as nutrient stress indicator in rice plants*. Remote Sensing of the Environment. Vol. 47, p. 45-50.
- Suits, G. H. 1972. *The calculation of the directional reflectance of a vegetative canopy*. Remote Sensing of Environment. Vol. 2, p. 117-125.
- Thimijan, R. W. and R. D. Heins. 1983. *Photometric, radiometric, and quantum light measure: a review of procedures for interconversion*. Hort Science. Vol. 18(6).

Tumbo, S. D., D. G. Wagner, and P. H. Heinemann. 2000. *Hyperspectral input-based neural network model for predicting chlorophyll status in corn*. Proceedings of ASAE.

Weiler, T. C. and M Sailus. 1996. Water and Nutrient Management for Greenhouses. Cornell Controlled Environment Agriculture Working Group, Cornell Cooperative Extension, College of Agriculture and Life Sciences. Northeast Regional Agriculture Engineering Service, Cooperative Extension, 152 Riley-Robb Hall, Ithaca, New York 14853.

Wells, E. C. 1995. "CEA Hydroponic Lettuce Production Handbook," <http://www.cals.cornell.edu/flori/lettuce>, May, 2000.

Widrow, Bernard, and Hoff, Marcian, E. 1960. *Adaptive switching circuits*, 1960 IRE WESCON Convention Record, New York: IRE pp. 96-104

Widrow, Bernard. 1962. "Generalization and Information Storage in Networks of Adaline Neurons". Self-Organizing Systems. Spartan Books. Washington D.C.

Wiegand, C. L., S. J. Maas, J. K. Aase, J. L. Hatfield, P. J. Pinter, R. D. Jackson, E. T. Kanemasu, and R. L. Lapitan. 1992. *Mutisite analyses of spectral-biophysical data for wheat*. Remote Sensing of Environment. Vol. 42, p. 1-21.

Wilkerson, J. B., R. Sui, W. E. Hart, L. R. Wilhelm, and D. D. Howard. 1999. *Artificial neural networks for determining nitrogen status in cotton*. 1999 ASAE/CSAE-SCGR Annual International Meeting, Paper No. 993042. ASAE, 2950 Niles Rd., St. Joseph, MI.

Wilkes, Alan L. and Wade, Nicholas, J. 1997. *Bain on Neural Networks*. Brain and Cognition. Vol. 33, p 295-305.

Winder, R.O. 1964. *Threshold logic in artificial intelligence*, Artificial Intelligence, IEEE Publication S-142, p. 107-128.

Yang, C. C., S. O. Prasher, and J. A. Landry. 1998. *Application of artificial neural network to image recognition in precision farming*. 1998 ASAE Annual International Meeting. Paper No. 983074. ASAE, 2950 Niles Rd., St. Joseph, MI.

## **APPENDIX A.) Cultivation Information**

## Lettuce Control Nutrient Solution, Days 1-35

Nutrient	conc.	compound	Atomic Wt (g/mol)	Ratio (mol/mol)	amount of compound to add	
	(M)				g/gallon	g/30gallon
N	1.56E-03	NH4NO3	80.04	2.0	2.36E-01	7.0815
N	1.39E-03	Ca(NO3)2*4H2O	236.2	2.0	6.20E-01	18.5852
K,N	4.48E-03	KNO3	101.1	1.0	1.72E+00	51.4583
P	9.88E-04	KH2PO4	136.11	1.0	5.09E-01	15.2657
S	8.68E-04	H2SO4	98.079	1.0	3.22E-01	9.6668
Fe	1.65E-05	FeSO4*7H2O	278	1.0	1.73E-02	0.5201
Mn	2.41E-06	MnSO4*H2O	169	1.0	1.54E-03	0.0462
B	1.50E-05	H3BO3	61.83	1.0	3.51E-03	0.1053
Zn	1.46E-06	ZnSO4*7H2O	287.5	1.0	1.59E-03	0.0478
Mo	3.00E-07	(NH4)6Mo7O24*4(H2O)	1235.9	7.0	2.00E-04	0.0060

	Tap Water	Atomic Wt	Tap Water	Fertilizer	Add
	mg/L	g/mol	M	mol/L	mol/L
N	1.22	14.0067	8.71E-05	8.90E-03	8.81E-03
P	0.38	30.9738	1.23E-05	1.00E-03	9.88E-04
K	1.165	39.0983	2.98E-05	5.50E-03	5.47E-03
Ca	28.62	40.078	7.14E-04	2.10E-03	1.39E-03
Mg	63.35	24.305	2.61E-03	1.00E-03	-1.61E-03
S	6.787	32.066	2.12E-04	1.10E-03	8.88E-04
Fe	0.018	55.847	3.22E-07	1.68E-05	1.65E-05
Mn	0.005	54.938	9.10E-08	2.50E-06	2.41E-06
Zn	0.035	65.39	5.35E-07	2.00E-06	1.46E-06
Cu	0.065	63.546	1.02E-06	4.00E-07	-6.23E-07
B		11	--	1.50E-05	1.50E-05
Mo		96	--	3.00E-07	3.00E-07
Cl	22.88	35.4527	6.45E-04		-6.45E-04

## Lettuce 5% Nitrogen Solution, Days 1-35

Nutrient	conc. (M)	compound	Atomic Wt (g/mol)	Ratio (mol/mol)	amount of compound to add	
					g/gallon	g/30 gallon
N	4.41E-04	NH4NO3	80.04	2.0	6.67E-02	2.0023
P	9.88E-04	KH2PO4	136.11	1.0	5.09E-01	15.2657
K	4.48E-03	K2CO3	138.2	2.0	1.17E+00	35.1708
Ca	1.39E-03	Ca(OH)2	74.09	1.0	3.89E-01	11.6594
S	8.68E-04	H2SO4	98.079	1.0	3.22E-01	9.6668
Fe	1.65E-05	FeSO4*7H2O	278	1.0	1.73E-02	0.5201
Mn	2.41E-06	MnSO4*H2O	169	1.0	1.54E-03	0.0462
B	1.50E-05	H3BO3	61.83	1.0	3.51E-03	0.1053
Zn	1.46E-06	ZnSO4*7H2O	287.5	1.0	1.59E-03	0.0478
Mo	3.00E-07	(NH4)6Mo7O24*4(H2O)	1235.9	7.0	2.00E-04	0.0060

## Lettuce 25% Nitrogen Solution, Days 1-35

Nutrient	conc. (M)	compound	Atomic Wt (g/mol)	Ratio (mol/mol)	amount of compound to add	
					g/gallon	g/30 gallon
N	2.20E-03	NH4NO3	80.04	2.0	3.34E-01	10.0117
P	9.88E-04	KH2PO4	136.11	1.0	5.09E-01	15.2657
K	4.48E-03	K2CO3	138.2	2.0	1.17E+00	35.1708
Ca	1.39E-03	Ca(OH)2	74.09	1.0	3.89E-01	11.6594
S	8.68E-04	H2SO4	98.079	1.0	3.22E-01	9.6668
Fe	1.65E-05	FeSO4*7H2O	278	1.0	1.73E-02	0.5201
Mn	2.41E-06	MnSO4*H2O	169	1.0	1.54E-03	0.0462
B	1.50E-05	H3BO3	61.83	1.0	3.51E-03	0.1053
Zn	1.46E-06	ZnSO4*7H2O	287.5	1.0	1.59E-03	0.0478
Mo	3.00E-07	(NH4)6Mo7O24*4(H2O)	1235.9	7.0	2.00E-04	0.0060

## Lettuce 5% Phosphorous Solution, Days 1-35

Nutrient	conc. (M)	compound	Atomic Wt (g/mol)	Ratio (mol/mol)	amount of compound to add g/gallon	g/30 gallon
N	6.20E-04	NH4NO3	80.04	2.0	9.39E-02	2.8174
N	1.39E-03	Ca(NO3)2*4H2O	236.2	2.0	6.20E-01	18.5852
N	5.42E-03	KNO3	101.1	1.0	2.07E+00	62.2305
K						
P	4.94E-05	KH2PO4	136.11	1.0	2.54E-02	0.7633
S	8.68E-04	H2SO4	98.079	1.0	3.22E-01	9.6668
Fe	1.65E-05	FeSO4*7H2O	278	1.0	1.73E-02	0.5201
Mn	2.41E-06	MnSO4*H2O	169	1.0	1.54E-03	0.0462
B	1.50E-05	H3BO3	61.83	1.0	3.51E-03	0.1053
Zn	1.46E-06	ZnSO4*7H2O	287.5	1.0	1.59E-03	0.0478
Mo	3.00E-07	(NH4)6Mo7O24*4(H2O)	1235.9	7.0	2.00E-04	0.0060

## Lettuce 25% Phosphorous Solution, Days 1-35

Nutrient	conc. (M)	compound	Atomic Wt (g/mol)	Ratio (mol/mol)	amount of compound to add g/gallon	g/30 gallon
N	8.18E-04	NH4NO3	80.04	2.0	1.24E-01	3.7151
N	1.39E-03	Ca(NO3)2*4H2O	236.2	2.0	6.20E-01	18.5852
N	5.22E-03	KNO3	101.1	1.0	2.00E+00	59.9626
K						
P	2.47E-04	KH2PO4	136.11	1.0	1.27E-01	3.8164
S	8.68E-04	H2SO4	98.079	1.0	3.22E-01	9.6668
Fe	1.65E-05	FeSO4*7H2O	278	1.0	1.73E-02	0.5201
Mn	2.41E-06	MnSO4*H2O	169	1.0	1.54E-03	0.0462
B	1.50E-05	H3BO3	61.83	1.0	3.51E-03	0.1053
Zn	1.46E-06	ZnSO4*7H2O	287.5	1.0	1.59E-03	0.0478
Mo	3.00E-07	(NH4)6Mo7O24*4(H2O)	1235.9	7.0	2.00E-04	0.0060



<b>Test 1, Day 1</b>							
<b>Temperature (C)</b>		<b>Relative Humidity (%)</b>		<b>Lighting (<math>\mu\text{mole m}^{-2} \text{s}^{-1}</math>)</b>			
<b>Min</b>	<b>Max</b>	<b>Min</b>	<b>Max</b>	<b>Min</b>	<b>Max</b>		
20	26	32	68	243	250		
22	27	31	65				
<b>pH</b>							
1	2	3	4	5	6	7	8
5.8	5.6	5.9	6.0	5.7	5.4	6.0	5.8
9	10	11	12	13	14	15	16
6.0	5.3	5.7	5.8	5.7	5.4	5.5	5.9
17	18	19	20	21	22	23	24
6.0	5.9	5.9	6.0	5.7	5.8	5.9	5.7
<b>EC (<math>\text{mS cm}^{-1}</math>)</b>							
1	2	3	4	5	6	7	8
1.25	1.30	1.43	1.55	1.32	1.42	1.35	1.29
9	10	11	12	13	14	15	16
1.35	1.46	1.28	1.37	1.42	1.44	1.60	1.52
17	18	19	20	21	22	23	24
1.37	1.43	1.45	1.51	1.48	1.37	1.44	1.56

<b>Test 1, Day 3</b>							
<b>Temperature (C)</b>		<b>Relative Humidity (%)</b>		<b>Lighting (<math>\mu\text{mole m}^{-2} \text{s}^{-1}</math>)</b>			
<b>Min</b>	<b>Max</b>	<b>Min</b>	<b>Max</b>	<b>Min</b>	<b>Max</b>		
21	27	31	69	240	249		
22	27	30	67				
<b>pH</b>							
1	2	3	4	5	6	7	8
5.9	5.4	5.9	6.0	5.8	5.0	5.7	5.8
9	10	11	12	13	14	15	16
6.0	5.7	6.0	5.8	5.5	5.1	5.6	5.8
17	18	19	20	21	22	23	24
6.0	5.6	5.6	5.5	6.0	5.9	5.9	6.0
<b>EC (<math>\text{mS cm}^{-1}</math>)</b>							
1	2	3	4	5	6	7	8
1.29	1.34	1.40	1.58	1.41	1.50	1.35	1.20
9	10	11	12	13	14	15	16
1.48	1.60	1.41	1.49	1.57	1.39	1.54	1.46
17	18	19	20	21	22	23	24
1.48	1.41	1.36	1.58	1.51	1.42	1.38	1.51

<b>Test 1, Day 5</b>							
<b>Temperature (C)</b>		<b>Relative Humidity (%)</b>		<b>Lighting (<math>\mu\text{mole m}^{-2} \text{s}^{-1}</math>)</b>			
<b>Min</b>	<b>Max</b>	<b>Min</b>	<b>Max</b>	<b>Min</b>	<b>Max</b>		
21	26	31	80	236	240		
21	27	32	87				
<b>pH</b>							
1	2	3	4	5	6	7	8
5.9	5.5	6.0	5.8	5.7	5.0	6.0	5.9
9	10	11	12	13	14	15	16
5.5	6.0	6.0	5.7	5.7	5.9	6.0	6.0
17	18	19	20	21	22	23	24
5.6	5.7	5.9	6.0	6.0	5.9	5.9	5.8
<b>EC (<math>\text{mS cm}^{-1}</math>)</b>							
1	2	3	4	5	6	7	8
1.24	1.27	1.25	1.40	1.65	1.33	1.25	1.22
9	10	11	12	13	14	15	16
1.43	1.30	1.24	1.56	1.24	1.46	1.44	1.53
17	18	19	20	21	22	23	24
1.56	1.35	1.20	1.41	1.41	1.23	1.31	1.30

<b>Test 1, Day 7</b>							
<b>Temperature (C)</b>		<b>Relative Humidity (%)</b>		<b>Lighting (<math>\mu\text{mole m}^{-2} \text{s}^{-1}</math>)</b>			
<b>Min</b>	<b>Max</b>	<b>Min</b>	<b>Max</b>	<b>Min</b>	<b>Max</b>		
21	27	33	87	247	253		
20	27	37	80				
<b>pH</b>							
1	2	3	4	5	6	7	8
5.9	5.9	6.0	5.5	5.5	6.0	5.5	5.5
9	10	11	12	13	14	15	16
5.8	6.0	6.0	5.9	5.9	5.9	6.0	6.0
17	18	19	20	21	22	23	24
5.8	6.0	6.0	5.9	5.7	5.7	5.5	5.5
<b>EC (<math>\text{mS cm}^{-1}</math>)</b>							
1	2	3	4	5	6	7	8
1.26	1.22	1.35	1.44	1.66	1.26	1.30	1.56
9	10	11	12	13	14	15	16
1.27	1.45	1.28	1.62	1.32	1.41	1.35	1.49
17	18	19	20	21	22	23	24
1.61	1.34	1.40	1.47	1.46	1.26	1.33	1.28

Test 1, Day 9							
Temperature (C)		Relative Humidity (%)		Lighting ( $\mu\text{mole m}^{-2} \text{s}^{-1}$ )			
Min	Max	Min	Max	Min	Max		
21	27	50	87	240	246		
20	27	48	80				
pH							
1	2	3	4	5	6	7	8
5.7	5.5	5.8	5.9	5.9	5.9	6.0	5.7
9	10	11	12	13	14	15	16
5.8	6.0	6.0	5.9	5.7	6.0	5.7	5.7
17	18	19	20	21	22	23	24
5.7	5.7	5.8	5.9	5.6	6.0	6.0	6.0
EC ( $\text{mS cm}^{-1}$ )							
1	2	3	4	5	6	7	8
1.21	1.23	1.34	1.43	1.52	1.30	1.35	1.46
9	10	11	12	13	14	15	16
1.33	1.45	1.22	1.59	1.40	1.44	1.42	1.46
17	18	19	20	21	22	23	24
1.50	1.32	1.49	1.51	1.42	1.25	1.32	1.32

Test 1, Day 11							
Temperature (C)		Relative Humidity (%)		Lighting ( $\mu\text{mole m}^{-2} \text{s}^{-1}$ )			
Min	Max	Min	Max	Min	Max		
21	27	56	85	236	246		
21	27	55	87				
pH							
1	2	3	4	5	6	7	8
5.8	5.6	6.0	5.6	6.0	5.9	6.0	6.0
9	10	11	12	13	14	15	16
5.8	6.0	6.0	5.9	5.7	5.6	6.0	6.0
17	18	19	20	21	22	23	24
5.5	6.0	5.5	5.5	5.7	5.8	5.8	5.6
EC ( $\text{mS cm}^{-1}$ )							
1	2	3	4	5	6	7	8
1.06	1.17	1.21	1.78	1.32	1.43	1.39	1.46
9	10	11	12	13	14	15	16
1.09	1.00	1.34	1.20	1.46	1.39	1.78	1.55
17	18	19	20	21	22	23	24
1.32	1.12	1.32	1.11	1.28	1.33	1.13	1.78

Test 1, Day 13							
Temperature (C)		Relative Humidity (%)		Lighting ( $\mu\text{mole m}^{-2} \text{s}^{-1}$ )			
Min	Max	Min	Max	Min	Max		
21	27	50	87	240	246		
20	27	48	80				
pH							
1	2	3	4	5	6	7	8
5.7	5.5	5.8	5.9	5.9	5.9	6.0	5.7
9	10	11	12	13	14	15	16
5.8	6.0	6.0	5.9	5.7	6.0	5.7	5.7
17	18	19	20	21	22	23	24
5.7	5.7	5.8	5.9	5.6	6.0	6.0	6.0
EC ( $\text{mS cm}^{-1}$ )							
1	2	3	4	5	6	7	8
1.21	1.23	1.34	1.43	1.52	1.30	1.35	1.46
9	10	11	12	13	14	15	16
1.33	1.45	1.22	1.59	1.40	1.44	1.42	1.46
17	18	19	20	21	22	23	24
1.50	1.32	1.49	1.51	1.42	1.25	1.32	1.32

Test 1, Day 15							
Temperature (C)		Relative Humidity (%)		Lighting ( $\mu\text{mole m}^{-2} \text{s}^{-1}$ )			
Min	Max	Min	Max	Min	Max		
21	27	32	85	257	260		
22	27	34	87				
pH							
1	2	3	4	5	6	7	8
5.7	5.7	6.0	5.8	5.6	6.0	5.6	5.6
9	10	11	12	13	14	15	16
5.9	5.7	5.5	6.0	5.8	5.7	5.6	5.9
17	18	19	20	21	22	23	24
5.9	5.9	5.8	5.6	5.8	5.7	5.2	5.8
EC ( $\text{mS cm}^{-1}$ )							
1	2	3	4	5	6	7	8
1.20	1.30	1.04	1.2	1.28	1.52	1.37	1.02
9	10	11	12	13	14	15	16
1.11	1.00	1.42	1.32	1.47	1.31	1.24	1.25
17	18	19	20	21	22	23	24
1.35	1.67	1.30	1.69	1.31	1.20	1.21	1.44

Test 1, Day 17							
Temperature (C)		Relative Humidity (%)		Lighting ( $\mu\text{mole m}^{-2} \text{s}^{-1}$ )			
Min	Max	Min	Max	Min	Max		
21	27	49	85	250	254		
21	27	48	87				
PH							
1	2	3	4	5	6	7	8
6.0	6.0	5.9	6.0	5.6	6.0	6.0	6.0
9	10	11	12	13	14	15	16
5.8	6.0	5.6	5.9	5.9	5.7	5.9	6.0
17	18	19	20	21	22	23	24
5.7	5.8	6.0	5.8	6.0	5.9	5.6	5.3
EC ( $\text{mS cm}^{-1}$ )							
1	2	3	4	5	6	7	8
1.02	1.22	1.04	1.27	1.32	1.21	1.28	1.28
9	10	11	12	13	14	15	16
1.39	1.21	1.50	1.42	1.45	1.26	1.25	1.17
17	18	19	20	21	22	23	24
1.29	1.32	1.27	1.35	1.25	1.22	1.03	1.42

Test 1, Day 19							
Temperature (C)		Relative Humidity (%)		Lighting ( $\mu\text{mole m}^{-2} \text{s}^{-1}$ )			
Min	Max	Min	Max	Min	Max		
21	27	47	85	249	255		
22	27	49	87				
PH							
1	2	3	4	5	6	7	8
5.6	5.9	5.8	5.8	5.8	5.8	5.6	6.0
9	10	11	12	13	14	15	16
6.0	5.5	5.6	5.5	6.0	5.9	5.6	6.0
17	18	19	20	21	22	23	24
6.0	6.0	5.9	5.5	5.7	5.9	6.0	5.7
EC ( $\text{mS cm}^{-1}$ )							
1	2	3	4	5	6	7	8
1.03	1.10	1.23	1.41	1.46	1.28	1.41	1.36
9	10	11	12	13	14	15	16
1.23	1.03	1.17	1.02	1.09	1.57	1.14	1.50
17	18	19	20	21	22	23	24
1.50	1.36	1.10	1.22	1.26	1.02	1.07	1.58

<b>Test 1, Day 21</b>							
<b>Temperature (C)</b>		<b>Relative Humidity (%)</b>		<b>Lighting (<math>\mu\text{mole m}^{-2} \text{s}^{-1}</math>)</b>			
<b>Min</b>	<b>Max</b>	<b>Min</b>	<b>Max</b>	<b>Min</b>	<b>Max</b>		
21	27	45	89	243	252		
21	27	41	85				
<b>pH</b>							
1	2	3	4	5	6	7	8
5.9	6.0	6.0	6.0	6.0	6.0	6.0	5.9
9	10	11	12	13	14	15	16
5.6	6.0	5.6	5.5	5.7	5.8	5.6	6.0
17	18	19	20	21	22	23	24
6.0	5.9	6.0	6.0	5.5	5.6	5.8	5.9
<b>EC (<math>\text{mS cm}^{-1}</math>)</b>							
1	2	3	4	5	6	7	8
1.02	1.35	1.04	1.44	1.24	1.32	1.21	1.09
9	10	11	12	13	14	15	16
1.27	1.04	1.08	1.30	1.43	1.48	1.27	1.14
17	18	19	20	21	22	23	24
1.19	1.17	1.00	1.45	1.27	1.36	1.17	1.20

<b>Test 1, Day 23</b>							
<b>Temperature (C)</b>		<b>Relative Humidity (%)</b>		<b>Lighting (<math>\mu\text{mole m}^{-2} \text{s}^{-1}</math>)</b>			
<b>Min</b>	<b>Max</b>	<b>Min</b>	<b>Max</b>	<b>Min</b>	<b>Max</b>		
21	29	53	85	246	253		
22	29	59	89				
<b>pH</b>							
1	2	3	4	5	6	7	8
5.6	6.0	5.7	6.0	5.9	5.9	5.9	5.8
9	10	11	12	13	14	15	16
5.7	6.0	6.0	5.6	5.5	6.0	6.0	6.0
17	18	19	20	21	22	23	24
5.6	5.9	6.0	5.8	5.6	5.8	5.5	5.2
<b>EC (<math>\text{mS cm}^{-1}</math>)</b>							
1	2	3	4	5	6	7	8
1.14	1.17	1.00	1.20	1.10	1.18	1.28	1.17
9	10	11	12	13	14	15	16
1.14	1.00	1.34	1.07	1.63	1.16	1.18	1.05
17	18	19	20	21	22	23	24
1.17	1.12	1.04	1.18	1.29	1.20	1.18	1.29

<b>Test 1, Day 25</b>							
<b>Temperature (C)</b>		<b>Relative Humidity (%)</b>		<b>Lighting (<math>\mu\text{mole m}^{-2} \text{s}^{-1}</math>)</b>			
<b>Min</b>	<b>Max</b>	<b>Min</b>	<b>Max</b>	<b>Min</b>	<b>Max</b>		
21	29	44	89	238	253		
20	29	44	85				
<b>pH</b>							
1	2	3	4	5	6	7	8
5.8	5.9	5.9	5.8	5.6	5.8	5.8	6.0
9	10	11	12	13	14	15	16
6.0	6.0	5.6	5.6	5.9	5.6	5.9	6.0
17	18	19	20	21	22	23	24
5.9	6.0	5.9	6.0	5.9	6.0	6.0	5.9
<b>EC (<math>\text{mS cm}^{-1}</math>)</b>							
1	2	3	4	5	6	7	8
1.16	1.33	1.11	1.24	1.29	1.43	1.36	1.22
9	10	11	12	13	14	15	16
1.22	1.40	1.34	1.34	1.41	1.07	1.13	1.03
17	18	19	20	21	22	23	24
1.49	0.99	1.54	1.60	1.18	1.10	1.04	1.55

<b>Test 1, Day 27</b>							
<b>Temperature (C)</b>		<b>Relative Humidity (%)</b>		<b>Lighting (<math>\mu\text{mole m}^{-2} \text{s}^{-1}</math>)</b>			
<b>Min</b>	<b>Max</b>	<b>Min</b>	<b>Max</b>	<b>Min</b>	<b>Max</b>		
21	29	61	89	243	246		
20	29	59	90				
<b>pH</b>							
1	2	3	4	5	6	7	8
6.0	6.0	6.0	5.8	5.9	5.9	5.9	6.0
9	10	11	12	13	14	15	16
6.0	6.0	6.0	6.0	5.6	6.0	5.9	5.9
17	18	19	20	21	22	23	24
5.7	5.8	6.0	5.6	6.0	5.8	5.6	5.7
<b>EC (<math>\text{mS cm}^{-1}</math>)</b>							
1	2	3	4	5	6	7	8
1.11	1.20	1.13	1.24	1.22	1.30	1.29	1.11
9	10	11	12	13	14	15	16
1.48	1.23	1.47	1.62	1.20	1.32	1.36	1.05
17	18	19	20	21	22	23	24
1.62	1.32	1.24	1.74	1.54	1.29	1.13	1.22

Test 1, Day 29							
Temperature (C)		Relative Humidity (%)		Lighting ( $\mu\text{mole m}^{-2} \text{s}^{-1}$ )			
Min	Max	Min	Max	Min	Max		
21	29	47	88	243	256		
21	28	46	85				
pH							
1	2	3	4	5	6	7	8
5.7	5.5	5.8	5.9	5.9	5.9	6.0	5.7
9	10	11	12	13	14	15	16
5.8	6.0	6.0	5.9	5.7	6.0	5.7	5.7
17	18	19	20	21	22	23	24
5.7	5.7	5.8	5.9	5.6	6.0	6.0	6.0
EC ( $\text{mS cm}^{-1}$ )							
1	2	3	4	5	6	7	8
1.21	1.23	1.34	1.43	1.52	1.30	1.35	1.46
9	10	11	12	13	14	15	16
1.33	1.45	1.22	1.59	1.40	1.44	1.42	1.46
17	18	19	20	21	22	23	24
1.50	1.32	1.49	1.51	1.42	1.25	1.32	1.32

Test 1, Day 31							
Temperature (C)		Relative Humidity (%)		Lighting ( $\mu\text{mole m}^{-2} \text{s}^{-1}$ )			
Min	Max	Min	Max	Min	Max		
20	29	46	92	238	249		
21	29	44	90				
pH							
1	2	3	4	5	6	7	8
5.6	5.7	5.8	5.8	5.3	5.7	5.9	6.0
9	10	11	12	13	14	15	16
5.9	5.9	5.6	5.8	5.8	5.6	5.7	6.0
17	18	19	20	21	22	23	24
6.0	5.9	5.7	5.5	5.9	5.7	5.2	5.8
EC ( $\text{mS cm}^{-1}$ )							
1	2	3	4	5	6	7	8
1.00	1.23	1.00	1.30	1.16	1.47	1.33	1.22
9	10	11	12	13	14	15	16
1.33	1.02	1.07	1.30	1.27	1.26	1.63	1.01
17	18	19	20	21	22	23	24
1.31	1.02	1.12	1.23	1.29	1.71	1.47	1.42



<b>Test 1, Day 33</b>							
<b>Temperature (C)</b>		<b>Relative Humidity (%)</b>		<b>Lighting (<math>\mu\text{mole m}^{-2} \text{s}^{-1}</math>)</b>			
<b>Min</b>	<b>Max</b>	<b>Min</b>	<b>Max</b>	<b>Min</b>	<b>Max</b>		
21	30	59	92	239	248		
21	29	56	95				
<b>pH</b>							
1	2	3	4	5	6	7	8
6.0	5.5	5.6	5.6	5.9	5.7	6.0	6.0
9	10	11	12	13	14	15	16
5.5	6.0	5.8	5.9	5.7	6.0	5.6	5.9
17	18	19	20	21	22	23	24
5.6	5.5	5.7	5.7	5.6	6.0	5.5	5.6
<b>EC (<math>\text{mS cm}^{-1}</math>)</b>							
1	2	3	4	5	6	7	8
1.20	1.34	1.36	1.56	1.39	1.25	1.42	1.53
9	10	11	12	13	14	15	16
1.19	1.32	1.16	1.63	1.37	1.51	1.33	1.43
17	18	19	20	21	22	23	24
1.45	1.28	1.45	1.53	1.46	1.29	1.45	1.48

<b>Test 1, Day 35</b>							
<b>Temperature (C)</b>		<b>Relative Humidity (%)</b>		<b>Lighting (<math>\mu\text{mole m}^{-2} \text{s}^{-1}</math>)</b>			
<b>Min</b>	<b>Max</b>	<b>Min</b>	<b>Max</b>	<b>Min</b>	<b>Max</b>		
21	29	48	89	257	259		
22	29	45	90				
<b>pH</b>							
1	2	3	4	5	6	7	8
5.6	5.7	6.0	5.8	5.3	5.8	5.5	5.6
9	10	11	12	13	14	15	16
5.6	5.7	5.5	6.0	5.8	5.9	5.6	5.9
17	18	19	20	21	22	23	24
5.9	5.9	5.8	5.3	5.8	5.7	5.5	6.0
<b>EC (<math>\text{mS cm}^{-1}</math>)</b>							
1	2	3	4	5	6	7	8
1.17	1.33	1.00	1.21	1.28	1.61	1.36	1.12
9	10	11	12	13	14	15	16
1.18	1.16	1.37	1.32	1.40	1.35	1.24	1.25
17	18	19	20	21	22	23	24
1.33	1.58	1.33	1.56	1.37	1.19	1.32	1.46

<b>Test 2, Day 1</b>							
<b>Temperature (C)</b>		<b>Relative Humidity (%)</b>		<b>Lighting (<math>\mu\text{mole m}^{-2} \text{s}^{-1}</math>)</b>			
<b>Min</b>	<b>Max</b>	<b>Min</b>	<b>Max</b>	<b>Min</b>	<b>Max</b>		
20	29	42	95	243	246		
21	30	45	98				
<b>pH</b>							
1	2	3	4	5	6	7	8
5.6	6.0	5.7	6.0	5.5	5.8	5.7	5.9
9	10	11	12	13	14	15	16
6.0	5.4	5.6	5.8	5.7	5.4	5.5	5.9
17	18	19	20	21	22	23	24
6.0	5.9	5.9	6.0	5.8	5.9	6.0	6.0
<b>EC (<math>\text{mS cm}^{-1}</math>)</b>							
1	2	3	4	5	6	7	8
1.05	1.26	1.34	1.17	1.47	1.37	1.26	1.20
9	10	11	12	13	14	15	16
1.01	1.69	1.59	1.40	1.76	1.58	1.74	1.33
17	18	19	20	21	22	23	24
1.03	1.33	1.27	1.52	1.03	1.07	1.36	1.23

<b>Test 2, Day 3</b>							
<b>Temperature (C)</b>		<b>Relative Humidity (%)</b>		<b>Lighting (<math>\mu\text{mole m}^{-2} \text{s}^{-1}</math>)</b>			
<b>Min</b>	<b>Max</b>	<b>Min</b>	<b>Max</b>	<b>Min</b>	<b>Max</b>		
20	29	46	94	246	249		
21	30	49	97				
<b>pH</b>							
1	2	3	4	5	6	7	8
5.9	6.0	6.0	6.0	5.8	5.9	5.9	5.9
9	10	11	12	13	14	15	16
6.0	5.9	5.9	6.0	5.9	5.9	5.8	6.0
17	18	19	20	21	22	23	24
6.0	5.9	5.9	5.9	6.0	6.0	5.7	5.9
<b>EC (<math>\text{mS cm}^{-1}</math>)</b>							
1	2	3	4	5	6	7	8
1.40	1.24	1.42	1.32	1.35	1.46	1.27	1.37
9	10	11	12	13	14	15	16
1.30	1.63	1.27	1.34	1.39	1.49	1.46	1.31
17	18	19	20	21	22	23	24
1.21	1.27	1.23	1.60	1.34	1.41	1.58	1.25

Test 2, Day 5							
Temperature (C)		Relative Humidity (%)		Lighting ( $\mu\text{mole m}^{-2} \text{s}^{-1}$ )			
Min	Max	Min	Max	Min	Max		
21	29	44	96	247	267		
22	30	45	96				
pH							
1	2	3	4	5	6	7	8
5.5	6.0	5.5	6.0	6.0	5.9	5.7	5.8
9	10	11	12	13	14	15	16
6.0	6.0	5.8	6.0	5.7	5.8	5.9	5.5
17	18	19	20	21	22	23	24
5.8	5.6	5.7	6.0	6.0	6.0	5.7	5.9
EC ( $\text{mS cm}^{-1}$ )							
1	2	3	4	5	6	7	8
1.37	1.20	1.31	1.32	1.26	1.50	1.32	1.31
9	10	11	12	13	14	15	16
1.30	1.54	1.43	1.46	1.37	1.54	1.54	1.29
17	18	19	20	21	22	23	24
1.36	1.56	1.32	1.63	1.23	1.40	1.48	1.31

Test 2, Day 7							
Temperature (C)		Relative Humidity (%)		Lighting ( $\mu\text{mole m}^{-2} \text{s}^{-1}$ )			
Min	Max	Min	Max	Min	Max		
21	29	42	95	242	244		
20	30	43	98				
pH							
1	2	3	4	5	6	7	8
5.8	5.6	5.9	5.7	5.7	5.6	5.6	5.9
9	10	11	12	13	14	15	16
5.8	5.9	5.9	6.0	6.0	5.8	5.0	6.0
17	18	19	20	21	22	23	24
5.9	5.5	5.5	5.0	6.0	5.0	5.0	5.6
EC ( $\text{mS cm}^{-1}$ )							
1	2	3	4	5	6	7	8
1.05	1.31	1.25	1.41	1.23	1.13	1.40	1.30
9	10	11	12	13	14	15	16
1.38	1.23	1.21	1.45	1.51	1.27	1.35	1.45
17	18	19	20	21	22	23	24
1.26	1.34	1.61	1.43	1.38	1.48	1.15	1.26

Test 2, Day 9							
Temperature (C)		Relative Humidity (%)		Lighting ( $\mu\text{mole m}^{-2} \text{s}^{-1}$ )			
Min	Max	Min	Max	Min	Max		
21	28	50	97	245	253		
21	29	48	96				
pH							
1	2	3	4	5	6	7	8
5.7	5.5	5.9	5.0	5.4	5.7	6.0	5.7
9	10	11	12	13	14	15	16
5.8	6.0	6.0	5.9	5.7	6.0	5.9	5.7
17	18	19	20	21	22	23	24
5.3	5.7	5.8	5.2	5.6	6.0	6.0	5.8
EC ( $\text{mS cm}^{-1}$ )							
1	2	3	4	5	6	7	8
1.27	1.44	1.23	1.17	1.60	1.32	1.27	1.46
9	10	11	12	13	14	15	16
1.39	1.42	1.32	1.48	1.37	1.27	1.49	1.38
17	18	19	20	21	22	23	24
1.57	1.38	1.52	1.64	1.35	1.49	1.40	1.42

Test 2, Day 11							
Temperature (C)		Relative Humidity (%)		Lighting ( $\mu\text{mole m}^{-2} \text{s}^{-1}$ )			
Min	Max	Min	Max	Min	Max		
21	30	46	95	246	252		
21	29	48	97				
pH							
1	2	3	4	5	6	7	8
5.7	5.4	6.0	5.9	5.3	5.7	6.0	5.8
9	10	11	12	13	14	15	16
5.8	5.6	6.0	5.8	5.7	5.5	6.0	5.8
17	18	19	20	21	22	23	24
5.2	5.7	5.5	5.9	5.7	5.9	5.8	5.9
EC ( $\text{mS cm}^{-1}$ )							
1	2	3	4	5	6	7	8
1.14	1.21	1.32	1.45	1.58	1.38	1.43	1.45
9	10	11	12	13	14	15	16
1.22	1.17	1.30	1.32	1.49	1.36	1.60	1.54
17	18	19	20	21	22	23	24
1.42	1.21	1.34	1.27	1.23	1.27	1.36	1.48

Test 2, Day 13							
Temperature (C)		Relative Humidity (%)		Lighting ( $\mu\text{mole m}^{-2} \text{s}^{-1}$ )			
Min	Max	Min	Max	Min	Max		
21	29	43	95	235	239		
20	30	40	98				
PH							
1	2	3	4	5	6	7	8
5.8	5.0	5.8	5.0	5.0	5.5	5.6	5.9
9	10	11	12	13	14	15	16
6.0	5.6	5.0	5.5	5.7	5.8	5.0	5.8
17	18	19	20	21	22	23	24
5.0	6.0	5.7	5.9	5.9	5.8	5.6	5.0
EC ( $\text{mS cm}^{-1}$ )							
1	2	3	4	5	6	7	8
1.02	1.25	1.55	1.31	1.50	1.34	1.36	1.66
9	10	11	12	13	14	15	16
1.72	1.24	1.77	1.78	1.79	1.53	1.54	1.46
17	18	19	20	21	22	23	24
1.66	1.46	1.78	1.71	1.65	1.40	1.12	1.63

Test 2, Day 15							
Temperature (C)		Relative Humidity (%)		Lighting ( $\mu\text{mole m}^{-2} \text{s}^{-1}$ )			
Min	Max	Min	Max	Min	Max		
21	30	53	98	243	249		
22	30	54	96				
PH							
1	2	3	4	5	6	7	8
5.7	5.7	6.0	5.8	5.6	6.0	5.6	5.6
9	10	11	12	13	14	15	16
5.9	5.7	5.5	6.0	5.8	5.7	5.6	5.9
17	18	19	20	21	22	23	24
5.9	5.9	5.8	5.6	5.8	5.7	5.2	5.8
EC ( $\text{mS cm}^{-1}$ )							
1	2	3	4	5	6	7	8
1.20	1.30	1.04	1.2	1.28	1.52	1.37	1.02
9	10	11	12	13	14	15	16
1.11	1.00	1.42	1.32	1.47	1.31	1.24	1.25
17	18	19	20	21	22	23	24
1.35	1.67	1.30	1.69	1.31	1.20	1.21	1.44

Test 2, Day 17							
Temperature (C)		Relative Humidity (%)		Lighting ( $\mu\text{mole m}^{-2} \text{s}^{-1}$ )			
Min	Max	Min	Max	Min	Max		
21	30	32	98	238	244		
22	29	35	97				
PH							
1	2	3	4	5	6	7	8
5.7	6.0	5.5	5.0	5.6	6.0	5.6	5.8
9	10	11	12	13	14	15	16
5.3	6.0	5.6	5.9	5.3	5.7	5.8	5.7
17	18	19	20	21	22	23	24
5.7	5.9	6.0	5.7	5.6	5.9	5.6	5.5
EC ( $\text{mS cm}^{-1}$ )							
1	2	3	4	5	6	7	8
1.14	1.24	1.09	1.33	1.39	1.30	1.29	1.41
9	10	11	12	13	14	15	16
1.36	1.29	1.48	1.48	1.54	1.32	1.27	1.30
17	18	19	20	21	22	23	24
1.36	1.41	1.25	1.32	1.34	1.36	1.15	1.36

Test 2, Day 19							
Temperature (C)		Relative Humidity (%)		Lighting ( $\mu\text{mole m}^{-2} \text{s}^{-1}$ )			
Min	Max	Min	Max	Min	Max		
21	30	40	98	247	248		
22	31	42	96				
PH							
1	2	3	4	5	6	7	8
5.7	5.0	5.0	5.9	5.0	5.0	5.0	5.8
9	10	11	12	13	14	15	16
5.0	5.5	5.8	5.0	6.0	6.0	5.5	5.0
17	18	19	20	21	22	23	24
6.0	6.0	5.0	5.3	5.0	5.0	6.0	5.0
EC ( $\text{mS cm}^{-1}$ )							
1	2	3	4	5	6	7	8
1.13	1.23	1.32	1.39	1.42	1.31	1.38	1.34
9	10	11	12	13	14	15	16
1.31	1.18	1.26	1.33	1.26	1.46	1.3	1.52
17	18	19	20	21	22	23	24
1.47	1.39	1.24	1.29	1.33	1.26	1.17	1.49

<b>Test 2, Day 21</b>							
<b>Temperature (C)</b>		<b>Relative Humidity (%)</b>		<b>Lighting (<math>\mu\text{mole m}^{-2} \text{s}^{-1}</math>)</b>			
<b>Min</b>	<b>Max</b>	<b>Min</b>	<b>Max</b>	<b>Min</b>	<b>Max</b>		
21	29	46	97	244	253		
21	30	43	95				
<b>pH</b>							
1	2	3	4	5	6	7	8
5.4	5.0	6.0	5.9	6.0	5.3	5.5	5.7
9	10	11	12	13	14	15	16
5.6	5.5	5.3	5.5	5.7	5.8	5.6	6.0
17	18	19	20	21	22	23	24
5.8	5.9	5.5	6.0	5.5	5.6	5.8	5.3
<b>EC (<math>\text{mS cm}^{-1}</math>)</b>							
1	2	3	4	5	6	7	8
1.20	1.51	1.22	1.34	1.32	1.30	1.29	1.18
9	10	11	12	13	14	15	16
1.29	1.34	1.25	1.32	1.45	1.52	1.33	1.23
17	18	19	20	21	22	23	24
1.21	1.19	1.20	1.38	1.25	1.33	1.27	1.28

<b>Test 2, Day 23</b>							
<b>Temperature (C)</b>		<b>Relative Humidity (%)</b>		<b>Lighting (<math>\mu\text{mole m}^{-2} \text{s}^{-1}</math>)</b>			
<b>Min</b>	<b>Max</b>	<b>Min</b>	<b>Max</b>	<b>Min</b>	<b>Max</b>		
21	29	53	85	246	253		
22	29	59	89				
<b>pH</b>							
1	2	3	4	5	6	7	8
5.6	6.0	5.7	5.0	5.9	5.4	5.9	5.6
9	10	11	12	13	14	15	16
5.7	6.0	6.0	5.6	5.5	6.0	6.0	6.0
17	18	19	20	21	22	23	24
5.6	5.3	6.0	5.5	5.6	5.8	5.3	5.2
<b>EC (<math>\text{mS cm}^{-1}</math>)</b>							
1	2	3	4	5	6	7	8
1.18	1.25	1.30	1.22	1.19	1.27	1.32	1.38
9	10	11	12	13	14	15	16
1.19	1.35	1.58	1.34	1.67	1.24	1.21	1.10
17	18	19	20	21	22	23	24
1.21	1.24	1.26	1.22	1.32	1.25	1.22	1.32

<b>Test 2, Day 25</b>							
<b>Temperature (C)</b>		<b>Relative Humidity (%)</b>		<b>Lighting (<math>\mu\text{mole m}^{-2} \text{s}^{-1}</math>)</b>			
<b>Min</b>	<b>Max</b>	<b>Min</b>	<b>Max</b>	<b>Min</b>	<b>Max</b>		
21	30	52	90	242	249		
20	29	51	93				
<b>pH</b>							
1	2	3	4	5	6	7	8
5.6	5.9	5.9	5.8	5.6	5.9	5.8	5.5
9	10	11	12	13	14	15	16
6.0	5.3	5.6	5.6	5.7	5.6	5.9	6.0
17	18	19	20	21	22	23	24
5.9	6.0	5.9	5.1	5.3	6.0	5.6	5.4
<b>EC (<math>\text{mS cm}^{-1}</math>)</b>							
1	2	3	4	5	6	7	8
1.24	1.32	1.17	1.28	1.31	1.40	1.33	1.16
9	10	11	12	13	14	15	16
1.25	1.56	1.41	1.31	1.37	1.13	1.24	1.16
17	18	19	20	21	22	23	24
1.33	1.12	1.45	1.49	1.24	1.09	1.26	1.45

<b>Test 2, Day 27</b>							
<b>Temperature (C)</b>		<b>Relative Humidity (%)</b>		<b>Lighting (<math>\mu\text{mole m}^{-2} \text{s}^{-1}</math>)</b>			
<b>Min</b>	<b>Max</b>	<b>Min</b>	<b>Max</b>	<b>Min</b>	<b>Max</b>		
21	29	60	89	247	252		
21	30	59	90				
<b>pH</b>							
1	2	3	4	5	6	7	8
6.0	5.0	6.0	5.7	5.9	5.6	5.9	6.0
9	10	11	12	13	14	15	16
6.0	5.3	5.0	6.0	5.6	5.8	5.9	5.9
17	18	19	20	21	22	23	24
5.7	5.6	5.7	5.5	6.0	5.2	5.6	5.5
<b>EC (<math>\text{mS cm}^{-1}</math>)</b>							
1	2	3	4	5	6	7	8
1.19	1.23	1.19	1.45	1.32	1.28	1.37	1.28
9	10	11	12	13	14	15	16
1.52	1.32	1.43	1.55	1.19	1.33	1.38	1.16
17	18	19	20	21	22	23	24
1.48	1.29	1.31	1.42	1.44	1.37	1.13	1.21



Test 2, Day 29							
Temperature (C)		Relative Humidity (%)		Lighting ( $\mu\text{mole m}^{-2} \text{s}^{-1}$ )			
Min	Max	Min	Max	Min	Max		
21	29	54	98	244	255		
21	30	56	97				
pH							
1	2	3	4	5	6	7	8
5.7	5.5	5.8	5.5	5.9	5.9	6.0	5.6
9	10	11	12	13	14	15	16
5.8	6.0	5.2	5.9	5.7	6.0	5.7	5.7
17	18	19	20	21	22	23	24
5.7	5.7	5.8	5.9	5.3	6.0	5.9	6.0
EC ( $\text{mS cm}^{-1}$ )							
1	2	3	4	5	6	7	8
1.20	1.28	1.31	1.40	1.51	1.44	1.32	1.48
9	10	11	12	13	14	15	16
1.46	1.51	1.30	1.69	1.45	1.44	1.38	1.32
17	18	19	20	21	22	23	24
1.47	1.29	1.50	1.47	1.43	1.21	1.23	1.32

Test 2, Day 31							
Temperature (C)		Relative Humidity (%)		Lighting ( $\mu\text{mole m}^{-2} \text{s}^{-1}$ )			
Min	Max	Min	Max	Min	Max		
20	29	50	92	242	256		
21	29	54	96				
pH							
1	2	3	4	5	6	7	8
5.6	5.6	5.6	6.0	5.5	5.0	5.8	5.9
9	10	11	12	13	14	15	16
5.7	5.9	5.6	5.8	5.6	6.0	5.7	6.0
17	18	19	20	21	22	23	24
6.0	5.9	5.1	5.5	5.9	5.4	5.2	5.6
EC ( $\text{mS cm}^{-1}$ )							
1	2	3	4	5	6	7	8
1.08	1.30	1.11	1.32	1.26	1.54	1.34	1.28
9	10	11	12	13	14	15	16
1.43	1.13	1.19	1.41	1.25	1.27	1.55	1.23
17	18	19	20	21	22	23	24
1.38	1.14	1.22	1.28	1.31	1.63	1.21	1.39

Test 2, Day 33							
Temperature (C)		Relative Humidity (%)		Lighting ( $\mu\text{mole m}^{-2} \text{s}^{-1}$ )			
Min	Max	Min	Max	Min	Max		
21	30	59	97	25	254		
21	29	56	98				
PH							
1	2	3	4	5	6	7	8
5.8	5.4	5.3	5.6	5.9	5.5	6.0	5.0
9	10	11	12	13	14	15	16
5.5	6.0	5.7	5.9	5.7	6.0	5.6	5.9
17	18	19	20	21	22	23	24
5.6	5.9	5.7	5.7	5.6	5.0	5.5	5.6
EC ( $\text{mS cm}^{-1}$ )							
1	2	3	4	5	6	7	8
1.21	1.30	1.33	1.52	1.41	1.32	1.40	1.45
9	10	11	12	13	14	15	16
1.27	1.34	1.38	1.55	1.32	1.45	1.31	1.36
17	18	19	20	21	22	23	24
1.40	1.25	1.36	1.45	1.40	1.39	1.22	1.43

Test 2, Day 35							
Temperature (C)		Relative Humidity (%)		Lighting ( $\mu\text{mole m}^{-2} \text{s}^{-1}$ )			
Min	Max	Min	Max	Min	Max		
21	29	54	94	256	261		
22	30	56	98				
PH							
1	2	3	4	5	6	7	8
5.4	5.8	5.5	6.0	5.6	5.9	5.3	5.8
9	10	11	12	13	14	15	16
6.0	5.7	5.9	5.0	5.8	5.7	5.6	5.9
17	18	19	20	21	22	23	24
5.9	5.4	5.8	5.7	5.8	5.7	5.5	5.8
EC ( $\text{mS cm}^{-1}$ )							
1	2	3	4	5	6	7	8
1.19	1.37	1.41	1.32	1.38	1.45	1.32	1.25
9	10	11	12	13	14	15	16
1.19	1.21	1.54	1.30	1.37	1.32	1.28	1.35
17	18	19	20	21	22	23	24
1.34	1.32	1.28	1.49	1.42	1.21	1.35	1.41

## **APPENDIX B.) Results for COLORBLOCK Neural Net**

**COLORBLOCK: Temporal and Reflectance Input  
Test 1: Training Set  
Large FOV, D =15-cm (or) 6-in**

<b>Test Day</b>	12	14	16	18	20	22	24	26	28	30	32	34
	<b>Percent (%) Correct Per Case Per Day</b>											
<b>Control</b>	25	50	75	75	50	25	25	50	50	50	50	0
<b>25%P</b>	0	25	25	75	100	75	75	75	0	50	25	0
<b>25%N</b>	50	0	0	75	75	25	50	75	0	25	50	50
<b>5%P</b>	25	50	25	25	75	100	75	50	50	75	50	0
<b>5%N</b>	100	100	75	100	100	100	100	100	100	100	100	100
	<b>Total Percent (%) Correct Per Case</b>											
	<b>Control</b>	<b>25%P</b>	<b>25%N</b>	<b>5%P</b>	<b>5%N</b>							
	44	44	40	50	98							
<b>Sum Square Error</b>	137											
<b>Total % Correct</b>	55											

**COLORBLOCK: Temporal and Reflectance Input  
Test 2: Validation Set  
Large FOV, D =15-cm (or) 6-in**

<b>Test Day</b>	12	14	16	18	20	22	24	26	28	30	32	34
	<b>Percent (%) Correct Per Case Per Day</b>											
<b>Control</b>	0	0	50	75	25	75	25	25	25	0	25	0
<b>25%P</b>	50	50	25	25	50	50	25	75	75	50	25	25
<b>25%N</b>	0	0	25	25	25	25	75	25	25	0	25	25
<b>5%P</b>	0	50	25	25	0	50	100	75	50	0	0	0
<b>5%N</b>	0	0	0	75	75	75	75	100	100	100	100	75
	<b>Total Percent (%) Correct Per Case</b>											
	<b>Control</b>	<b>25%P</b>	<b>25%N</b>	<b>5%P</b>	<b>5%N</b>							
	27	44	23	31	65							
<b>Sum Square Error</b>	212											
<b>Total % Correct</b>	38											

**COLORBLOCK: Temporal and Reflectance Input  
Test 1: Training Set  
Medium FOV, D = 7.5-cm (3.0-in)**

<b>Test Day</b>	12	14	16	18	20	22	24	26	28	30	32	34
	<b>Percent (%) Correct Per Case Per Day</b>											
<b>Control</b>	100	75	75	100	75	50	0	50	0	0	0	0
<b>25%P</b>	0	0	0	75	50	75	50	50	75	50	75	75
<b>25%N</b>	75	25	50	100	100	75	75	25	75	100	100	100
<b>5%P</b>	0	50	75	100	75	100	75	50	50	50	25	75
<b>5%N</b>	100	75	100	100	100	100	100	100	100	100	100	100
	<b>Total Percent (%) Correct Per Case</b>											
	<b>Control</b>	<b>25%P</b>	<b>25%N</b>	<b>5%P</b>	<b>5%N</b>							
	44	48	75	60	98							
<b>Sum Square Error</b>	113											
<b>Total % Correct</b>	65											

**COLORBLOCK: Temporal and Reflectance Input  
Test 2: Validation Set  
Medium FOV, D = 7.5-cm (3.0-in)**

<b>Test Day</b>	12	14	16	18	20	22	24	26	28	30	32	34
	<b>Percent (%) Correct Per Case Per Day</b>											
<b>Control</b>	0	75	25	25	0	0	0	0	25	0	0	0
<b>25%P</b>	0	0	0	0	0	50	25	75	25	50	75	25
<b>25%N</b>	0	25	25	25	25	25	0	0	25	25	75	75
<b>5%P</b>	0	0	25	50	100	75	75	100	50	0	25	25
<b>5%N</b>	100	25	50	100	100	100	100	100	75	100	50	100
	<b>Total Percent (%) Correct Per Case</b>											
	<b>Control</b>	<b>25%P</b>	<b>25%N</b>	<b>5%P</b>	<b>5%N</b>							
	13	27	27	44	83							
<b>Sum Square Error</b>	186											
<b>Total % Correct</b>	39											

**COLORBLOCK: Temporal and Reflectance Input  
Test 1: Training Set  
Small FOV, D = 3.75-cm (1.5-in)**

<b>Test Day</b>	12	14	16	18	20	22	24	26	28	30	32	34
	<b>Percent (%) Correct Per Case Per Day</b>											
<b>Control</b>	0	0	0	50	75	50	75	25	75	25	0	25
<b>25%P</b>	50	50	75	50	50	50	25	25	25	50	0	75
<b>25%N</b>	50	0	75	100	100	50	50	50	25	100	75	100
<b>5%P</b>	0	50	50	75	100	100	75	50	50	100	75	75
<b>5%N</b>	75	75	75	100	100	100	100	100	100	100	100	100
	<b>Total Percent (%) Correct Per Case</b>											
	<b>Control</b>	<b>25%P</b>	<b>25%N</b>	<b>5%P</b>	<b>5%N</b>							
	33	44	65	67	94							
<b>Sum Square Error</b>	118											
<b>Total % Correct</b>	60											

**COLORBLOCK: Temporal and Reflectance Input  
Test 2: Validation Set  
Small FOV, D = 3.75-cm (1.5-in)**

<b>Test Day</b>	12	14	16	18	20	22	24	26	28	30	32	34
	<b>Percent (%) Correct Per Case Per Day</b>											
<b>Control</b>	0	0	25	25	25	25	25	25	50	25	50	75
<b>25%P</b>	0	25	25	50	25	25	50	50	25	50	25	0
<b>25%N</b>	0	25	0	0	0	25	0	25	0	50	50	0
<b>5%P</b>	0	0	0	50	100	75	100	50	50	0	0	0
<b>5%N</b>	100	25	50	100	75	100	100	100	75	75	75	75
	<b>Total Percent (%) Correct Per Case</b>											
	<b>Control</b>	<b>25%P</b>	<b>25%N</b>	<b>5%P</b>	<b>5%N</b>							
	29	29	15	35	79							
<b>Sum Square Error</b>	187											
<b>Total % Correct</b>	38											

**COLORBLOCK: Temporal and Fluorescence Input  
Test 1: Training Set  
Large FOV, D =15-cm (or) 6-in**

<b>Test Day</b>	12	14	16	18	20	22	24	26	28	30	32	34
	<b>Percent (%) Correct Per Case Per Day</b>											
<b>Control</b>	50	0	25	0	25	0	0	0	0	25	50	0
<b>25%P</b>	50	50	75	25	50	75	75	100	100	75	50	75
<b>25%N</b>	50	50	0	50	25	100	50	100	75	100	100	75
<b>5%P</b>	25	0	25	50	50	50	25	25	25	25	25	25
<b>5%N</b>	75	75	100	75	100	100	50	100	75	75	100	100
	<b>Total Percent (%) Correct Per Case</b>											
	<b>Control</b>	<b>25%P</b>	<b>25%N</b>	<b>5%P</b>	<b>5%N</b>							
	15	67	65	29	85							
<b>Sum Square Error</b>	142											
<b>Total % Correct</b>	52											

**COLORBLOCK: Temporal and Fluorescence Input  
Test 2: Validation Set  
Large FOV, D =15-cm (or) 6-in**

<b>Test Day</b>	12	14	16	18	20	22	24	26	28	30	32	34
	<b>Percent (%) Correct Per Case Per Day</b>											
<b>Control</b>	0	0	0	25	25	25	50	0	0	0	0	0
<b>25%P</b>	25	0	0	0	0	75	50	25	0	0	0	0
<b>25%N</b>	0	0	0	50	0	25	50	75	50	50	25	50
<b>5%P</b>	0	0	0	0	0	0	0	50	50	0	75	0
<b>5%N</b>	75	75	100	75	50	75	75	50	25	50	25	75
	<b>Total Percent (%) Correct Per Case</b>											
	<b>Control</b>	<b>25%P</b>	<b>25%N</b>	<b>5%P</b>	<b>5%N</b>							
	10	15	31	15	63							
<b>Sum Square Error</b>	215											
<b>Total % Correct</b>	27											

**COLORBLOCK: Temporal and Fluorescence Input  
Test 1: Training Set  
Medium FOV, D = 7.5-cm (3.0-in)**

<b>Test Day</b>	12	14	16	18	20	22	24	26	28	30	32	34
	<b>Percent (%) Correct Per Case Per Day</b>											
<b>Control</b>	75	50	25	75	75	50	75	100	25	25	75	75
<b>25%P</b>	50	25	75	50	50	25	100	50	25	0	25	0
<b>25%N</b>	0	25	25	75	75	100	75	75	75	100	75	75
<b>5%P</b>	0	0	75	75	0	50	0	0	50	25	25	0
<b>5%N</b>	25	100	75	100	100	100	75	100	100	100	100	100
	<b>Total Percent (%) Correct Per Case</b>											
	<b>Control</b>	<b>25%P</b>	<b>25%N</b>	<b>5%P</b>	<b>5%N</b>							
	60	40	65	25	90							
<b>Sum Square Error</b>	142											
<b>Total % Correct</b>	56											

**COLORBLOCK: Temporal and Fluorescence Input  
Test 2: Validation Set  
Medium FOV, D = 7.5-cm (3.0-in)**

<b>Test Day</b>	12	14	16	18	20	22	24	26	28	30	32	34
	<b>Percent (%) Correct Per Case Per Day</b>											
<b>Control</b>	0	25	50	0	50	75	75	25	75	25	50	75
<b>25%P</b>	0	25	0	0	0	25	0	0	25	0	0	0
<b>25%N</b>	0	0	0	25	50	50	25	0	50	25	50	75
<b>5%P</b>	0	0	25	0	0	25	25	25	0	50	25	0
<b>5%N</b>	75	25	50	75	100	75	100	50	0	0	25	25
	<b>Total Percent (%) Correct Per Case</b>											
	<b>Control</b>	<b>25%P</b>	<b>25%N</b>	<b>5%P</b>	<b>5%N</b>							
	44	6	29	15	50							
<b>Sum Square Error</b>	211											
<b>Total % Correct</b>	29											



**COLORBLOCK: Temporal and Fluorescence Input  
Test 1: Training Set  
Small FOV, D = 3.75-cm (1.5-in)**

<b>Test Day</b>	12	14	16	18	20	22	24	26	28	30	32	34
	<b>Percent (%) Correct Per Case Per Day</b>											
<b>Control</b>	0	0	0	100	50	50	50	75	25	0	75	75
<b>25%P</b>	25	50	75	75	50	25	75	100	100	75	50	75
<b>25%N</b>	75	25	25	0	0	0	50	50	100	100	50	25
<b>5%P</b>	0	0	75	25	75	100	25	50	0	50	0	0
<b>5%N</b>	0	100	75	100	75	100	100	100	100	100	100	100
	<b>Total Percent (%) Correct Per Case</b>											
	<b>Control</b>	<b>25%P</b>	<b>25%N</b>	<b>5%P</b>	<b>5%N</b>							
	47	65	42	33	89							
<b>Sum Square Error</b>	137											
<b>Total % Correct</b>	54											

**COLORBLOCK: Temporal and Fluorescence Input  
Test 2: Validation Set  
Small FOV, D = 3.75-cm (1.5-in)**

<b>Test Day</b>	12	14	16	18	20	22	24	26	28	30	32	34
	<b>Percent (%) Correct Per Case Per Day</b>											
<b>Control</b>	0	0	0	25	25	25	50	50	25	25	0	0
<b>25%P</b>	25	25	0	75	25	75	0	25	75	75	50	25
<b>25%N</b>	50	0	0	0	0	25	50	0	0	0	0	0
<b>5%P</b>	25	50	0	75	50	50	50	0	0	25	0	0
<b>5%N</b>	0	25	50	50	75	75	25	50	0	50	75	50
	<b>Total Percent (%) Correct Per Case</b>											
	<b>Control</b>	<b>25%P</b>	<b>25%N</b>	<b>5%P</b>	<b>5%N</b>							
	19	40	10	27	44							
<b>Sum Square Error</b>	203											
<b>Total % Correct</b>	28											

**COLORBLOCK: Temporal, Reflectance, and Fluorescence Input  
Test 1: Training Set  
Large FOV, D =15-cm (or) 6-in**

<b>Test Day</b>	12	14	16	18	20	22	24	26	28	30	32	34
	<b>Percent (%) Correct Per Case Per Day</b>											
<b>Control</b>	50	50	50	50	50	75	50	75	50	75	75	25
<b>25%P</b>	25	50	50	75	100	50	75	75	75	75	75	75
<b>25%N</b>	100	75	50	50	75	100	75	50	25	50	100	75
<b>5%P</b>	0	25	50	25	75	75	100	50	100	75	25	25
<b>5%N</b>	100	100	75	100	100	100	100	100	100	100	100	100
	<b>Total Percent (%) Correct Per Case</b>											
	<b>Control</b>	<b>25%P</b>	<b>25%N</b>	<b>5%P</b>	<b>5%N</b>							
	56	67	69	52	98							
<b>Sum Square Error</b>	111											
<b>Total % Correct</b>	68											

**COLORBLOCK: Temporal, Reflectance, and Fluorescence Input  
Test 2: Validation Set  
Large FOV, D =15-cm (or) 6-in**

<b>Test Day</b>	12	14	16	18	20	22	24	26	28	30	32	34
	<b>Percent (%) Correct Per Case Per Day</b>											
<b>Control</b>	75	50	50	50	25	25	25	25	25	0	0	0
<b>25%P</b>	75	25	25	25	25	25	50	50	50	50	25	25
<b>25%N</b>	0	0	0	0	75	50	0	25	0	0	0	0
<b>5%P</b>	0	25	0	0	0	25	100	25	0	25	25	0
<b>5%N</b>	0	0	0	75	100	75	75	100	100	100	100	75
	<b>Total Percent (%) Correct Per Case</b>											
	<b>Control</b>	<b>25%P</b>	<b>25%N</b>	<b>5%P</b>	<b>5%N</b>							
	29	38	13	19	67							
<b>Sum Square Error</b>	237											
<b>Total % Correct</b>	33											

**COLORBLOCK: Temporal, Reflectance, and Fluorescence Input  
Test 1: Training Set  
Medium FOV, D = 7.5-cm (3.0-in)**

<b>Test Day</b>	12	14	16	18	20	22	24	26	28	30	32	34
	<b>Percent (%) Correct Per Case Per Day</b>											
<b>Control</b>	25	50	75	100	100	50	75	75	75	50	50	50
<b>25%P</b>	25	50	75	50	100	75	100	75	75	100	75	50
<b>25%N</b>	0	0	75	100	100	100	75	75	100	100	100	100
<b>5%P</b>	100	75	75	100	100	75	100	100	75	100	50	75
<b>5%N</b>	75	75	100	100	100	100	100	100	100	100	100	100
	<b>Total Percent (%) Correct Per Case</b>											
	<b>Control</b>	<b>25%P</b>	<b>25%N</b>	<b>5%P</b>	<b>5%N</b>							
	65	71	77	85	96							
<b>Sum Square Error</b>	73											
<b>Total % Correct</b>	79											

**COLORBLOCK: Temporal, Reflectance, and Fluorescence Input  
Test 2: Validation Set  
Medium FOV, D = 7.5-cm (3.0-in)**

<b>Test Day</b>	12	14	16	18	20	22	24	26	28	30	32	34
	<b>Percent (%) Correct Per Case Per Day</b>											
<b>Control</b>	0	0	0	25	25	25	25	25	0	50	0	50
<b>25%P</b>	0	25	25	0	25	75	50	75	75	100	100	75
<b>25%N</b>	0	75	0	50	50	25	25	0	0	0	25	75
<b>5%P</b>	25	0	0	25	25	50	50	25	50	25	25	25
<b>5%N</b>	50	50	100	100	100	100	100	75	100	100	75	100
	<b>Total Percent (%) Correct Per Case</b>											
	<b>Control</b>	<b>25%P</b>	<b>25%N</b>	<b>5%P</b>	<b>5%N</b>							
	19	52	27	27	88							
<b>Sum Square Error</b>	221											
<b>Total % Correct</b>	43											

**COLORBLOCK: Temporal, Reflectance, and Fluorescence Input  
Test 1: Training Set  
Small FOV, D = 3.75-cm (1.5-in)**

<b>Test Day</b>	12	14	16	18	20	22	24	26	28	30	32	34
	<b>Percent (%) Correct Per Case Per Day</b>											
<b>Control</b>	25	75	50	100	75	100	25	100	100	75	75	100
<b>25%P</b>	75	50	100	100	100	100	75	100	100	50	75	50
<b>25%N</b>	50	25	75	100	100	75	50	50	25	50	75	50
<b>5%P</b>	50	25	50	50	50	75	50	50	75	75	75	25
<b>5%N</b>	50	100	100	100	100	100	100	100	100	100	100	100
	<b>Total Percent (%) Correct Per Case</b>											
	<b>Control</b>		<b>25%P</b>		<b>25%N</b>		<b>5%P</b>		<b>5%N</b>			
	75		81		60		54		96			
<b>Sum Square Error</b>	93											
<b>Total % Correct</b>	73											

**COLORBLOCK: Temporal, Reflectance, and Fluorescence Input  
Test 2: Validation Set  
Small FOV, D = 3.75-cm (1.5-in)**

<b>Day</b>	12	14	16	18	20	22	24	26	28	30	32	34
	<b>Percent (%) Correct Per Case Per Day</b>											
<b>Control</b>	0	25	0	50	75	50	25	25	75	25	75	50
<b>25%P</b>	25	0	75	25	50	100	50	50	50	0	0	0
<b>25%N</b>	0	0	0	0	25	25	0	25	0	25	25	50
<b>5%P</b>	0	25	0	25	25	0	75	50	75	0	0	0
<b>5%N</b>	50	25	50	75	100	100	100	75	75	25	75	75
	<b>Total Percent (%) Correct Per Case</b>											
	<b>Control</b>		<b>25%P</b>		<b>25%N</b>		<b>5%P</b>		<b>5%N</b>			
	40		35		15		23		69			
<b>Sum Square Error</b>	242											
<b>Total % Correct</b>	36											

## **APPENDIX C.) Results for 10-nm Neural Net**

**10-nm NN: Temporal and Reflectance Input  
Test 1: Training Set  
Large FOV, D =15-cm (or) 6-in**

<b>Test Day</b>	12	14	16	18	20	22	24	26	28	30	32	34
	<b>Percent (%) Correct Per Case Per Day</b>											
<b>Control</b>	0	75	75	100	75	50	25	0	0	50	75	25
<b>25%P</b>	75	25	50	75	75	50	100	75	75	50	25	25
<b>25%N</b>	75	0	25	75	100	75	25	75	50	0	75	50
<b>5%P</b>	25	50	100	100	100	100	75	50	75	100	75	50
<b>5%N</b>	100	100	75	75	100	100	100	100	100	100	100	100
	<b>Total Percent (%) Correct Per Case</b>											
	<b>Control</b>	<b>25%P</b>	<b>25%N</b>	<b>5%P</b>	<b>5%N</b>							
	46	58	52	75	96							
<b>Sum Square Error</b>	126											
<b>Total % Correct</b>	65											

**10-nm NN: Temporal and Reflectance Input  
Test 2: Validation Set  
Large FOV, D =15-cm (or) 6-in**

<b>Test Day</b>	12	14	16	18	20	22	24	26	28	30	32	34
	<b>Percent (%) Correct Per Case Per Day</b>											
<b>Control</b>	0	0	0	50	25	25	0	50	50	25	25	25
<b>25%P</b>	25	25	25	25	25	50	75	50	50	50	25	25
<b>25%N</b>	0	0	0	0	25	25	25	0	0	0	50	25
<b>5%P</b>	0	0	25	25	0	50	75	25	50	50	50	50
<b>5%N</b>	100	75	100	75	100	75	50	75	100	100	100	100
	<b>Total Percent (%) Correct Per Case</b>											
	<b>Control</b>	<b>25%P</b>	<b>25%N</b>	<b>5%P</b>	<b>5%N</b>							
	23	38	13	33	88							
<b>Sum Square Error</b>	182											
<b>Total % Correct</b>	39											

**10-nm NN: Temporal and Reflectance Input  
Test 1: Training Set  
Medium FOV, D = 7.5-cm (3.0-in)**

<b>Test Day</b>	12	14	16	18	20	22	24	26	28	30	32	34
	<b>Percent (%) Correct Per Case Per Day</b>											
<b>Control</b>	25	50	75	75	100	100	50	50	100	100	25	50
<b>25%P</b>	50	75	50	100	50	75	75	100	50	25	100	50
<b>25%N</b>	50	25	75	100	100	50	25	0	25	25	50	50
<b>5%P</b>	0	25	75	100	100	100	100	100	50	100	100	100
<b>5%N</b>	100	50	75	100	100	100	100	100	100	100	100	100
	<b>Total Percent (%) Correct Per Case</b>											
	<b>Control</b>	<b>25%P</b>	<b>25%N</b>	<b>5%P</b>	<b>5%N</b>							
	67	67	48	79	94							
<b>Sum Square Error</b>	106											
<b>Total % Correct</b>	71											

**10-nm NN: Temporal and Reflectance Input  
Test 2: Validation Set  
Medium FOV, D = 7.5-cm (3.0-in)**

<b>Test Day</b>	12	14	16	18	20	22	24	26	28	30	32	34
	<b>Percent (%) Correct Pre Case Per Day</b>											
<b>Control</b>	0	25	0	25	25	0	25	100	75	75	50	25
<b>25%P</b>	25	0	25	0	25	75	50	100	25	25	50	25
<b>25%N</b>	0	25	25	0	50	50	0	25	0	25	0	25
<b>5%P</b>	0	0	100	25	75	75	50	75	75	50	75	50
<b>5%N</b>	75	25	50	100	100	100	100	100	100	100	100	100
	<b>Total Percent (%) Correct Per Case</b>											
	<b>Control</b>	<b>25%P</b>	<b>25%N</b>	<b>5%P</b>	<b>5%N</b>							
	35	35	19	54	88							
<b>Sum Square Error</b>	163											
<b>Total % Correct</b>	46											

**10-nm NN: Temporal and Reflectance Input  
Test 1: Training Set  
Small FOV, D = 3.75-cm (1.5-in)**

<b>Test Day</b>	12	14	16	18	20	22	24	26	28	30	32	34
	<b>Percent (%) Correct Per Case Per Day</b>											
<b>Control</b>	25	25	75	75	75	75	75	75	100	50	0	75
<b>25%P</b>	50	25	25	50	50	75	25	50	25	50	25	50
<b>25%N</b>	0	0	50	100	75	25	25	50	0	25	25	25
<b>5%P</b>	0	50	50	75	100	100	25	50	75	100	100	100
<b>5%N</b>	100	50	75	100	100	100	100	100	100	100	100	100
	<b>Total Percent (%) Correct Per Case</b>											
	<b>Control</b>		<b>25%P</b>		<b>25%N</b>		<b>5%P</b>		<b>5%N</b>			
	60		42		33		69		94			
<b>Sum Square Error</b>	127											
<b>Total % Correct</b>	60											

**10-nm NN: Temporal and Reflectance Input  
Test 2: Validation Set  
Small FOV, D = 3.75-cm (1.5-in)**

<b>Test Day</b>	12	14	16	18	20	22	24	26	28	30	32	34
	<b>Percent (%) Correct Per Case Per Day</b>											
<b>Control</b>	0	25	25	0	50	25	0	0	75	50	50	25
<b>25%P</b>	0	0	0	0	50	100	75	75	50	75	50	0
<b>25%N</b>	0	50	0	0	0	25	0	0	25	25	25	50
<b>5%P</b>	0	0	0	75	75	50	75	50	75	100	50	100
<b>5%N</b>	100	50	50	100	100	100	100	100	75	100	75	100
	<b>Total Percent Correct (%) Per Case</b>											
	<b>Control</b>		<b>25%P</b>		<b>25%N</b>		<b>5%P</b>		<b>5%N</b>			
	27		40		17		54		88			
<b>Sum Square Error</b>	162											
<b>Total % Correct</b>	45											



**10-nm NN: Temporal and Fluorescence Input  
Test 1: Training Set  
Large FOV, D =15-cm (or) 6-in**

<b>Test Day</b>	12	14	16	18	20	22	24	26	28	30	32	34
	<b>Percent (%) Correct Per Case Per Day</b>											
<b>Control</b>	50	25	50	75	75	25	25	50	75	75	75	50
<b>25%P</b>	50	50	25	50	50	50	75	100	75	75	50	75
<b>25%N</b>	0	0	50	75	100	100	25	100	75	75	75	75
<b>5%P</b>	25	50	50	50	50	75	100	50	50	100	25	50
<b>5%N</b>	25	100	100	100	100	100	100	100	100	100	100	100
	<b>Total Percent (%) Correct Per Case</b>											
	<b>Control</b>	<b>25%P</b>	<b>25%N</b>	<b>5%P</b>	<b>5%N</b>							
	54	60	63	56	94							
<b>Sum Square Error</b>	113											
<b>Total % Correct</b>	65											

**10-nm NN: Temporal and Fluorescence Input  
Test 2: Validation Set  
Large FOV, D =15-cm (or) 6-in**

<b>Test Day</b>	12	14	16	18	20	22	24	26	28	30	32	34
	<b>Percent (%) Correct Per Case Per Day</b>											
<b>Control</b>	25	25	50	50	75	50	50	50	25	0	25	0
<b>25%P</b>	25	25	25	0	0	75	25	0	0	25	25	0
<b>25%N</b>	0	25	0	0	50	50	0	0	50	25	50	100
<b>5%P</b>	0	0	0	50	25	50	25	50	100	25	25	25
<b>5%N</b>	25	0	75	25	75	75	50	100	50	100	100	75
	<b>Total Percent (%) Correct Per Case</b>											
	<b>Control</b>	<b>25%P</b>	<b>25%N</b>	<b>5%P</b>	<b>5%N</b>							
	35	19	29	31	63							
<b>Sum Square Error</b>	180											
<b>Total % Correct</b>	35											

**10-nm NN: Temporal and Fluorescence Input  
Test 1: Training Set  
Medium FOV, D = 7.5-cm (3.0-in)**

<b>Test Day</b>	12	14	16	18	20	22	24	26	28	30	32	34
	<b>Percent (%) Correct Per Case Per Day</b>											
<b>Control</b>	50	100	75	75	75	50	75	50	50	50	75	50
<b>25%P</b>	50	25	100	50	100	75	100	100	75	100	100	75
<b>25%N</b>	25	0	25	75	75	100	75	75	75	75	100	75
<b>5%P</b>	75	50	75	75	75	25	100	100	75	100	50	75
<b>5%N</b>	75	100	100	100	100	100	100	100	100	100	100	100
	<b>Total Percent (%) Correct Per Case</b>											
	<b>Control</b>	<b>25%P</b>	<b>25%N</b>	<b>5%P</b>	<b>5%N</b>							
	65	79	65	73	98							
<b>Sum Square Error</b>	100											
<b>Total % Correct</b>	76											

**10-nm NN: Temporal and Fluorescence Input  
Test 2: Validation Set  
Medium FOV, D = 7.5-cm (3.0-in)**

<b>Test Day</b>	12	14	16	18	20	22	24	26	28	30	32	34
	<b>Percent (%) Correct Per Case Per Day</b>											
<b>Control</b>	0	0	25	0	50	25	75	50	75	25	50	75
<b>25%P</b>	0	25	25	50	50	75	100	50	75	50	75	25
<b>25%N</b>	0	25	0	50	75	50	50	0	50	0	50	100
<b>5%P</b>	25	0	50	50	25	25	25	75	75	75	75	25
<b>5%N</b>	50	25	50	75	100	100	75	50	25	25	50	75
	<b>Total Percent (%) Correct Per Case</b>											
	<b>Control</b>	<b>25%P</b>	<b>25%N</b>	<b>5%P</b>	<b>5%N</b>							
	38	50	38	44	58							
<b>Sum Square Error</b>	170											
<b>Total % Correct</b>	45											

**10-nm NN: Temporal and Fluorescence Input  
Test 1: Training Set  
Small FOV, D = 3.75-cm (1.5-in)**

<b>Test Day</b>	12	14	16	18	20	22	24	26	28	30	32	34
	<b>Percent (%) Correct Per Case Per Day</b>											
<b>Control</b>	25	75	50	100	75	100	75	25	25	75	25	50
<b>25%P</b>	50	50	100	100	100	100	100	75	50	100	50	50
<b>25%N</b>	75	100	100	100	75	75	75	75	50	100	100	100
<b>5%P</b>	75	75	75	100	75	100	100	75	100	75	100	75
<b>5%N</b>	75	100	75	100	100	100	100	100	100	100	100	100
	<b>Total Percent (%) Correct Per Case</b>											
	<b>Control</b>	<b>25%P</b>	<b>25%N</b>	<b>5%P</b>	<b>5%N</b>							
	58	77	85	85	96							
<b>Sum Square Error</b>	80											
<b>Total % Correct</b>	80											

**10-nm NN: Temporal and Fluorescence Input  
Test 2: Validation Set  
Small FOV, D = 3.75-cm (1.5-in)**

<b>Test Day</b>	12	14	16	18	20	22	24	26	28	30	32	34
	<b>Percent (%) Correct Per Case Per Day</b>											
<b>Control</b>	25	0	0	25	75	50	25	50	25	25	0	0
<b>25%P</b>	25	25	50	75	50	75	50	75	25	50	25	25
<b>25%N</b>	50	50	0	100	50	75	25	25	50	50	50	25
<b>5%P</b>	25	0	50	50	0	75	50	0	0	25	75	0
<b>5%N</b>	0	0	50	50	75	75	50	100	75	100	100	75
	<b>Total Percent (%) Correct Per Case</b>											
	<b>Control</b>	<b>25%P</b>	<b>25%N</b>	<b>5%P</b>	<b>5%N</b>							
	25	46	46	29	63							
<b>Sum Square Error</b>	188											
<b>Total % Correct</b>	42											

**10-nm NN: Temporal, Reflectance, and Fluorescence Input  
Test 1: Training Set  
Large FOV, D =15-cm (or) 6-in**

<b>Test Day</b>	12	14	16	18	20	22	24	26	28	30	32	34
	<b>Percent (%) Correct Per Case Per Day</b>											
<b>Control</b>	25	25	50	50	50	50	0	0	0	75	75	50
<b>25%P</b>	25	50	25	50	75	50	100	100	100	75	50	50
<b>25%N</b>	75	75	75	100	100	100	50	100	75	75	50	75
<b>5%P</b>	50	25	75	100	75	100	75	50	50	100	25	25
<b>5%N</b>	100	100	75	100	100	100	100	100	100	100	100	100
	<b>Total Percent (%) Correct Per Case</b>											
	<b>Control</b>	<b>25%P</b>	<b>25%N</b>	<b>5%P</b>	<b>5%N</b>							
	38	63	79	63	98							
<b>Sum Square Error</b>	117											
<b>Total % Correct</b>	68											

**10-nm NN: Temporal, Reflectance, and Fluorescence Input  
Test 2: Validation Set  
Large FOV, D =15-cm (or) 6-in**

<b>Test Day</b>	12	14	16	18	20	22	24	26	28	30	32	34
	<b>Percent (%) Correct Per Case Per Day</b>											
<b>Control</b>	0	0	25	50	75	25	50	100	25	50	25	0
<b>25%P</b>	25	25	25	50	0	75	50	25	0	25	25	0
<b>25%N</b>	0	25	25	25	25	25	25	0	0	0	50	50
<b>5%P</b>	0	25	25	0	25	75	100	50	75	50	75	75
<b>5%N</b>	100	50	100	75	75	100	75	75	100	100	100	100
	<b>Total Percent (%) Correct Per Case</b>											
	<b>Control</b>	<b>25%P</b>	<b>25%N</b>	<b>5%P</b>	<b>5%N</b>							
	36	27	21	48	88							
<b>Sum Square Error</b>	168											
<b>Total % Correct</b>	44											

**10-nm NN: Temporal, Reflectance, and Fluorescence Input  
Test 1: Training Set  
Medium FOV, D = 7.5-cm (3.0-in)**

<b>Test Day</b>	12	14	16	18	20	22	24	26	28	30	32	34
	<b>Percent (%) Correct Per Case Per Day</b>											
<b>Control</b>	25	50	75	75	100	100	50	50	25	100	75	75
<b>25%P</b>	75	75	75	50	75	50	50	100	50	0	50	50
<b>25%N</b>	25	25	75	100	100	100	50	75	75	75	75	100
<b>5%P</b>	25	25	75	100	75	100	50	75	75	100	100	100
<b>5%N</b>	100	100	75	100	100	100	100	100	100	100	100	100
	<b>Total Percent (%) Correct Per Case</b>											
	<b>Control</b>	<b>25%P</b>	<b>25%N</b>	<b>5%P</b>	<b>5%N</b>							
	67	58	73	75	98							
<b>Sum Square Error</b>	105											
<b>Total % Correct</b>	74											

**10-nm NN: Temporal, Reflectance, and Fluorescence Input  
Test 2: Validation Set  
Medium FOV, D = 7.5-cm (3.0-in)**

<b>Test Day</b>	12	14	16	18	20	22	24	26	28	30	32	34
	<b>Percent (%) Correct Per Case Per Day</b>											
<b>Control</b>	0	25	25	25	75	75	75	50	75	75	50	50
<b>25%P</b>	25	0	50	0	0	50	0	50	100	75	25	25
<b>25%N</b>	0	50	25	25	50	50	50	0	25	25	75	75
<b>5%P</b>	0	0	25	50	50	50	25	75	25	50	0	50
<b>5%N</b>	100	75	100	75	100	100	100	75	100	75	75	100
	<b>Total Percent (%) Correct Per Case</b>											
	<b>Control</b>	<b>25%P</b>	<b>25%N</b>	<b>5%P</b>	<b>5%N</b>							
	50	33	38	33	90							
<b>Sum Square Error</b>	154											
<b>Total % Correct</b>	49											

**10-nm NN: Temporal, Reflectance, and Fluorescence Input  
Test 1: Training Set  
Small FOV, D = 3.75-cm (1.5-in)**

<i>Test Day</i>	12	14	16	18	20	22	24	26	28	30	32	34
	<b>Percent (%) Correct Per Case Per Day</b>											
<b>Control</b>	25	50	50	100	75	100	75	25	50	50	50	50
<b>25%P</b>	0	25	75	100	100	100	75	100	100	50	75	75
<b>25%N</b>	25	0	0	100	100	100	50	75	25	100	75	100
<b>5%P</b>	75	100	100	100	100	100	75	50	75	75	100	75
<b>5%N</b>	75	75	100	100	100	100	100	100	100	100	100	100
	<b>Total Percent (%) Correct Per Case</b>											
	<b>Control</b>		<b>25%P</b>		<b>25%N</b>		<b>5%P</b>		<b>5%N</b>			
	58		73		63		85		96			
<b>Sum Square Error</b>	101											
<b>Total % Correct</b>	75											

**10-nm NN: Temporal, Reflectance, and Fluorescence Input  
Test 2: Validation Set  
Small FOV, D = 3.75-cm (1.5-in)**

<i>Test Day</i>	12	14	16	18	20	22	24	26	28	30	32	34
	<b>Percent (%) Correct Per Case Per Day</b>											
<b>Control</b>	0	0	0	0	75	50	25	0	50	25	50	50
<b>25%P</b>	0	0	25	50	50	100	50	75	75	100	50	25
<b>25%N</b>	0	0	0	50	50	100	25	25	0	0	50	50
<b>5%P</b>	25	50	50	25	25	50	50	25	75	50	25	25
<b>5%N</b>	50	50	50	50	100	100	100	75	75	75	75	75
	<b>Total Percent (%) Correct Per Case</b>											
	<b>Control</b>		<b>25%P</b>		<b>25%N</b>		<b>5%P</b>		<b>5%N</b>			
	27		50		29		40		73			
<b>Sum Square Error</b>	168											
<b>Total % Correct</b>	44											

## **APPENDIX D.) Results for 1-nm Neural Net**

**1-nm NN: Temporal and Reflectance Input  
Test 1: Training Set  
Large FOV, D =15-cm (or) 6-in**

<b>Test Day</b>	12	14	16	18	20	22	24	26	28	30	32	34
	<b>Percent (%) Correct Per Case Per Day</b>											
<b>Control</b>	0	50	50	50	50	25	75	50	25	0	0	50
<b>25%P</b>	0	0	25	50	75	50	75	50	75	75	50	75
<b>25%N</b>	100	25	25	25	50	100	50	25	25	25	25	50
<b>5%P</b>	25	100	50	75	75	100	75	75	25	100	75	0
<b>5%N</b>	100	100	75	100	100	100	100	100	100	100	100	100
	<b>Total Percent (%) Correct Per Case</b>											
	<b>Control</b>	<b>25%P</b>	<b>25%N</b>	<b>5%P</b>	<b>5%N</b>							
	35	50	44	65	98							
<b>Sum Square Error</b>	141											
<b>Total % Correct</b>	58											

**1-nm NN: Temporal and Reflectance Input  
Test 2: Validation Set  
Large FOV, D =15-cm (or) 6-in**

<b>Test Day</b>	12	14	16	18	20	22	24	26	28	30	32	34
	<b>Percent (%) Correct Per Case Per Day</b>											
<b>Control</b>	0	0	0	25	0	0	0	75	0	25	0	0
<b>25%P</b>	0	0	0	25	25	50	75	75	50	25	25	50
<b>25%N</b>	25	25	0	0	25	0	0	25	50	25	50	50
<b>5%P</b>	0	0	0	25	50	25	50	25	75	25	25	50
<b>5%N</b>	75	100	75	100	100	75	50	75	100	100	75	100
	<b>Total Percent (%) Correct Per Case</b>											
	<b>Control</b>	<b>25%P</b>	<b>25%N</b>	<b>5%P</b>	<b>5%N</b>							
	10	33	23	29	85							
<b>Sum Square Error</b>	192											
<b>Total % Correct</b>	36											



**1-nm NN: Temporal and Reflectance Input  
Test 1: Training Set  
Medium FOV, D = 7.5-cm (3.0-in)**

<b>Test Day</b>	12	14	16	18	20	22	24	26	28	30	32	34
	<b>Percent (%) Correct Per Case Per Day</b>											
<b>Control</b>	25	0	0	50	25	75	25	50	100	50	25	50
<b>25%P</b>	50	0	50	100	25	75	100	25	75	50	75	50
<b>25%N</b>	0	0	0	75	100	25	25	0	0	50	50	50
<b>5%P</b>	75	75	50	25	100	75	75	50	25	100	25	50
<b>5%N</b>	100	100	100	100	100	100	100	100	100	100	100	100
	<b>Total Percent (%) Correct Per Case</b>											
	<b>Control</b>	<b>25%P</b>	<b>25%N</b>	<b>5%P</b>	<b>5%N</b>							
	40	56	31	60	100							
<b>Sum Square Error</b>	134											
<b>Total % Correct</b>	58											

**1-nm NN: Temporal and Reflectance Input  
Test 2: Validation Set  
Medium FOV, D = 7.5-cm (3.0-in)**

<b>Test Day</b>	12	14	16	18	20	22	24	26	28	30	32	34
	<b>Percent (%) Correct Per Case Per Day</b>											
<b>Control</b>	0	0	0	0	25	0	0	25	25	50	25	25
<b>25%P</b>	0	25	50	0	50	100	75	75	75	75	75	50
<b>25%N</b>	0	25	0	0	25	0	0	0	25	0	25	50
<b>5%P</b>	0	0	25	100	100	75	25	50	50	0	25	50
<b>5%N</b>	100	50	75	100	100	100	100	100	100	100	75	100
	<b>Total Percent (%) Correct Per Case</b>											
	<b>Control</b>	<b>25%P</b>	<b>25%N</b>	<b>5%P</b>	<b>5%N</b>							
	15	54	13	42	92							
<b>Sum Square Error</b>	171											
<b>Total % Correct</b>	43											

**1-nm NN: Temporal and Reflectance Input  
Test 1: Training Set  
Small FOV, D = 3.75-cm (1.5-in)**

<b>Test Day</b>	12	14	16	18	20	22	24	26	28	30	32	34
	<b>Percent (%) Correct Per Case Per Day</b>											
<b>Control</b>	25	25	50	50	50	50	75	50	100	50	0	0
<b>25%P</b>	0	0	50	75	100	50	50	100	25	50	0	75
<b>25%N</b>	75	25	75	100	75	25	0	50	25	50	75	50
<b>5%P</b>	75	75	100	100	100	100	50	50	100	100	75	75
<b>5%N</b>	100	75	75	100	100	100	100	100	100	100	100	100
	<b>Total Percent (%) Correct Per Case</b>											
	<b>Control</b>		<b>25%P</b>		<b>25%N</b>		<b>5%P</b>		<b>5%N</b>			
	44		48		52		83		96			
<b>Sum Square Error</b>	126											
<b>Total % Correct</b>	65											

**1-nm NN: Temporal and Reflectance Input  
Test 2: Validation Set  
Small FOV, D = 3.75-cm (1.5-in)**

<b>Test Day</b>	12	14	16	18	20	22	24	26	28	30	32	34
	<b>Percent (%) Correct Per Case Per Day</b>											
<b>Control</b>	0	50	25	0	75	25	0	25	75	25	50	75
<b>25%P</b>	0	0	25	25	25	100	50	100	50	75	50	25
<b>25%N</b>	25	50	0	25	0	25	0	0	0	25	0	0
<b>5%P</b>	0	0	25	50	50	50	50	25	75	50	25	75
<b>5%N</b>	100	50	50	100	100	100	100	100	75	75	75	50
	<b>Total Percent (%) Correct Per Case</b>											
	<b>Control</b>		<b>25%P</b>		<b>25%N</b>		<b>5%P</b>		<b>5%N</b>			
	35		44		13		40		81			
<b>Sum Square Error</b>	172											
<b>Total % Correct</b>	43											

**1-nm NN: Temporal and Fluorescence Input  
Test 1: Training Set  
Large FOV, D =15-cm (or) 6-in**

<b>Test Day</b>	12	14	16	18	20	22	24	26	28	30	32	34
	<b>Percent (%) Correct Per Case Per Day</b>											
<b>Control</b>	75	0	0	25	50	75	0	25	25	100	75	25
<b>25%P</b>	75	75	75	75	75	25	75	100	100	50	75	100
<b>25%N</b>	25	0	25	25	0	0	0	0	0	0	0	0
<b>5%P</b>	0	0	25	0	25	0	0	75	25	50	0	0
<b>5%N</b>	25	100	100	100	100	100	100	100	100	100	100	100
	<b>Total Percent (%) Correct Per Case</b>											
	<b>Control</b>	<b>25%P</b>	<b>25%N</b>	<b>5%P</b>	<b>5%N</b>							
	40	75	6	17	94							
<b>Sum Square Error</b>	156											
<b>Total % Correct</b>	46											

**1-nm NN: Temporal and Fluorescence Input  
Test 2: Validation Set  
Large FOV, D =15-cm (or) 6-in**

<b>Test Day</b>	12	14	16	18	20	22	24	26	28	30	32	34
	<b>Percent (%) Correct Per Case Per Day</b>											
<b>Control</b>	0	0	0	25	75	50	0	0	50	25	25	25
<b>25%P</b>	50	50	25	25	0	75	50	25	75	50	50	50
<b>25%N</b>	0	25	0	0	0	0	0	0	0	0	0	25
<b>5%P</b>	0	25	25	0	0	25	0	0	25	0	25	0
<b>5%N</b>	75	50	100	50	100	100	75	100	50	100	100	100
	<b>Total Percent (%) Correct Per Case</b>											
	<b>Control</b>	<b>25%P</b>	<b>25%N</b>	<b>5%P</b>	<b>5%N</b>							
	23	44	4	10	83							
<b>Sum Square Error</b>	212											
<b>Total % Correct</b>	33											

**1-nm NN: Temporal and Fluorescence Input  
Test 1: Training Set  
Medium FOV, D = 7.5-cm (3.0-in)**

<b>Test Day</b>	12	14	16	18	20	22	24	26	28	30	32	34
	<b>Percent (%) Correct Per Case Per Day</b>											
<b>Control</b>	50	50	50	75	100	50	75	75	50	75	100	75
<b>25%P</b>	100	75	75	75	75	75	100	100	75	100	75	50
<b>25%N</b>	25	0	50	100	100	100	75	100	100	75	75	75
<b>5%P</b>	0	50	50	50	75	75	100	100	50	100	75	75
<b>5%N</b>	100	100	100	100	100	100	100	100	100	100	100	100
	<b>Total Percent (%) Correct Per Case</b>											
	<b>Control</b>	<b>25%P</b>	<b>25%N</b>	<b>5%P</b>	<b>5%N</b>							
	69	81	73	67	100							
<b>Sum Square Error</b>	96											
<b>Total % Correct</b>	78											

**1-nm NN: Temporal and Fluorescence Input  
Test 2: Validation Set  
Medium FOV, D = 7.5-cm (3.0-in)**

<b>Test Day</b>	12	14	16	18	20	22	24	26	28	30	32	34
	<b>Percent (%) Correct Per Case Per Day</b>											
<b>Control</b>	0	25	25	25	75	75	75	25	75	25	50	75
<b>25%P</b>	0	25	50	75	25	75	100	50	25	50	50	50
<b>25%N</b>	0	50	25	75	100	75	75	25	50	50	25	25
<b>5%P</b>	25	25	25	50	25	25	0	75	0	50	50	25
<b>5%N</b>	75	50	50	75	100	100	50	75	50	50	75	75
	<b>Total Percent (%) Correct Per Case</b>											
	<b>Control</b>	<b>25%P</b>	<b>25%N</b>	<b>5%P</b>	<b>5%N</b>							
	46	48	48	31	69							
<b>Sum Square Error</b>	168											
<b>Total % Correct</b>	48											

**1-nm NN: Temporal and Fluorescence Input  
Test 1: Training Set  
Small FOV, D = 3.75-cm (1.5-in)**

<b>Test Day</b>	12	14	16	18	20	22	24	26	28	30	32	34
	<b>Percent (%) Correct Per Case Per Day</b>											
<b>Control</b>	25	50	75	100	100	100	100	100	100	100	100	100
<b>25%P</b>	0	0	0	0	0	0	0	0	0	0	0	0
<b>25%N</b>	0	0	0	0	0	0	0	0	0	0	0	0
<b>5%P</b>	0	0	0	0	0	0	0	0	0	0	0	0
<b>5%N</b>	100	75	50	50	50	75	100	50	50	25	25	50
	<b>Total Percent (%) Correct Per Case</b>											
	<b>Control</b>	<b>25%P</b>	<b>25%N</b>	<b>5%P</b>	<b>5%N</b>							
	88	0	0	0	58							
<b>Sum Square Error</b>	219											
<b>Total % Correct</b>	29											

**1-nm NN: Temporal and Fluorescence Input  
Test 2: Validation Set  
Small FOV, D = 3.75-cm (1.5-in)**

<b>Test Day</b>	12	14	16	18	20	22	24	26	28	30	32	34
	<b>Percent (%) Correct Per Case Per Day</b>											
<b>Control</b>	25	100	50	100	100	100	100	100	100	100	100	100
<b>25%P</b>	0	0	0	0	0	0	0	0	0	0	0	0
<b>25%N</b>	0	0	0	0	0	0	0	0	0	0	0	0
<b>5%P</b>	0	0	0	0	0	0	0	0	0	0	0	0
<b>5%N</b>	0	0	75	0	0	25	50	25	25	50	0	50
	<b>Total Percent (%) Correct Per Case</b>											
	<b>Control</b>	<b>25%P</b>	<b>25%N</b>	<b>5%P</b>	<b>5%N</b>							
	90	0	0	0	25							
<b>Sum Square Error</b>	234											
<b>Total % Correct</b>	23											

**1-nm NN: Temporal, Reflectance, and Fluorescence Input  
Test 1: Training Set  
Large FOV, D =15-cm (or) 6-in**

<b>Test Day</b>	12	14	16	18	20	22	24	26	28	30	32	34
	<b>Percent (%) Correct Per Case Per Day</b>											
<b>Control</b>	100	75	50	50	50	25	50	100	25	75	100	75
<b>25%P</b>	75	50	50	50	75	100	100	75	100	100	100	75
<b>25%N</b>	75	50	50	100	100	100	50	75	100	75	75	100
<b>5%P</b>	75	50	50	75	75	100	100	50	75	100	25	50
<b>5%N</b>	100	100	100	100	100	100	100	100	100	100	100	100
	<b>Total Percent (%) Correct Per Case</b>											
	<b>Control</b>	<b>25%P</b>	<b>25%N</b>	<b>5%P</b>	<b>5%N</b>							
	65	79	79	69	100							
<b>Sum Square Error</b>	96											
<b>Total % Correct</b>	78											

**1-nm NN: Temporal, Reflectance, and Fluorescence Input  
Test 2: Validation Set  
Large FOV, D =15-cm (or) 6-in**

<b>Test Day</b>	12	14	16	18	20	22	24	26	28	30	32	34
	<b>Percent (%) Correct Per Case Per Day</b>											
<b>Control</b>	0	0	25	75	0	50	25	100	50	100	25	0
<b>25%P</b>	0	0	25	25	50	50	50	0	25	0	25	0
<b>25%N</b>	25	25	25	0	25	25	25	25	0	0	25	25
<b>5%P</b>	50	25	0	0	50	75	50	25	50	25	75	75
<b>5%N</b>	75	75	100	75	75	100	75	75	100	100	100	75
	<b>Total Percent (%) Correct Per Case</b>											
	<b>Control</b>	<b>25%P</b>	<b>25%N</b>	<b>5%P</b>	<b>5%N</b>							
	38	21	19	42	85							
<b>Sum Square Error</b>	188											
<b>Total % Correct</b>	41											

**1-nm NN: Temporal, Reflectance, and Fluorescence Input  
Test 1: Training Set  
Medium FOV, D = 7.5-cm (3.0-in)**

<b>Test Day</b>	12	14	16	18	20	22	24	26	28	30	32	34
	<b>Percent (%) Correct Per Case Per Day</b>											
<b>Control</b>	25	75	50	75	100	75	75	100	50	100	75	100
<b>25%P</b>	25	25	75	50	100	75	75	75	100	50	75	25
<b>25%N</b>	25	50	50	100	100	100	75	75	25	50	100	100
<b>5%P</b>	50	50	50	100	100	100	75	100	50	75	75	50
<b>5%N</b>	100	75	100	100	100	100	100	100	100	100	100	100
	<b>Total Percent (%) Correct Per Case</b>											
	<b>Control</b>		<b>25%P</b>		<b>25%N</b>		<b>5%P</b>		<b>5%N</b>			
	75		63		71		73		98			
<b>Sum Square Error</b>	93											
<b>Total % Correct</b>	76											

**1-nm NN: Temporal, Reflectance, and Fluorescence Input  
Test 2: Validation Set  
Medium FOV, D = 7.5-cm (3.0-in)**

<b>Test Day</b>	12	14	16	18	20	22	24	26	28	30	32	34
	<b>Percent (%) Correct Per Case Per Day</b>											
<b>Control</b>	0	25	25	0	50	75	50	25	50	25	25	75
<b>25%P</b>	0	25	25	25	25	100	25	25	25	25	50	50
<b>25%N</b>	0	0	25	25	25	25	0	0	25	25	50	25
<b>5%P</b>	0	25	75	25	50	50	25	75	75	75	0	50
<b>5%N</b>	75	50	100	75	100	100	100	100	100	50	75	100
	<b>Total Percent (%) Correct Per Case</b>											
	<b>Control</b>		<b>25%P</b>		<b>25%N</b>		<b>5%P</b>		<b>5%N</b>			
	35		33		19		44		85			
<b>Sum Square Error</b>	175											
<b>Total % Correct</b>	43											

**1-nm NN: Temporal, Reflectance, and Fluorescence Input  
Test 1: Training Set  
Small FOV, D = 3.75-cm (1.5-in)**

<b>Test Day</b>	12	14	16	18	20	22	24	26	28	30	32	34
	<b>Percent (%) Correct Per Case Per Day</b>											
<b>Control</b>	0	0	25	100	75	100	75	75	100	50	25	75
<b>25%P</b>	50	50	75	100	75	75	50	75	50	75	75	75
<b>25%N</b>	75	25	75	100	75	100	50	75	25	75	75	100
<b>5%P</b>	50	75	100	100	100	100	100	75	75	75	75	100
<b>5%N</b>	100	100	100	75	100	100	100	100	100	100	100	100
	<b>Total Percent (%) Correct Per Case</b>											
	<b>Control</b>	<b>25%P</b>	<b>25%N</b>	<b>5%P</b>	<b>5%N</b>							
	58	69	71	85	98							
<b>Sum Square Error</b>	99											
<b>Total % Correct</b>	76											

**1-nm NN: Temporal, Reflectance, and Fluorescence Input  
Test 2: Validation Set  
Small FOV, D = 3.75-cm (1.5-in)**

<b>Test Day</b>	12	14	16	18	20	22	24	26	28	30	32	34
	<b>Percent (%) Correct Per Case Per Day</b>											
<b>Control</b>	0	0	0	0	50	25	25	0	75	50	75	50
<b>25%P</b>	0	0	50	50	25	75	50	75	50	75	25	0
<b>25%N</b>	25	0	0	25	25	25	25	0	25	0	0	25
<b>5%P</b>	25	100	50	50	75	50	50	50	50	0	0	50
<b>5%N</b>	50	50	75	50	100	75	100	100	100	75	75	75
	<b>Total Percent (%) Correct Per Day</b>											
	<b>Control</b>	<b>25%P</b>	<b>25%N</b>	<b>5%P</b>	<b>5%N</b>							
	29	40	15	46	77							
<b>Sum Square Error</b>	178											
<b>Total % Correct</b>	41											



## **APPENDIX E.) Results for 0.1-nm Neural Net**

**0.1-nm NN: Temporal and Reflectance Input  
Test 1: Training Set  
Large FOV, D =15-cm (or) 6-in**

<b>Test Day</b>	12	14	16	18	20	22	24	26	28	30	32	34
	<b>Percent (%) Correct Per Case Per Day</b>											
<b>Control</b>	0	0	25	50	50	50	75	50	25	50	75	100
<b>25%P</b>	0	25	25	50	50	50	100	75	50	75	25	50
<b>25%N</b>	75	50	0	75	50	100	50	50	25	50	50	50
<b>5%P</b>	0	0	50	75	50	75	75	25	25	75	75	0
<b>5%N</b>	100	100	100	100	100	100	100	100	100	100	100	100
	<b>Total Percent (%) Correct Per Case</b>											
	<b>Control</b>	<b>25%P</b>	<b>25%N</b>	<b>5%P</b>	<b>5%N</b>							
	46	48	52	44	100							
<b>Sum Square Error</b>	136											
<b>Total % Correct</b>	58											

**0.1-nm NN: Temporal and Reflectance Input  
Test 2: Validation Set  
Large FOV, D =15-cm (or) 6-in**

<b>Test Day</b>	12	14	16	18	20	22	24	26	28	30	32	34
	<b>Percent (%) Correct Per Case Per Day</b>											
<b>Control</b>	0	0	0	25	25	25	50	75	0	25	50	0
<b>25%P</b>	0	0	0	25	25	50	0	25	25	25	0	25
<b>25%N</b>	25	25	0	25	0	25	25	0	0	25	25	75
<b>5%P</b>	0	25	0	50	25	50	50	0	50	25	75	25
<b>5%N</b>	100	50	100	100	100	100	100	75	100	75	75	100
	<b>Total Percent (%) Correct Per Case</b>											
	<b>Control</b>	<b>25%P</b>	<b>25%N</b>	<b>5%P</b>	<b>5%N</b>							
	23	17	21	31	90							
<b>Sum Square Error</b>	201											
<b>Total % Correct</b>	36											

**0.1-nm NN: Temporal and Reflectance Input  
Test 1: Training Set  
Medium FOV, D = 7.5-cm (3.0-in)**

<b>Test Day</b>	12	14	16	18	20	22	24	26	28	30	32	34
	<b>Percent (%) Correct Per Case Per Day</b>											
<b>Control</b>	25	0	50	0	0	0	0	25	0	25	75	50
<b>25%P</b>	0	0	25	75	75	100	75	25	75	100	75	75
<b>25%N</b>	25	25	75	100	100	75	75	100	25	0	0	0
<b>5%P</b>	75	50	100	100	100	75	50	50	50	100	100	75
<b>5%N</b>	100	100	75	100	100	75	100	100	100	100	100	75
	<b>Total Percent (%) Correct Per Case</b>											
	<b>Control</b>		<b>25%P</b>		<b>25%N</b>		<b>5%P</b>		<b>5%N</b>			
	21		58		50		77		94			
<b>Sum Square Error</b>	137											
<b>Total % Correct</b>	60											

**0.1-nm NN: Temporal and Reflectance Input  
Test 2: Validation Set  
Medium FOV, D = 7.5-cm (3.0-in)**

<b>Test Day</b>	12	14	16	18	20	22	24	26	28	30	32	34
	<b>Percent (%) Correct Per Case Per Day</b>											
<b>Control</b>	0	0	25	50	0	25	0	0	0	0	0	0
<b>25%P</b>	0	0	0	0	25	25	75	25	75	50	25	75
<b>25%N</b>	0	25	0	25	25	0	0	0	0	25	50	50
<b>5%P</b>	0	0	0	25	100	75	0	50	50	50	25	25
<b>5%N</b>	50	75	75	50	100	75	25	50	25	0	75	75
	<b>Total Percent (%) Correct Per Case</b>											
	<b>Control</b>		<b>25%P</b>		<b>25%N</b>		<b>5%P</b>		<b>5%N</b>			
	8		31		17		33		56			
<b>Sum Square Error</b>	211											
<b>Total % Correct</b>	29											

**0.1-nm NN: Temporal and Reflectance Input  
Test 1: Training Set  
Small FOV, D = 3.75-cm (1.5-in)**

<b>Test Day</b>	12	14	16	18	20	22	24	26	28	30	32	34
	<b>Percent (%) Correct Per Case Per Day</b>											
<b>Control</b>	0	0	0	100	100	50	100	75	100	100	25	50
<b>25%P</b>	0	0	25	75	100	75	75	75	75	100	75	100
<b>25%N</b>	50	50	75	50	100	100	25	75	75	75	75	0
<b>5%P</b>	0	75	75	50	0	50	25	0	0	75	100	100
<b>5%N</b>	100	100	100	100	100	100	100	100	100	75	75	75
	<b>Total Percent (%) Correct Per Case</b>											
	<b>Control</b>	<b>25%P</b>	<b>25%N</b>	<b>5%P</b>	<b>5%N</b>							
	58	65	63	46	94							
<b>Sum Square Error</b>	125											
<b>Total % Correct</b>	65											

**0.1-nm NN: Temporal and Reflectance Input  
Test 2: Validation Set  
Small FOV, D = 3.75-cm (1.5-in)**

<b>Test Day</b>	12	14	16	18	20	22	24	26	28	30	32	34
	<b>Percent (%) Correct Per Case Per Day</b>											
<b>Control</b>	0	0	0	0	50	25	25	25	100	50	50	50
<b>25%P</b>	0	0	25	0	25	100	25	50	25	75	75	25
<b>25%N</b>	25	50	0	25	25	25	50	0	0	25	25	50
<b>5%P</b>	0	0	0	25	50	25	0	25	0	0	0	0
<b>5%N</b>	100	75	75	100	100	75	100	75	75	25	50	50
	<b>Total Percent (%) Correct Per Case</b>											
	<b>Control</b>	<b>25%P</b>	<b>25%N</b>	<b>5%P</b>	<b>5%N</b>							
	31	35	25	10	75							
<b>Sum Square Error</b>	202											
<b>Total % Correct</b>	35											

**0.1-nm NN: Temporal and Fluorescence Input  
Test 1: Training Set  
Large FOV, D =15-cm (or) 6-in**

<i>Test Day</i>	12	14	16	18	20	22	24	26	28	30	32	34
	<b>Percent (%) Correct Per Case Per Day</b>											
<b>Control</b>	25	0	0	25	50	100	75	75	75	100	75	100
<b>25%P</b>	100	75	75	50	100	75	100	100	75	75	75	75
<b>25%N</b>	50	50	50	50	75	100	50	75	100	75	100	50
<b>5%P</b>	25	0	25	25	0	0	50	50	0	0	0	25
<b>5%N</b>	25	100	100	100	75	100	75	100	100	100	100	100
	<b>Total Percent (%) Correct Per Case</b>											
	<b>Control</b>	<b>25%P</b>	<b>25%N</b>	<b>5%P</b>	<b>5%N</b>							
	58	81	69	17	90							
<b>Sum Square Error</b>	115											
<b>Total % Correct</b>	63											

**0.1-nm NN: Temporal and Fluorescence Input  
Test 2: Validation Set  
Large FOV, D =15-cm (or) 6-in**

<i>Test Day</i>	12	14	16	18	20	22	24	26	28	30	32	34
	<b>Percent (%) Correct Per Case Per Day</b>											
<b>Control</b>	0	0	0	50	25	50	75	25	75	0	0	25
<b>25%P</b>	75	50	50	25	0	75	50	50	0	0	0	0
<b>25%N</b>	0	0	25	0	0	25	25	75	0	50	0	25
<b>5%P</b>	0	0	0	0	0	0	0	25	25	25	75	0
<b>5%N</b>	25	25	75	50	50	100	75	75	25	100	75	75
	<b>Total Percent (%) Correct Per Case</b>											
	<b>Control</b>	<b>25%P</b>	<b>25%N</b>	<b>5%P</b>	<b>5%N</b>							
	27	31	19	13	63							
<b>Sum Square Error</b>	218											
<b>Total % Correct</b>	30											

**0.1-nm NN: Temporal and Fluorescence Input  
Test 1: Training Set  
Medium FOV, D = 7.5-cm (3.0-in)**

<b>Test Day</b>	12	14	16	18	20	22	24	26	28	30	32	34
	<b>Percent (%) Correct Per Case Per Day</b>											
<b>Control</b>	0	25	50	100	75	75	100	75	75	75	75	100
<b>25%P</b>	100	100	100	75	75	100	100	100	75	100	75	50
<b>25%N</b>	25	25	50	75	100	100	75	75	100	100	100	100
<b>5%P</b>	25	25	50	100	75	100	100	100	75	75	100	100
<b>5%N</b>	75	100	100	100	100	100	100	100	100	100	100	100
	<b>Total Percent (%) Correct Per Case</b>											
	<b>Control</b>	<b>25%P</b>	<b>25%N</b>	<b>5%P</b>	<b>5%N</b>							
	69	88	77	77	98							
<b>Sum Square Error</b>	84											
<b>Total % Correct</b>	82											

**10-nm NN: Temporal and Fluorescence Input  
Test 2: Validation Set  
Medium FOV, D = 7.5-cm (3.0-in)**

<b>Test Day</b>	12	14	16	18	20	22	24	26	28	30	32	34
	<b>Percent (%) Correct Per Case Per Day</b>											
<b>Control</b>	0	0	25	0	50	50	50	25	75	50	50	100
<b>25%P</b>	75	50	100	75	75	100	50	50	25	0	25	50
<b>25%N</b>	0	0	0	50	50	50	25	0	0	0	75	100
<b>5%P</b>	0	25	25	25	0	0	0	25	75	50	50	25
<b>5%N</b>	50	50	50	50	100	100	100	100	25	25	25	75
	<b>Total Percent (%) Correct Per Case</b>											
	<b>Control</b>	<b>25%P</b>	<b>25%N</b>	<b>5%P</b>	<b>5%N</b>							
	40	56	29	25	63							
<b>Sum Square Error</b>	185											
<b>Total % Correct</b>	43											

**0.1-nm NN: Temporal and Fluorescence Input  
Test 1: Training Set  
Small FOV, D = 3.75-cm (1.5-in)**

<b>Test Day</b>	12	14	16	18	20	22	24	26	28	30	32	34
	<b>Percent (%) Correct Per Case Per Day</b>											
<b>Control</b>	75	100	100	100	100	100	75	75	50	100	50	50
<b>25%P</b>	100	75	100	100	100	100	100	100	75	100	100	100
<b>25%N</b>	100	100	100	100	75	100	75	75	50	75	100	75
<b>5%P</b>	100	100	100	100	100	100	100	100	75	75	100	75
<b>5%N</b>	75	100	100	100	100	100	100	100	100	100	100	100
	<b>Total Percent (%) Correct Per Case</b>											
	<b>Control</b>	<b>25%P</b>	<b>25%N</b>	<b>5%P</b>	<b>5%N</b>							
	81	96	85	94	98							
<b>Sum Square Error</b>	68											
<b>Total % Correct</b>	91											

**0.1-nm NN: Temporal and Fluorescence Input  
Test 2: Validation Set  
Small FOV, D = 3.75-cm (1.5-in)**

<b>Test Day</b>	12	14	16	18	20	22	24	26	28	30	32	34
	<b>Percent (%) Correct Per Case Per Day</b>											
<b>Control</b>	25	0	25	75	25	75	50	25	50	25	25	0
<b>25%P</b>	25	25	25	50	25	25	50	25	50	50	0	0
<b>25%N</b>	50	25	0	0	25	25	0	25	25	50	25	50
<b>5%P</b>	0	50	0	75	25	75	25	25	25	0	50	25
<b>5%N</b>	0	50	75	50	75	50	50	100	25	50	75	100
	<b>Total Percent (%) Correct Per Case</b>											
	<b>Control</b>	<b>25%P</b>	<b>25%N</b>	<b>5%P</b>	<b>5%N</b>							
	33	29	25	31	58							
<b>Sum Square Error</b>	193											
<b>Total % Correct</b>	35											

**0.1-nm NN: Temporal, Reflectance, and Fluorescence Input  
Test 1: Training Set  
Large FOV, D =15-cm (or) 6-in**

<b>Test Day</b>	12	14	16	18	20	22	24	26	28	30	32	34
	<b>Percent (%) Correct Per Case Per Day</b>											
<b>Control</b>	100	50	25	100	100	75	100	100	50	100	100	100
<b>25%P</b>	100	50	75	100	100	100	100	100	100	75	100	75
<b>25%N</b>	100	75	50	50	75	100	75	100	100	100	100	75
<b>5%P</b>	50	75	50	100	75	100	75	100	50	100	75	50
<b>5%N</b>	100	100	100	100	100	100	100	100	100	100	100	100
	<b>Total Percent (%) Correct Per Case</b>											
	<b>Control</b>	<b>25%P</b>	<b>25%N</b>	<b>5%P</b>	<b>5%N</b>							
	83	90	83	75	100							
<b>Sum Square Error</b>	72											
<b>Total % Correct</b>	86											

**0.1-nm NN: Temporal, Reflectance, and Fluorescence Input  
Test 2: Validation Set  
Large FOV, D =15-cm (or) 6-in**

<b>Test Day</b>	12	14	16	18	20	22	24	26	28	30	32	34
	<b>Percent (%) Correct Per Case Per Day</b>											
<b>Control</b>	0	25	50	50	50	25	0	75	0	50	25	25
<b>25%P</b>	0	25	25	50	0	75	50	0	25	25	25	0
<b>25%N</b>	0	0	0	25	0	50	50	25	50	0	50	75
<b>5%P</b>	0	0	25	0	25	25	50	25	50	50	75	25
<b>5%N</b>	100	75	100	50	75	75	50	100	100	100	100	75
	<b>Total Percent (%) Correct Per Case</b>											
	<b>Control</b>	<b>25%P</b>	<b>25%N</b>	<b>5%P</b>	<b>5%N</b>							
	31	25	27	29	83							
<b>Sum Square Error</b>	194											
<b>Total % Correct</b>	39											



**0.1-nm NN: Temporal, Reflectance, and Fluorescence Input  
Test 1: Training Set  
Medium FOV, D = 7.5-cm (3.0-in)**

<b>Test Day</b>	12	14	16	18	20	22	24	26	28	30	32	34
	<b>Percent (%) Correct Per Case Per Day</b>											
<b>Control</b>	50	50	75	100	100	100	100	100	100	100	75	100
<b>25%P</b>	100	100	100	100	75	100	100	100	100	100	100	75
<b>25%N</b>	0	50	75	100	100	100	75	100	100	100	100	100
<b>5%P</b>	100	100	100	100	100	100	100	100	100	100	75	100
<b>5%N</b>	100	100	100	100	100	100	100	100	100	100	100	100
	<b>Total Percent (%) Correct Per Case</b>											
	<b>Control</b>	<b>25%P</b>	<b>25%N</b>	<b>5%P</b>	<b>5%N</b>							
	88	96	83	98	100							
<b>Sum Square Error</b>	42											
<b>Total % Correct</b>	93											

**0.1-nm NN: Temporal, Reflectance, and Fluorescence Input  
Test 2: Validation Set  
Medium FOV, D = 7.5-cm (3.0-in)**

<b>Test Day</b>	12	14	16	18	20	22	24	26	28	30	32	34
	<b>Percent (%) Correct Per Case Per Day</b>											
<b>Control</b>	0	25	0	0	50	75	50	50	100	0	75	25
<b>25%P</b>	0	0	25	0	25	50	25	50	25	25	0	25
<b>25%N</b>	0	0	0	0	50	0	50	25	25	0	25	75
<b>5%P</b>	0	50	75	50	75	25	0	50	25	75	0	25
<b>5%N</b>	75	50	75	75	100	50	100	75	50	50	75	50
	<b>Total Percent (%) Correct Per Case</b>											
	<b>Control</b>	<b>25%P</b>	<b>25%N</b>	<b>5%P</b>	<b>5%N</b>							
	38	21	21	38	69							
<b>Sum Square Error</b>	195											
<b>Total % Correct</b>	37											

**0.1-nm NN: Temporal, Reflectance, and Fluorescence Input  
Test 1: Training Set  
Small FOV, D = 3.75-cm (1.5-in)**

<b>Test Day</b>	12	14	16	18	20	22	24	26	28	30	32	34
	<b>Percent (%) Correct Per Case Per Day</b>											
<b>Control</b>	50	100	100	100	100	100	75	50	75	100	100	50
<b>25%P</b>	75	25	75	75	100	75	75	100	75	75	100	100
<b>25%N</b>	100	75	100	100	100	100	75	75	50	75	75	75
<b>5%P</b>	75	100	100	100	100	100	100	75	100	100	100	100
<b>5%N</b>	75	100	75	100	100	100	100	100	100	100	100	100
	<b>Total Percent (%) Correct Per Case</b>											
	<b>Control</b>	<b>25%P</b>	<b>25%N</b>	<b>5%P</b>	<b>5%N</b>							
	83	79	83	96	96							
<b>Sum Square Error</b>	64											
<b>Total % Correct</b>	88											

**0.1-nm NN: Temporal, Reflectance, and Fluorescence Input  
Test 2: Validation Set  
Small FOV, D = 3.75-cm (1.5-in)**

<b>Test Day</b>	12	14	16	18	20	22	24	26	28	30	32	34
	<b>Percent (%) Correct Per Case Per Day</b>											
<b>Control</b>	0	0	0	75	25	50	25	0	75	50	0	50
<b>25%P</b>	0	0	50	25	0	100	50	50	25	100	50	0
<b>25%N</b>	25	25	0	25	0	50	25	0	0	0	50	50
<b>5%P</b>	0	50	25	50	25	25	75	50	50	25	0	50
<b>5%N</b>	50	50	50	50	100	75	100	100	75	75	75	75
	<b>Total Percent (%) Correct Per Case</b>											
	<b>Control</b>	<b>25%P</b>	<b>25%N</b>	<b>5%P</b>	<b>5%N</b>							
	29	38	21	35	73							
<b>Sum Square Error</b>	191											
<b>Total % Correct</b>	39											

## **VITA EDIE SEARS**

**Edie Sears was born in Ft. Walton Beach, Florida. She graduated from Virginia Polytechnic and State University in 1994 with a Bachelors of Science in Biological Systems Engineering. Ms. Sears was awarded a Westinghouse/ARCO fellowship to conduct independent undergraduate research and present findings at International Professional Society Meeting, ASAE 1993. While at VA Tech, she also received the ASAE Student Honor Award and was voted Most Outstanding Senior by her departmental faculty.**

**In 1997 she received a Master of Science from the Pennsylvania State University in Biological Engineering which was funded by an ABE RA. While working on her Masters degree, Ms. Sears served two years on the Engineering Graduate Student Council where she participated in multiple recruitment activities for PSU's College of Engineering and in the organization of graduate student events. She served two terms as president of the student chapter of her professional honor society, Alpha Epsilon, and served as Team Leader for an Interdisciplinary research effort funded by a NASA STIR Grant.**

**Her Ph.D. program was conducted dually through PSU's Agricultural and Biological Engineering Department (ABE) and Electrical Engineering's (EE's) Communications and Space Science Laboratory (CSSL). Her work was funded by a three year NASA GSRP Fellowship from the Office of Life and Microgravity Science. Additional funding was provided by the Pennsylvania State University Graduate College and the Department of Agricultural and Biological Engineering. While working on her dissertation, Ms. Sears served as payload manager of Shuttle Small Payload G-064 where she lead six student teams, managed three experiments, conducted hardware fabrication, fundraising, PR, recruiting, and wrote all safety data reports/revisions as required by NASA GAS Office, Wallops, VA.**

**Ms. Sears belongs to SPIE, OSA, NSPE, Sigma Xi, Alpha Epsilon, NAUI, and AOPA. Her hobbies include: flying single engine aircraft, long distance running, scuba diving, and tai chi.**